U.S. DEPARTMENT OF THE INTERIOR
BUREAU OF RECLAMATION

# Seismic Tomography of Concrete Structures
# Phase I: Equipment Tests

U.S. Department of the Interior
1849-1999

**DSO-98-02**

Geophysics, Paleohydrology, and Seismotectonics Group

September 1998

DSO
DAM SAFETY OFFICE

# Seismic Tomography of Concrete Structures
# Phase I: Equipment Tests
# DSO-98-02

*by*
*Lisa Block*

**U.S. Department of Interior**
**Bureau of Reclamation**
**Dam Safety Office**
**Denver, Colorado**

**September 1998**

Prepared by

Lisa Block
Geophysicist

2/12/98
Date

Peer review by

Jerry Wright
Manager, Geophysics, Paleohydrology,
and Seismotectonics Group

2-12-98
Date

External peer review by
Kenneth D. Mahrer
Geophysicist

# TABLE OF CONTENTS

# LIST OF FIGURES

# LIST OF TABLES

# 1.0 INTRODUCTION

This report contains the results of Phase I of the seismic tomography research project currently being performed by the Seismotectonics and Geophysics Group, with funding from the Dam Safety Office. The ultimate goal of this research project is to develop Reclamation's capabilities for efficiently acquiring high-quality seismic tomography data on concrete structures for the purpose of imaging variations in concrete quality within the structure. As part of this project, the usefulness of the seismic tomography method as applied to concrete structures will be evaluated by acquiring and processing seismic data from one of Reclamation's concrete dams. The project is divided into 4 major phases: gathering background information from other researchers and testing various types of equipment (Phase I); preparing for the field test by purchasing and constructing equipment, modifying data processing software, and performing forward modeling (Phase II); data acquisition and preliminary on-site data processing (Phase III); and final data analysis and report preparation (Phase IV).

The primary purpose of Phase I of this research project is to determine the types of sources, receivers, and coupling methods that are likely to produce the highest quality seismic data on concrete structures. Other important factors that are considered when evaluating various field equipment are equipment costs and difficulty of installation. A secondary purpose of Phase I is to determine the frequencies of the seismic signals that are likely to be acquired through concrete dams over the distances and angles necessary for application of the seismic tomography method.

The methodology and results from Phase I are presented in the following sections of this report. The initial part of Phase I involved the gathering of information from various groups that have acquired and analyzed seismic data on concrete structures. The information obtained is summarized in Section 2 of this report. Most of the work performed during Phase I involved the acquisition and testing of various types of sources and receivers. Various types of surface receivers and coupling methods were compared by acquiring data in a laboratory on a large concrete block (5 ft x 5 ft x 5 ft). Different types of sources, as well as the feasibility of lowering sources and receivers into the reservoir immediately upstream of the dam, were evaluated with field tests performed at Monticello Dam, near Vacaville, California. These tests also provided further comparison data between the various types of surface receivers. Section 3 contains explanations of the

laboratory and field testing procedures, and Section 4 contains details about the specific types of sources and receivers tested. In Section 5, the responses of the surface receivers, from both laboratory and field tests, are presented and compared. Effects of different methods of mounting surface receivers are addressed in Section 6. Evaluations of the sources tested are presented in Section 7. While the tests performed during Phase I answered many questions, some issues remain unresolved and new issues arose. The conclusions of the Phase I work and the issues that need further investigation are discussed in Section 8.

# 2.0 THE CURRENT STATE OF PRACTICE

Although an in-depth investigation of the current state of practice in the evaluation of concrete quality using seismic data was not performed, some information was gathered from several sources. Most notably, a group of geophysicists at ISMES, a company in Italy, has been performing seismic tomography on concrete, masonry, and embankment dams for more than 10 years. (Bertacchi et al., 1991; Angeloni et al., 1995) They have tested approximately 100 dams with this method. In response to a letter containing a number of questions, ISMES sent a fax providing information about the equipment they use for acquiring seismic data on dams. The following information is summarized from that correspondence and from Angeloni et al. (1995). Seismic sources used by ISMES include hammers on dry surfaces and piezoelectric transmitters and a spark transducer below the water (in boreholes or in the reservoir upstream of a dam). The piezoelectric transmitters and spark transducer were designed and built in-house. Frequencies of 10 to 30 kHz are obtained with the piezoelectric transmitters over distances of a few meters (use of impulsive signals is implied). A piezoelectric transmitter is being developed whose signal emission is driven by a pseudo-random binary sequence and which is expected to transmit frequencies of 5 to 20 kHz over distances of tens of meters. The frequencies generated with the sparker source range from 2 to 4 kHz. The frequencies obtained with a hammer source are not stated in the correspondence or published papers. For receivers on dry surfaces, ISMES uses high-sensitivity vertical accelerometers, mounted with “threaded plugs”. In boreholes or in the reservoir below the water, ISMES uses low-noise hydrophones.

In addition to ISMES, a group of investigators, mostly located in Canada, are currently developing capabilities for recording and analyzing seismic tomography data on concrete dams. Diane Wiese

of MDC Geological Consultants Ltd., Professor Mike Thomas at the University of Toronto, Dr. Carlos Santamarina of Georgia Institute of Technology, and ANDEC Mfg. Ltd. are working together, with partial funding from the Canadian government, to develop the hardware and software needed to perform seismic tomography on concrete structures. They have performed seismic travel time tomography through 4 ft x 4 ft sections of a concrete lab sample using piezoelectric transducers with a resonance frequency of 50 kHz as the source and receiver. (Thomas et al., 1995). They have also performed some limited field tests, acquiring data up to a distance of about 100 ft with a maximum frequency content of 40 kHz (phone conversation, Professor Thomas, University of Toronto, May 23, 1997). They are currently preparing for a full-scale field trial at a concrete dam.

Several other groups are performing seismic testing of concrete, although not necessarily using the seismic tomography method. Olson Engineering, located in Lakewood, Colorado, routinely performs "crosshole sonic logging" in concrete. Olson records data using a sonic transmitter in one borehole and a matching receiver in a nearby borehole at the same depth. They have acquired good-quality 35-kHz seismic data over distances up to 25 feet without stacking (phone conversation, Dennis Sack, April 25, 1997). They have also acquired seismic data on concrete surfaces using vertical accelerometers mounted with either dental plaster, grease, or screwed onto metal plates epoxyed onto the surface.

Mount Sopris, a company that primarily builds geophysical logging equipment, in conjunction with InfraSeis Inc., a small company recently founded by Farrokh Jalinoos, is currently developing a crosshole sonic logging system that will operate at a resonance frequency of 40 kHz. This system is primarily intended to be used to test concrete piers, using an anticipated borehole separation of about 20 feet (phone conversations, Chuck Oden, Mount Sopris, February 28, 1997, and Farrokh Jalinoos, InfraSeis Inc, March 3, 1997).

Ernie Majer, at Lawrence Berkeley Laboratory, has acquired seismic data on concrete surfaces using piezoelectric transmitters designed and built in-house. He has acquired data ranging in frequency from 1 to 15 kHz over distances up to 10 meters through concrete (phone conversation, Ernie Majer, March 27, 1997). He can drive the transmitters using an impulsive signal or various coded sequences. An impulsive signal is preferred over sequences due to a sharper "first break" of the P-wave arrival. Ernie Majer is currently writing a paper documenting comparisons of various types of source

signatures.

# 3.0 TESTING PROCEDURES

## 3.1 Laboratory Tests

Seismic data were acquired on a concrete block measuring 5 ft x 5 ft x 5 ft using various types of receivers and receiver mountings. These tests were performed between April and June, 1997. The two purposes of these tests were to compare the responses of different types of surface receivers and to investigate the effects of a few different types of receiver mountings. Procedures specific to each test performed are given in Sections 5 and 6 as the data are presented. This section contains information common to all of the laboratory tests.

Before the laboratory tests were performed, a cylindrical hole with a diameter of 3.75 inches had been cored from the center of one block face through the block to the opposite face. The source and receivers used during these tests were placed on block faces that did not contain the corehole. The source and receiver used for each test were placed such that the direct, straight-ray path was at least 1 foot from the corehole.

In order to compare the responses of various types of receivers, a repeatable source was required. This was necessary so that the strength and frequency content of the seismic energy generated during each test was as similar as possible. To satisfy this requirement, a transducer consisting of 2 piezoelectric crystals and an inertial mass mounted between alluminum plates was constructed. The piezoelectric crystals, mass, and plates were held together by two bolts extending from one alluminum plate to the other. This transducer was threaded onto a masonry anchor bolt placed in the concrete block. One of the crystals in the transducer was driven with an electrical signal generated by a Hewlett Packard frequency analyzer. During all of the laboratory tests discussed in this report, the frequency analyzer output a short burst chirp signal (Figure 3-1). A 20-watt power amplifier and wide-bandwidth step-up transformer were used to boost the signal level. The amplifier has a 60-kHz bandwidth and a gain of about 20. (The transducer, amplifier, and transformer were constructed by Matrix-5 Technologies).

During the lab tests, the second piezoelectric crystal in the

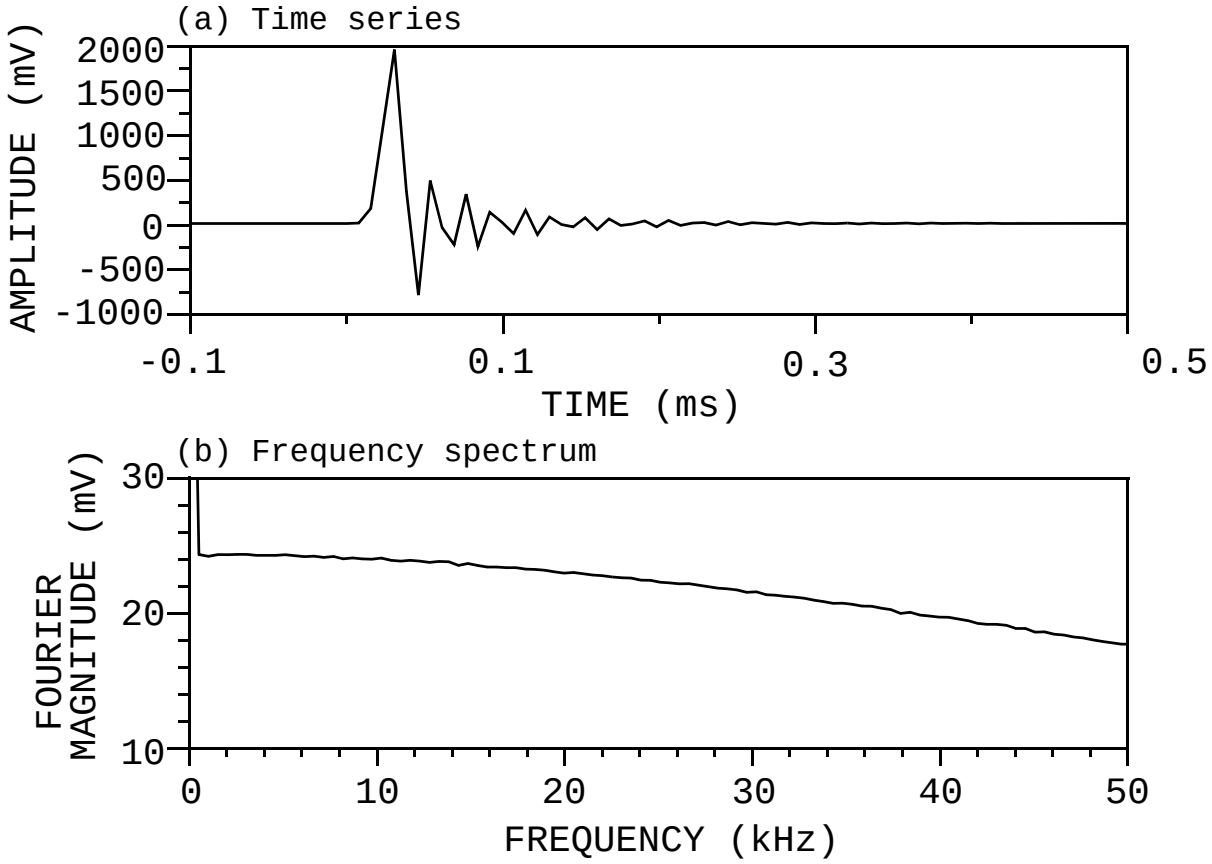


FIGURE 3-1: Burst chirp signal generated by the frequency analyzer during laboratory tests. This signal was sent through an amplifier and transformer and then used to drive a piezoelectric transmitter.

transducer was used as a receiver. It was originally thought that this receiver would provide a good indication of the seismic signal that was generated. However, because of severe electromagnetic crossfeed problems, the recorded signal is contaminated with electromagnetic energy and hence is not a reliable indicator of the seismic energy generated. Because of variable frequency response of the amplifier and transformer (not all frequencies are boosted equally) and the variable frequency response of the piezoelectric crystals, the precise signal put into the concrete, although repeatable, is not well characterized.

All data were recorded on the same frequency analyzer that generated the source signal. Although this frequency analyzer has 4 channels, only two channels can be recorded simultaneously at the highest sampling rate. The signal from the second crystal in the piezoelectric source described above was recorded on one channel, and the receiver being tested was recorded on the other channel.

A sample interval of 7.63 us was used for all laboratory tests. A recording delay time of -0.5 ms was used, so that some data were acquired before the source was fired. Time 0 corresponds to the moment when the source signal is generated by the frequency analyzer.

## 3.2 Field Tests

Limited field testing was conducted at Monticello Dam near Vacaville, California, in early May, 1997. All testing was done in block 8 (located immediately north of the main gallery entrance, Figure 3-2). Seismic data were acquired in the upstream-downstream direction across block 8. Three acquisition geometries were used. These geometries are shown in Figure 3-3 and include:

1. Data acquisition between the east gallery wall and the downstream face (Figure 3-3a). For each test, a source was activated on the gallery wall, and a receiver was mounted on the downstream dam face. The straight-ray angle between the source and receiver was about 5.5 degrees from horizontal, and the source-receiver separation was approximately 45 feet.

2. Data acquisition between the reservoir and the west gallery wall (Figure 3-3b). During these tests, the seismic source was located in the reservoir, and a receiver was mounted on the gallery wall. The straight-ray angle ranged from about 15 to 57 degrees from horizontal, and the source-receiver separation varied from approximately 24 to 43 feet.

3. Data acquisition between the reservoir and the downstream face (Figure 3-3c). For this geometry, tests were conducted with a source on the downstream face and a receiver in the resevoir, and vice versa. The straight-ray angle ranged from about 2 to 63 degrees from horizontal. The source-receiver separation varied from 67 to 148 feet.

No climbers or divers were used for these tests. The lower section of the downstream dam face and the dam gallery are easily accessible from the downstream toe. Sources and receivers were used in the reservoir immediately upstream of the dam by simply lowering them into the reservoir using a winch from the dam crest. As the source or receiver was lowered into the reservoir, it slid along the upstream dam face. Based on observations of the cable, there is no indication that it drifted significantly either upstream-downstream or laterally as it was lowered and raised. Hence, these tools likely stayed within inches of the upstream dam face.

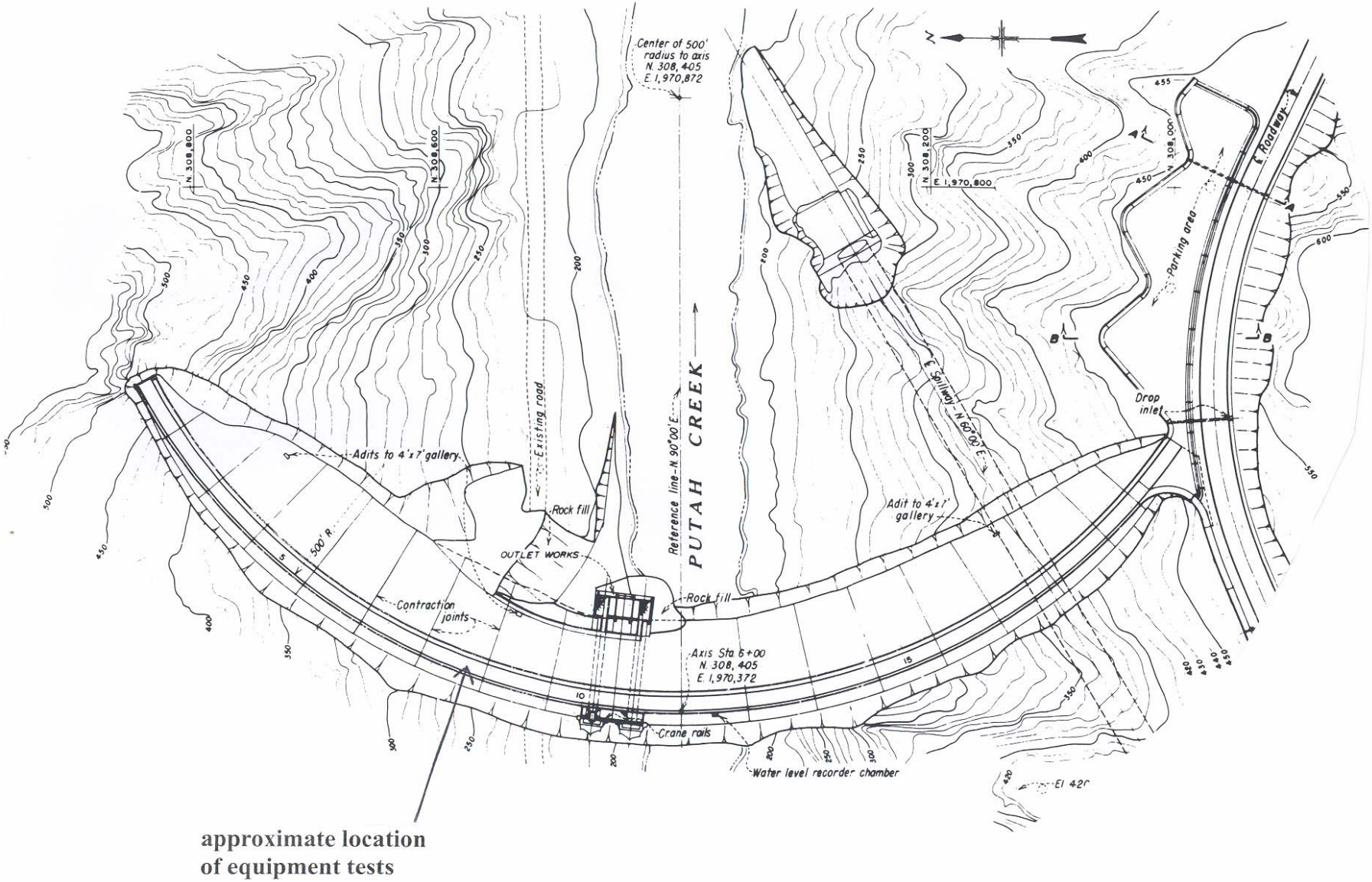


FIGURE 3-2: Plan map of Monticello Dam showing location of equipment tests conducted in May, 1997.

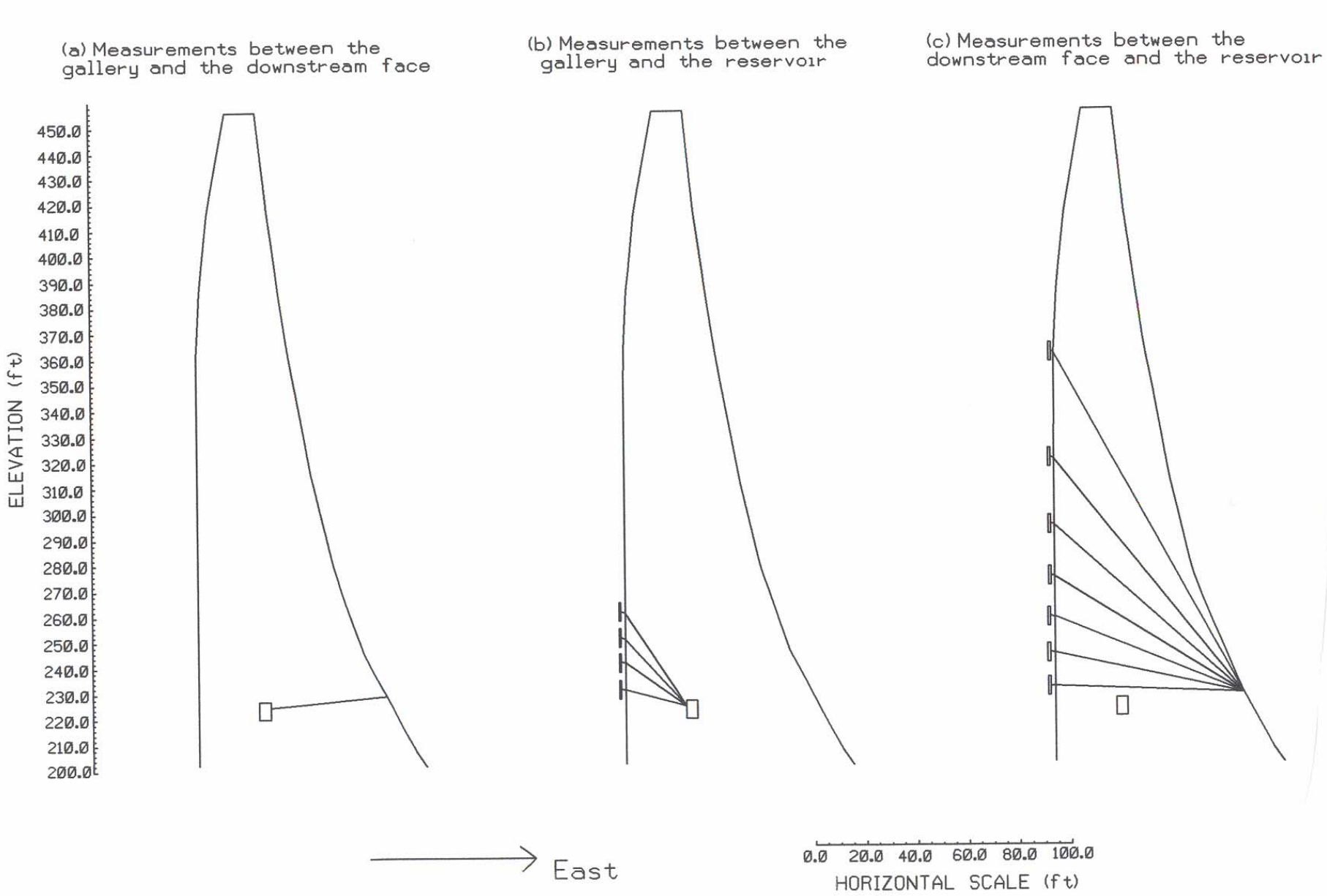


FIGURE 3-3: Data acquisition geometries used for equipment tests at Monticello Dam.

Because of limited time, not all types of sources and receivers were tested for each of the three geometries described above. The sources and receivers tested using each geometry are discussed as the field data are presented in Sections 5 and 7.

# 4.0 SOURCES AND RECEIVERS TESTED

The following sources were tested:

1. The piezoelectric transmitter described in Section 3.1. This source was only successfully used for the laboratory tests on the concrete block. Electronic problems and insufficient source strength hampered its use for the field testing.

2. A magnetorestrictive sonic logging source with a center frequency of about 15 kHz. This tool was manufactured by Simplec. When the tool is operated, it pulses repetitively approximately 15 times each second.

3. Size “N” Schmidt concrete test hammer (impact energy of 0.225 mkg), manufactured by Forney.

4. Size “M” Schmidt concrete test hammer (impact energy of 3 mkg), manufactured by Forney. This test hammer and the smaller version list above (#3) contain spring-loaded pistons that directly impact the concrete surface on which they are used.

5. Nail gun powered by 22 mm shot, with piston hitting steel plate bolted onto concrete. The type of nail gun used is triggered by applying a manual hammer hit to the back of the gun.

The following surface receivers were tested:

1. Piezoelectric accelerometer from Wilcoxon Research, Model No.736. Vertically-polarized; mounted resonant frequency: 52 kHz; sensitivity: 104 mV/g; cost: $345

2. Piezoelectric accelerometer from PCB Piezotronics, Inc., Model No. 353B17. Vertically-polarized; resonant frequency: 81 kHz; sensitivity: 10.5 mV/g; cost: $275

3. Piezoceramic accelerometer from Oceana Sensor Technologies,

Inc., Model No. A8000. Vertically-polarized; mounted resonant frequency: >20 kHz; sensitivity: 858 mV/g; cost: $99

4. Flat disk piezoelectric transducer from JODEX Applied Geoscience Limited. Resonant frequency and sensitivity: unknown; Cost: See #6 below.

5. Sensor #4 above, stiffened by epoxying a quarter to one side of the sensor. The modification, also done by JODEX, was intended to increase the resonant frequency of the receiver. Resonant frequency and sensitivity: unknown; Cost: See #6 below.

6. Sensor #5 above, further modified by JODEX by adding an amplifier. Resonant frequency and sensitivity: unknown The combined cost of developing sensors 4, 5, and 6 (2 of each), including materials and labor, was approximately $2300.

7. Flat disk piezoelectric transducer, removed from tweeter purchased at Radio Shack. Frequency range: 4 to 25 kHz, resonant frequency unknown; sensitivity: unknown; cost of tweeter: $5; approximate additional cost to wire sensor (approximately one half-hour staff time): $35.

8. Piezoelectric sensor built by Matrix-5 Technologies consisting of a rectangular piezoelectric crystal and an inertial mass between 2 alluminum plates. Frequency response and sensitivity: unknown; Approximate cost to design and build receiver: $260

Complete specifications for the accelerometers tested are included in Appendix A. The different types of sensors are sometimes referenced by the index numbers listed above in later sections of the report.

# 5.0 COMPARISON OF SURFACE RECEIVERS

We did not have access to a high-frequency shake table for testing various types of receivers. Therefore, the responses of the receivers were solely evaluated by analyzing data acquired on the 5-ft laboratory concrete block and at Monticello Dam.

## 5.1 Laboratory Tests

Each of the eight receivers listed in Section 4 above were tested on the concrete block. The piezoelectric source transducer

described in Section 3.1 was mounted on one side of the concrete block, 15 inches from the top of the block and 12 inches from one of the faces containing the corehole (See Section 3.1). Each receiver being tested was sequentially mounted on the opposite side of the block, within a two-inch area directly across from the source. (Not all receivers could be placed at exactly the same position, for reasons related to mounting techniques. Mountings are discussed below.) The responses presented here were recorded on the same day to minimize variations due to slight differences in source mounting or background noise.

Because of differences in the physical characteristics of the sensors tested, all sensors could not be mounted in the same manner. The Wilcoxon and PCB accelerometers were stud-mounted using a 1/4-inch steel masonry anchor bolt placed in the concrete block directly across from the source. (Sketches of these mountings are presented in Section 6, Figure 6-4). The accelerometer from Oceana does not have a mounting bolt or threaded hole built into its housing. For these tests it was epoxyed onto an alluminum block, and the alluminum block was then bolted onto the concrete surface using the same anchor used for the other accelerometers. The piezoelectric transducer from Matrix-5 Technologies (sensor #8) was also threaded onto this same masonry anchor bolt. The remaining piezoelectric transducers could not be stud-mounted. They were coupled to the concrete surface using silicon grease. These sensors were placed within two inches of the anchor used to mount the other receivers.

For each receiver, the averaged time and frequency responses from 20 transmitter firings were recorded on the frequency analyzer. (Averaging is performed by the frequency analyzer after each source activation.) The frequency spectrum presented below for each receiver is the magnitude of the Fourier transform of the entire recorded waveform.

The time responses of the three sensors constructed by JODEX, sensors 4, 5, and 6, are shown in Figure 5-1, and the corresponding frequency responses are presented in Figure 5-2. Significant background noise is seen on the responses from all of these sensors before the P-wave arrival at approximately 0.38 ms. Some of this noise is electromagnetic crossfeed. The signature of the source excitation itself is seen on the responses (at time 0 ms) and has a larger amplitude than the direct P wave. Strong electromagnetic crossfeed of the source excitation occurred on all of the piezoelectric transducers tested. This crossfeed could not be eliminated by grounding. The high-frequency signal at the beginning of the response from sensor #5 (time -0.5 ms, Figure 5-1b), which also

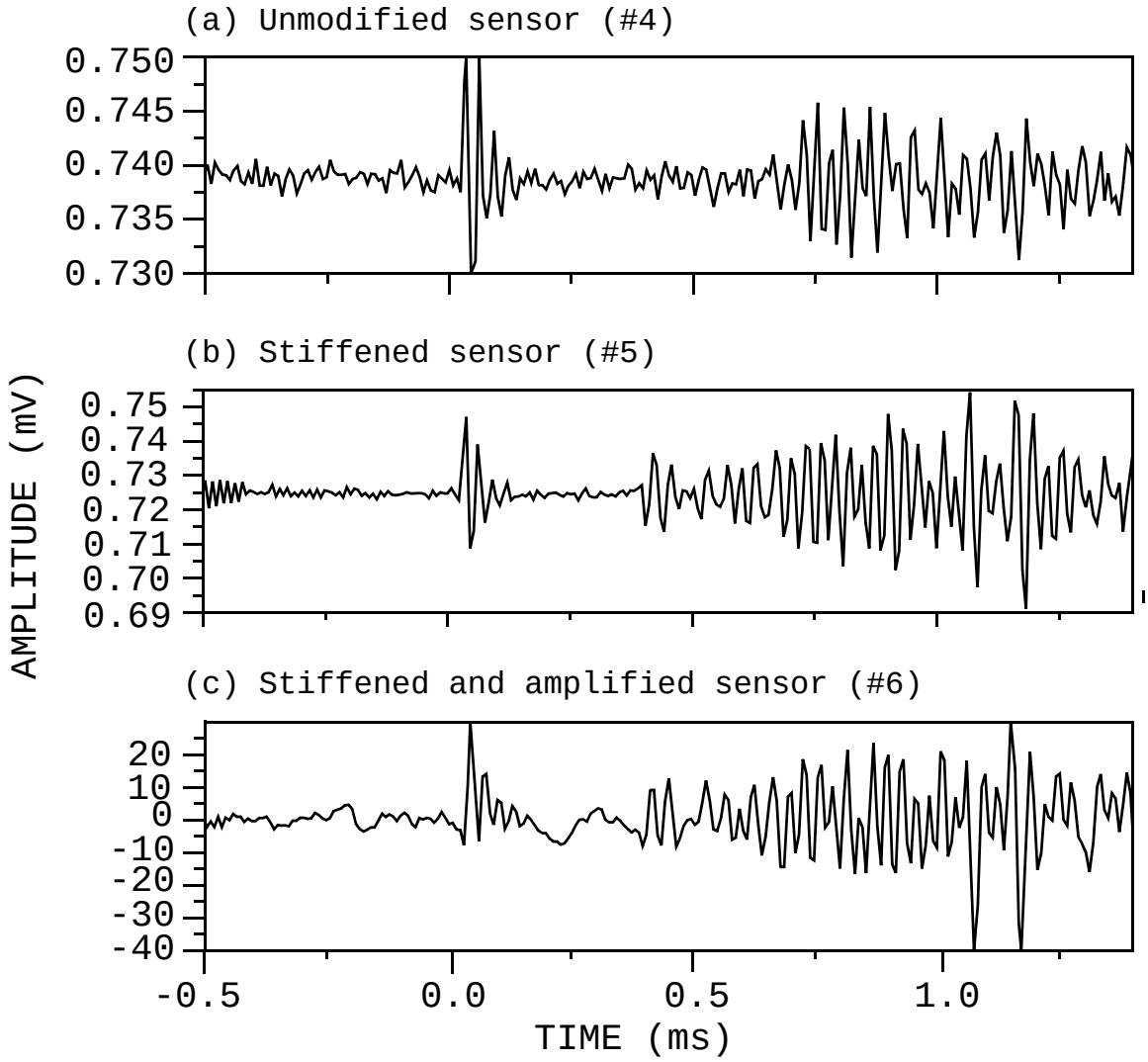


FIGURE 5-1: Time responses of the piezoelectric transducers from JODEX Applied Geoscience (sensors #4, #5, and #6) measured during the laboratory tests.

occurs on some of the other responses presented later, is believed to be related to something within the circuitry of the frequency analyzer that occurs when recording begins. Although not well understood, it was not of concern during these tests since it dies out before the onset of the P-wave arrival.

Stiffening the receiver by gluing a quarter to one side of the piezoelectric sensor changes the data in two ways. The signal-to-noise ratio improves (compare Figure 5-1b to Figure 5-1a), and the relative response to higher frequencies increases (Figure 5-2a and b). The improvement in the signal-to-noise ratio may be largely due to better coupling of the modified sensor to the concrete surface. The unmodified sensor has a ridge around its edge that

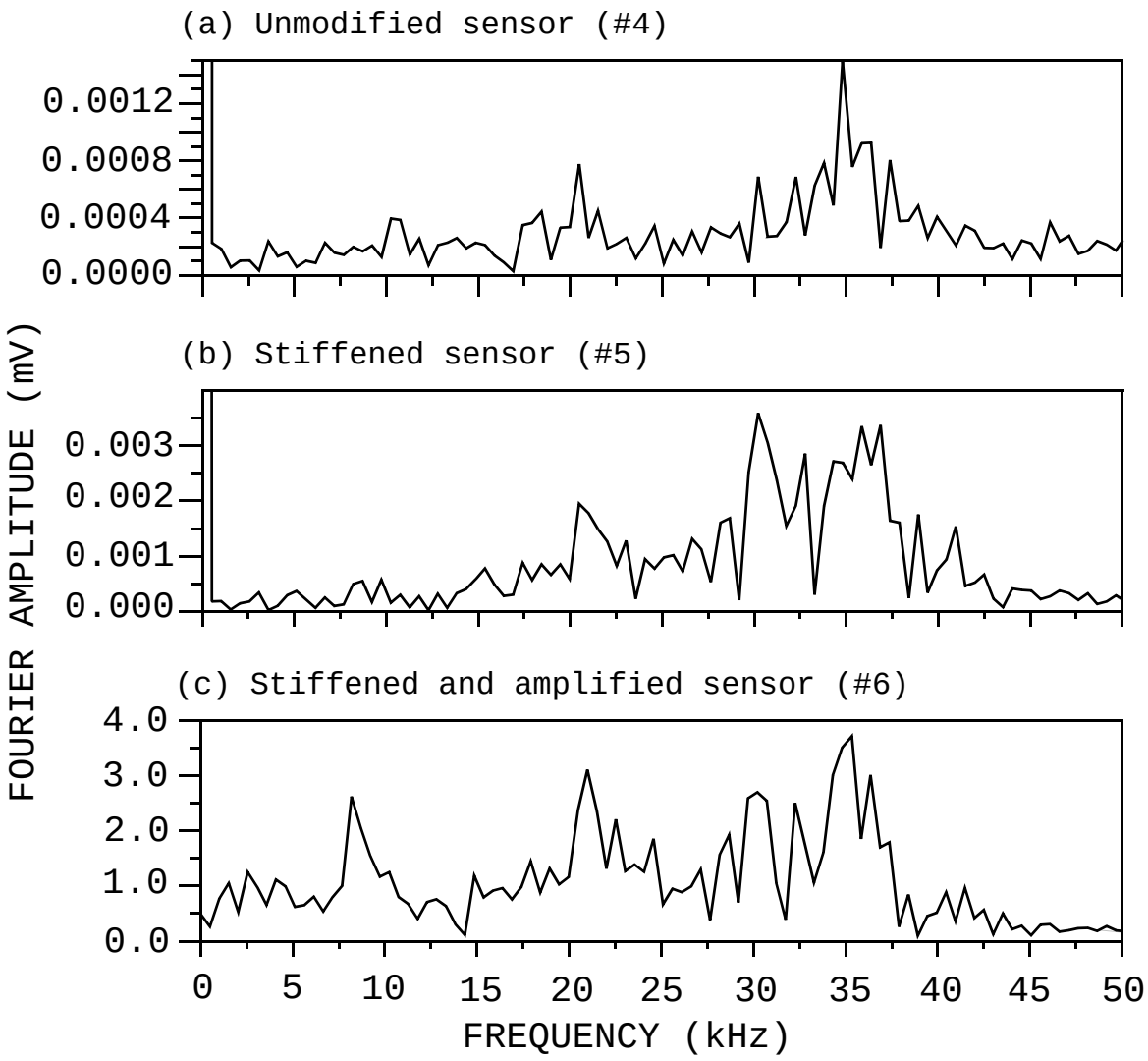


FIGURE 5-2: Frequency responses of the piezoelectric transducers from JODEX Applied Geoscience (sensors #4, #5, and #6) measured during the laboratory tests.

makes it difficult to mount flush with the surface (a lot of silicon grease had to be used between the concrete and the sensor), whereas the quarter mounts much more securely against the concrete face. The change in the frequency response of the modified sensor is presumably due to increasing the stiffness of the sensor.

The change in the frequency response of the modified sensor can be most easily seen by examining the ratio of the individual frequency responses of the modified and unmodified sensors. The individual frequency responses were smoothed, and then the smoothed response of the sensor with the quarter (sensor #5) was divided by the smoothed response of the unmodified sensor (sensor #4). The result

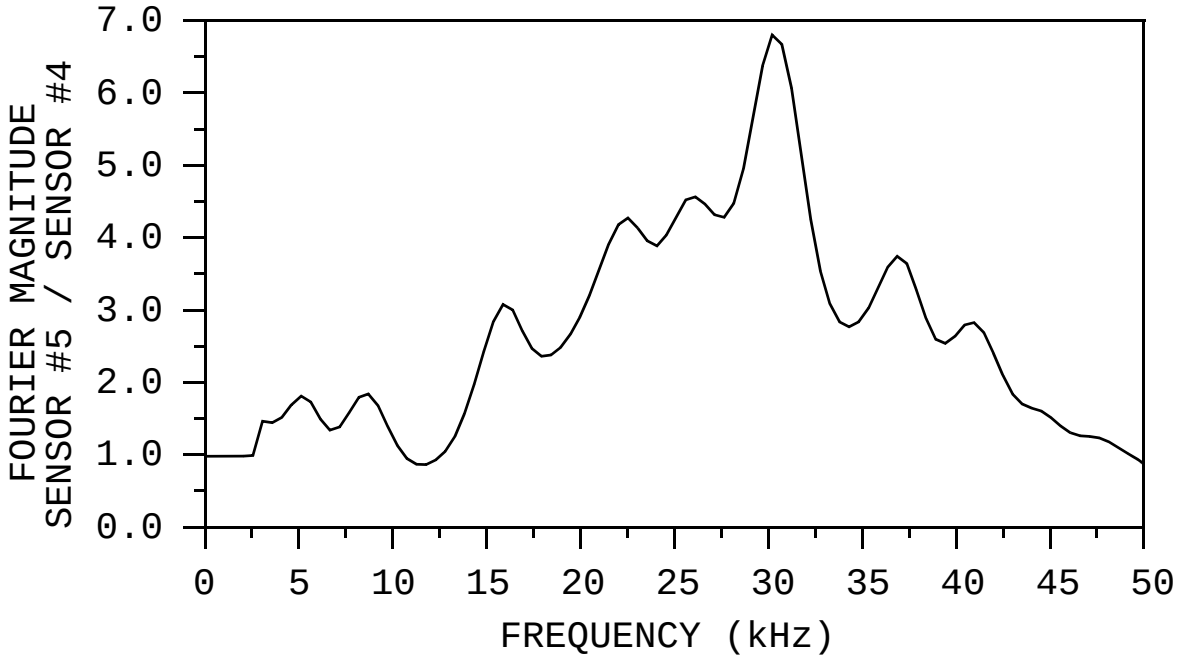


FIGURE 5-3: Ratio of the frequency spectrum of the stiffened JODEX sensor (#5) to the frequency spectrum of the unmodified JODEX sensor (#4), computed from the laboratory data.

is presented in Figure 5-3. It clearly shows that the relative response to frequencies above about 15 kHz has been increased. The maximum increase in response occurs at approximately 30 kHz.

The third sensor from JODEX, sensor #6, has the same quarter backing as sensor #5 but also has an amplifier. The addition of the amplifier increases the overall amplitude of the seismic trace, but it also appears to increase the relative background noise level and alter the frequency response. (Compare Figures 5-1c and 5-2c, showing the response of the sensor with the amplifier, to Figures 5-1b and 5-2b, showing the unamplified sensor response.) The ratio of the smoothed frequency spectrum of the amplified sensor to that of the unamplified one is presented in Figure 5-4. It clearly shows that the relative content of frequencies between about 2.5 and 14 kHz has been increased by the amplifier.

The response of the piezoelectric sensor from Matrix-5 Technologies is shown in Figure 5-5. The seismic trace is overwhelmed by a large response at about 2.5 kHz. It also exhibits strong crossfeed of the source excitation (at 0 ms), and contains the transient response from the frequency analyzer at the beginning of the record (-0.5 ms). Despite these significant flaws, the response of this sensor shows the least background seismic noise and the clearest

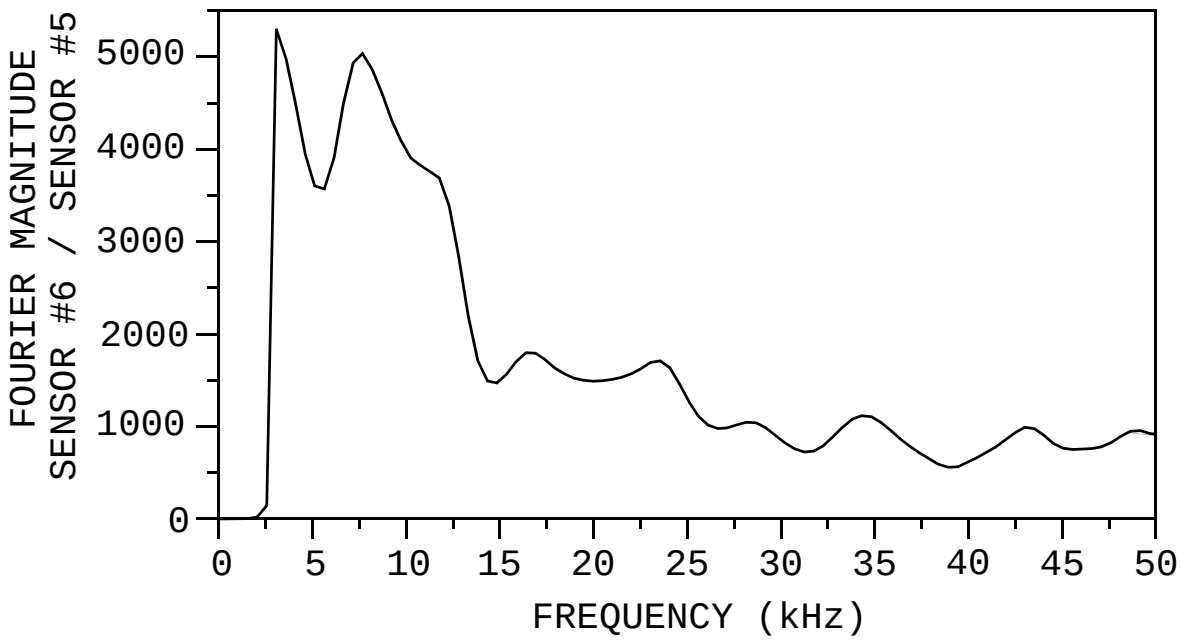


FIGURE 5-4: Ratio of the frequency spectrum of the amplified stiffened JODEX sensor (#6) to the frequency spectrum of the unamplified stiffened JODEX sensor (#5), computed from the laboratory data.

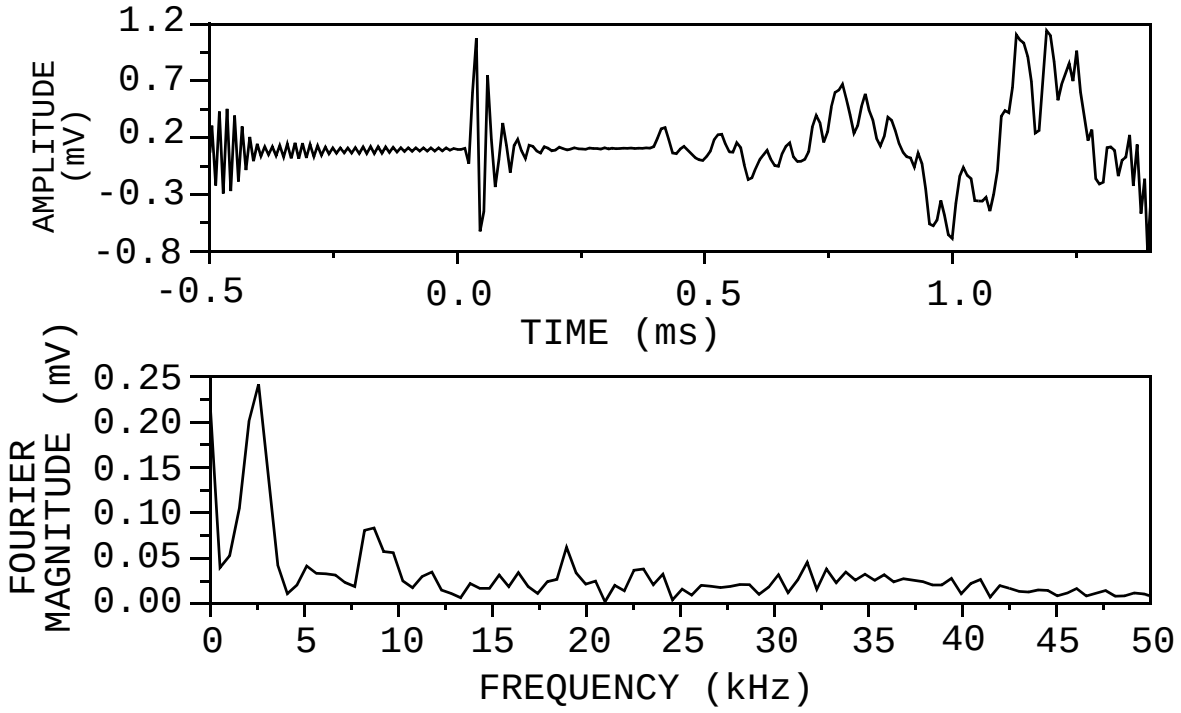


FIGURE 5-5: Time and frequency response of the piezoelectric transducer from Matrix-5 Technologies (sensor #8) measured during the laboratory tests.

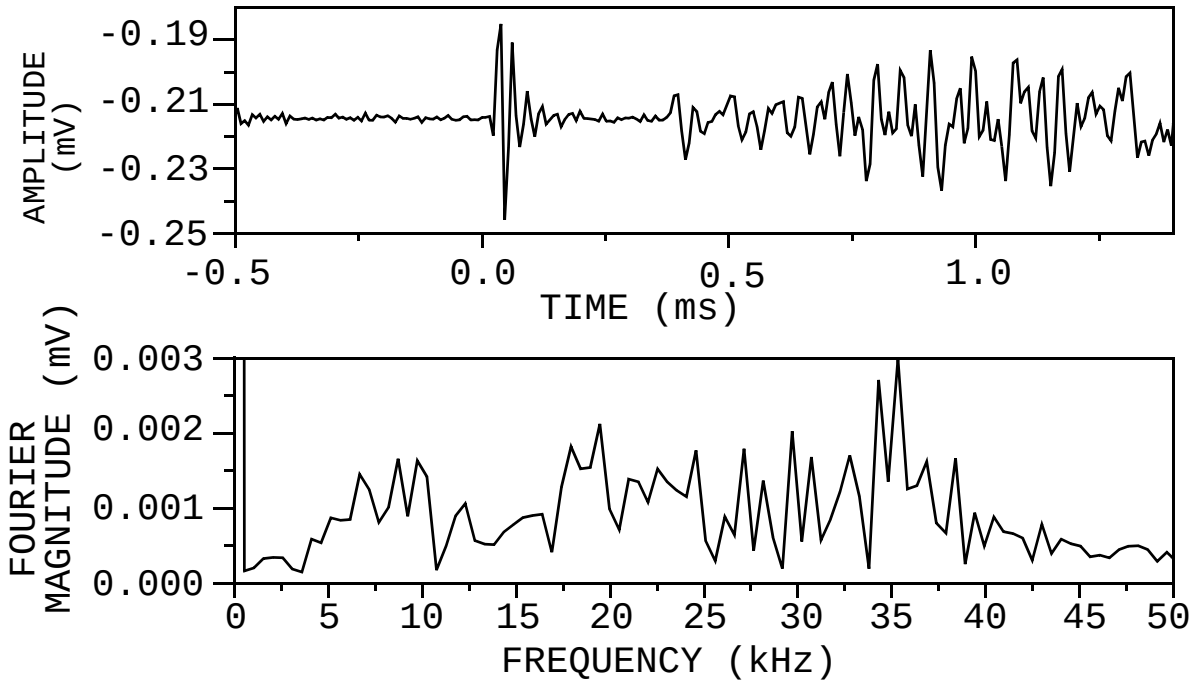


FIGURE 5-6: Time and frequency response of the piezoelectric transducer from the Radio Shack tweeter (sensor #7) measured during the laboratory tests.

first break of all of the piezoelectric transducers tested. The relatively good signal-to-noise ratio of this receiver could be related to the coupling, since it is bolt-mounted.

The tweeter piezo purchased at Radio Shack exhibits the broadest range of frequencies of the five piezoelectric transducers tested (Figure 5-6). Its response shows strong crossfeed of the source excitation and moderate signal-to-noise ratio.

The time responses of the three accelerometers are shown in Figure 5-7, and the corresponding frequency responses are presented in Figure 5-8. The most obvious differences between the responses of the accelerometers and the piezoelectric transducers is the lack of any crossfeed of the source excitation, and the much better ratio of signal to noise. The improved signal-to-noise ratio may be related to both the bolt mounting of the accelerometers and their lack of electrical crossfeed problems.

The accelerometer responses do not show the variation in sensitivities that are stated in their calibrations. (The sensitivities are listed in Section 4 of this report). Approximate relative sensitivies of the accelerometers were computed by simply measuring the maximum peak-to-peak amplitude on each time record

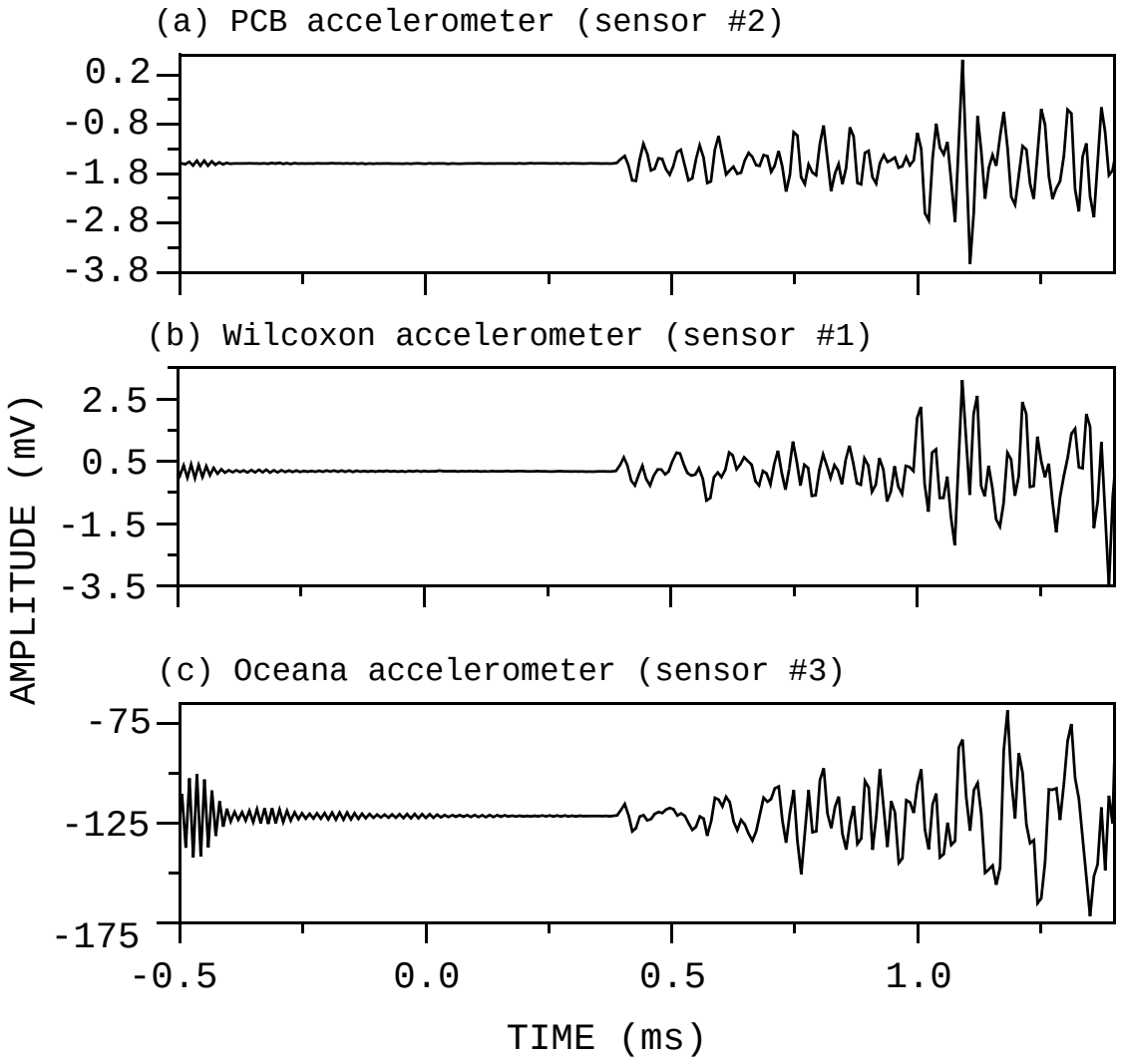


FIGURE 5-7: Time responses of the accelerometers measured during the laboratory tests.

shown in Figure 5-7. The Wilcoxon accelerometer (sensor #1) is stated to be 10 times more sensitive than the PCB accelerometer (sensor #2), but the data from this test indicate that the overall amplitude of the Wilcoxon response is only about 1.6 times the amplitude of the PCB response. Likewise, the Oceana accelerometer (sensor #3) is specified to be about 82 times as sensitive as the PCB accelerometer. However, the recorded waveform from the Oceana accelerometer only shows approximately 28 times the amplitude of the PCB waveform. The Oceana accelerometer should also be about 8 times as sensitive as the Wilcoxon accelerometer, but the results from this test show its overall amplitude to be about 17 times that of the Wilcoxon accelerometer.

According to their calibrations, the accelerometers from Wilcoxon

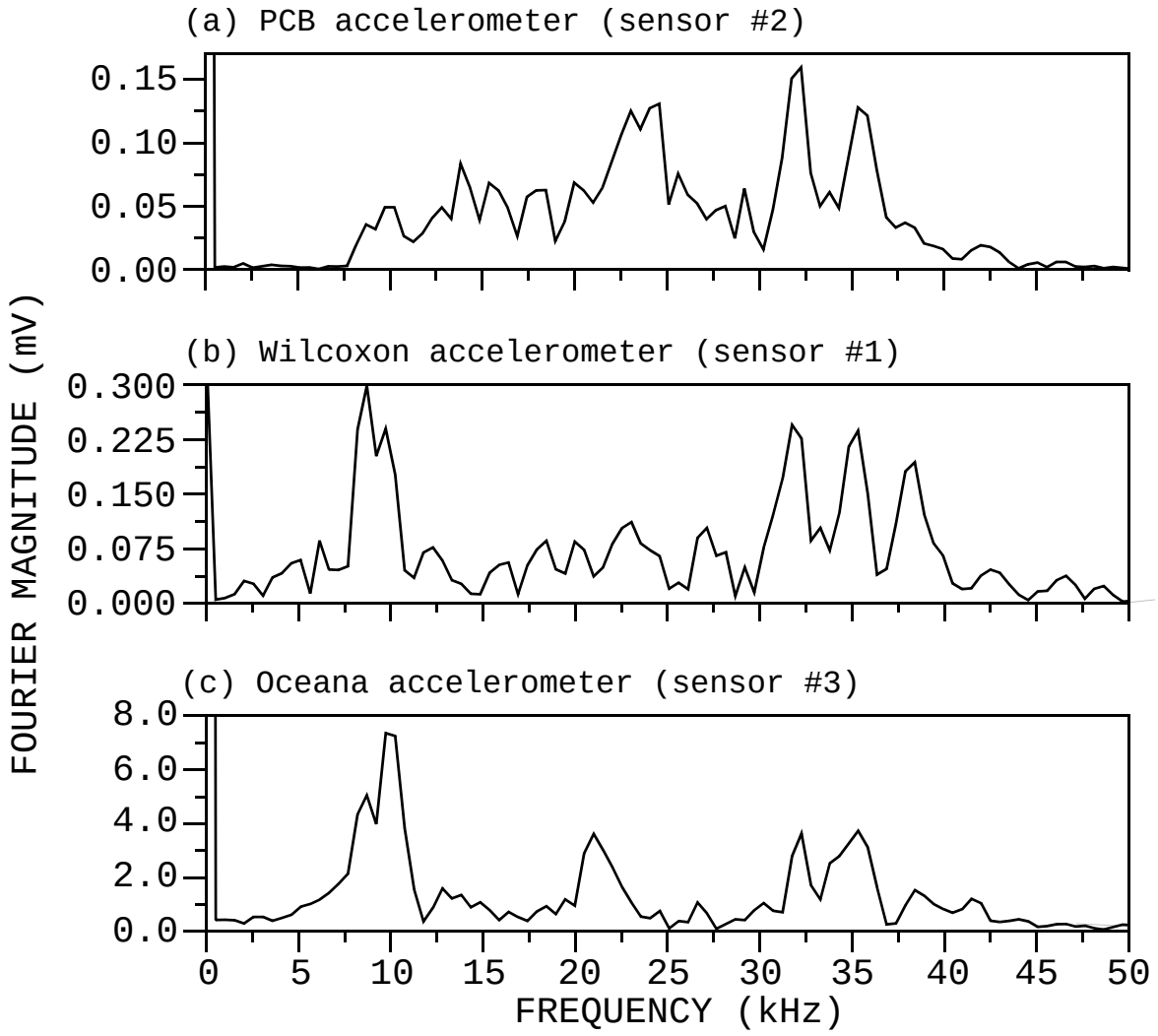


FIGURE 5-8: Frequency responses of the accelerometers measured during the laboratory tests.

and PCB have their resonances above 50 kHz. (The resonant frequency of each accelerometer is listed in Section 4.) Therefore, their response spectra should be fairly flat in the frequency band of these laboratory tests. Since they were mounted (sequentially) in exactly the same location (on the same anchor bolt), and since the source should be repeatable, their response spectra should be very similar (except for an overall change of scale due to different sensitivities). However, there are significant differences between their responses from these tests (Figure 5-8a and b). While their spectra both show peaks at about 32 and 35 kHz, the Wilcoxon accelerometer response also shows strong peaks at about 9 and 38 kHz. The PCB response contains an additional peak at 24 kHz, but is relatively flat otherwise. The spectrum of the Oceana accelerometer exhibits some similarities to the spectra of both of

the other two accelerometers. (The peak at about 21 kHz may be its resonance response.) The differences between the responses of the three accelerometers indicate that not all of them are exhibiting a flat frequency response for these tests. Differences between the frequency responses of the accelerometers were better understood after completing the field tests described below.

## 5.2 Field Tests

Some of the tests conducted at Monticello Dam involved lowering a sonic logging tool source into the reservoir from the dam crest and sequentially recording data with various receivers mounted on the west wall of the gallery (Figure 3-3b). The sonic tool was lowered to a predetermined depth and then kept in a fixed position as the data were recorded. Receivers were mounted within six inches of each other on the gallery wall. The piezoelectric transducers were coupled to the concrete wall using silicon grease, and the accelerometers were bolt-mounted using a 1/4-inch masonry anchor bolt.

Data were simultaneously recorded in the time and frequency domains with the frequency analyzer, using a sync signal from the sonic tool as the trigger. A recording delay time of -0.5 ms was used, so that some data were acquired before the source was fired (at time 0 ms). The time sampling interval is 7.63 us. Between 20 and 500 pulses from the sonic tool were averaged for each recorded response. (Averaging is performed by the frequency anlayzer after each trigger.) The number of averages used for each specific test is indicated in the figure captions. All frequency spectra presented below represent the magnitude of the Fourier transform of the entire recorded waveform.

Initially, data were acquired at what was believed to be a nearly horizontal ray path. The sonic tool was lowered to a depth of 230 feet below the top of the crest wall, and the receivers were mounted approximately 5 feet above the gallery floor. Upon returning to Denver, construction drawings were carefully reexamined. The ray angle from source to receiver was then recomputed to be 15.5 degrees below horizontal, and the source-receiver distance was computed as 24.4 feet.

The time responses from the stiffened unamplified and amplified sensors from JODEX (sensors #5 and #6), the transducer from the Radio Shack tweeter (sensor #7), and the accelerometer from PCB

Piezotronics (Sensor #2) are presented in Figure 5-9. As in the laboratory tests, the amplified sensor from JODEX (Figure 5-9b) exhibits much poorer signal-to-noise ratio than the corresponding unamplified sensor (Figure 5-9a). The Radio Shack tweeter (Figure 5-9c) exhibits almost as good signal-to-noise as the unamplified JODEX sensor. The accelerometer from PCB (Figure 5-9d) shows slightly lower signal-to-noise than either the Radio Shack tweeter or the unamplified JODEX sensor, but much better signal-to-noise than the amplified JODEX sensor.

The smoothed frequency responses for these sensors are shown in Figure 5-10. The data trace acquired with the accelerometer has the narrowest frequency spectrum, having a large peak centered at about 15 kHz (Figure 5-10d). Since a large peak at this frequency was not seen on the responses from this accelerometer during the laboratory tests (during which the same type of mounting was used), it is unlikely that this large 15 kHz response is due to a resonance associated with the accelerometer mounting. Barring any strong mounting effects, the PCB accelerometer should have a nearly flat frequency response over the frequency range examined during these tests. Furthermore, this sonic tool has a center frequency of about 15 kHz, consistent with the frequency spectrum of the data acquired with the accelerometer. Thus, the response of the PCB accelerometer shown in Figure 5-10d may be a fairly accurate representation of the seismic frequencies generated by the sonic tool and propagated through the dam.

Data acquired with the three piezoelectric transducers have frequency spectra that are significantly different from each other and from the accelerometer frequency spectrum. The frequency spectrum recorded with the tweeter transducer purchased at Radio Shack is similar to the spectrum recorded with the PCB accelerometer above approximately 14 kHz, having a peak at about 15.5 kHz (Figure 5-10c). At lower frequencies the two spectra diverge, and the frequency response from the Radio Shack receiver has another strong peak at 8.8 kHz. Neither of the frequency spectra recorded with the JODEX receivers have a peak at 15 kHz. The spectrum from the unamplified receiver shows a strong peak response between about 10.5 and 13 kHz (Figure 5-10a), whereas the spectrum from the amplified receiver contains a broad range of frequencies and a relatively minor peak at about 13 kHz (Figure 5-10b).

Additional data were acquired with the unamplified stiffened JODEX sensor (#5) and the PCB accelerometer at three different ray angles and corresponding source-receiver distances. These additional geometries were achieved by keeping the receivers fixed and raising

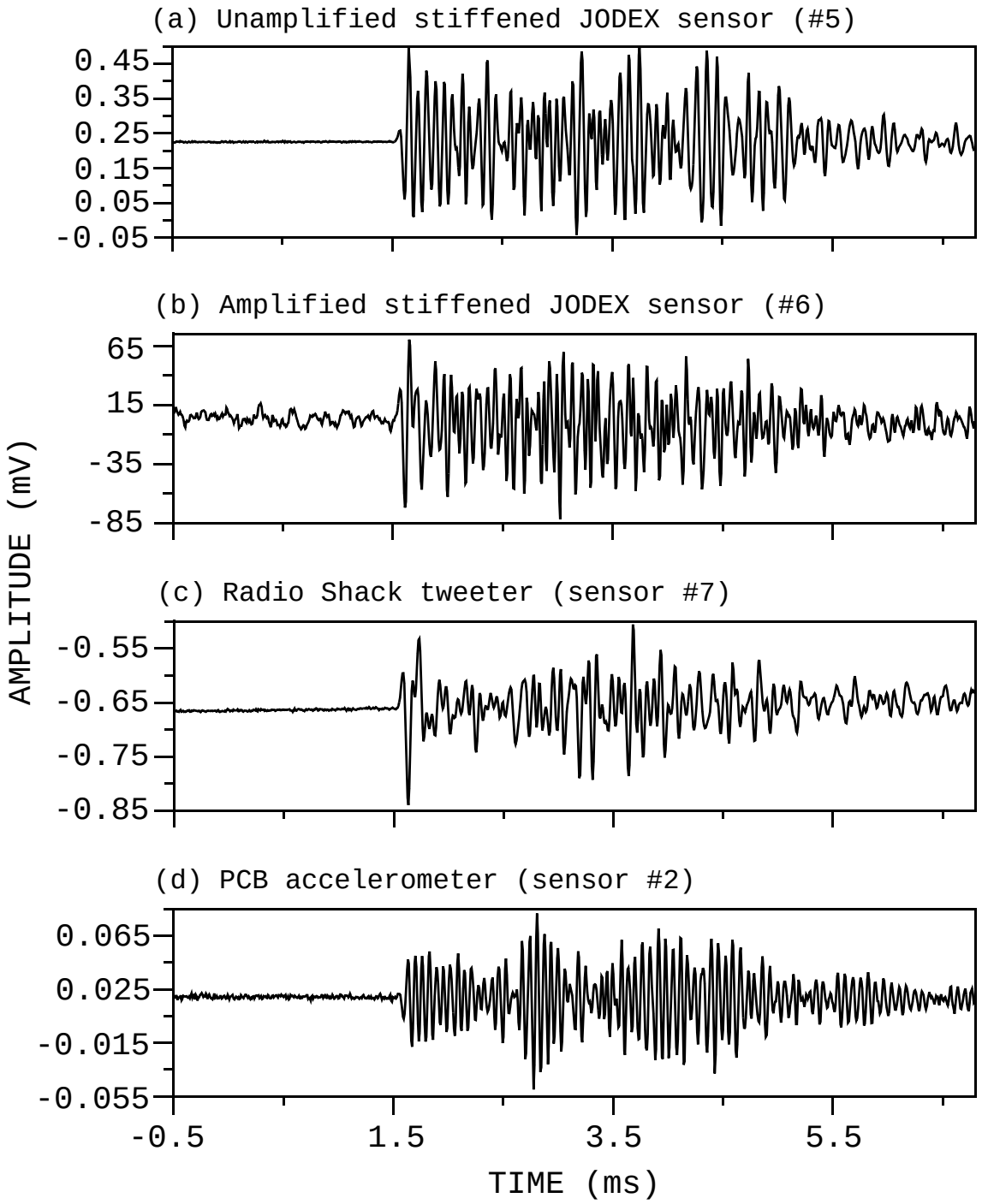


FIGURE 5-9: Time responses of three piezoelectric transducers and one accelerometer, recorded on the west gallery wall at Monticello Dam. The source was a sonic tool located in the reservoir. Each waveform represents the averaged response from 20 pulses of the sonic tool. The source-receiver separation was 24.4 feet, at an angle of 15.5 degrees from horizontal.

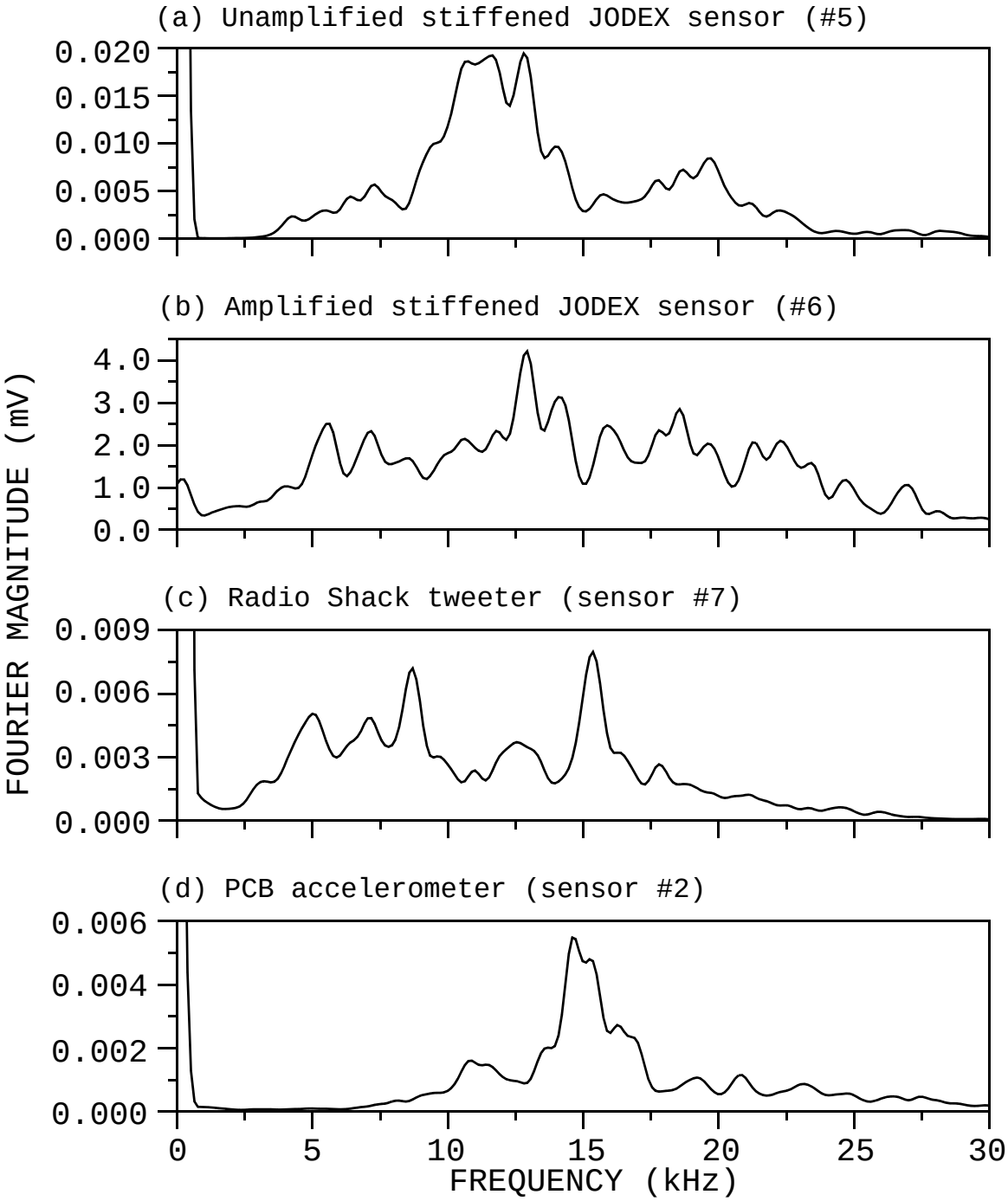


FIGURE 5-10: Frequency responses of three piezoelectric transducers and one accelerometer, recorded on the west gallery wall at Monticello Dam. The source was a sonic tool located in the reservoir. Each waveform represents the averaged response from 20 pulses of the sonic tool. The source-receiver separation was 24.4 feet, at an angle of 15.5 degrees from horizontal.

the sonic logging tool to depths of 220, 210, and 200 feet below the top of the crest wall (Figure 3-3b). The waveforms from the JODEX sensor are shown in Figure 5-11, and those from the PCB accelerometer are shown in Figure 5-12. The corresponding frequency spectra for these data sets are presented in Figure 5-13.

Figures 5-11 and 5-12 show that, although the piezoelectric transducer exhibits better signal-to-noise ratio than the accelerometer at a low ray angle (Figures 5-11a and 5-12a), the signal-to-noise ratios recorded by the two sensors are comparable at larger ray angles. Also, as the signal level becomes smaller with increasing source-receiver separation, the data from the piezoelectric transducer become noticeably affected by 60 Hz electrical crossfeed. This crossfeed is seen as the low-frequency signal superimposed on the data in Figure 5-11c and d. Strong 60-Hz electromagnetic energy is produced by a hydroelectric power plant located at the downstream toe of Monticello Dam, just outside the main gallery entrance.

The frequency spectra of the accelerometer data are consistent at all ray angles (Figure 5-13b). As the ray angle and source-receiver distance increases, the peak frequency generally decreases very slightly and the highest frequencies (above 20 kHz) are severely attenuated. Stronger attenuation of higher frequencies relative to lower frequencies is a characteristic effect of intrinsic attenuation. In contrast, the data from the JODEX piezoelectric transducer show inconsistent frequency patterns (Figure 5-13a). The frequency variations with changing ray angle and source-receiver separation are so dramatic that they can easily be seen in the time domain (Figure 5-11). The data from this sensor show frequency variations that are not consistent with attenuation effects. These data suggest that either the frequency response of this sensor varies with angle of incidence, or that the response is so variable with frequency that small changes in the frequency content of the incoming seismic waves results in large changes in the frequency content of the recorded data.

Seismic data were also acquired at Monticello Dam between the east gallery wall and downstream face (Figure 3-3a), using two sizes of Schmidt hammers and a nail gun powered by a 22 mm shot as sources. The sources were used inside the gallery, and the receivers were mounted on the downstream face. The distance between source and receiver was about 45 feet, and the angle of the direct raypath from source to receiver was about 5.5 degrees above horizontal. An accelerometer was bolt-mounted on the gallery wall, within 2 feet of the source. The response from this accelerometer was used to

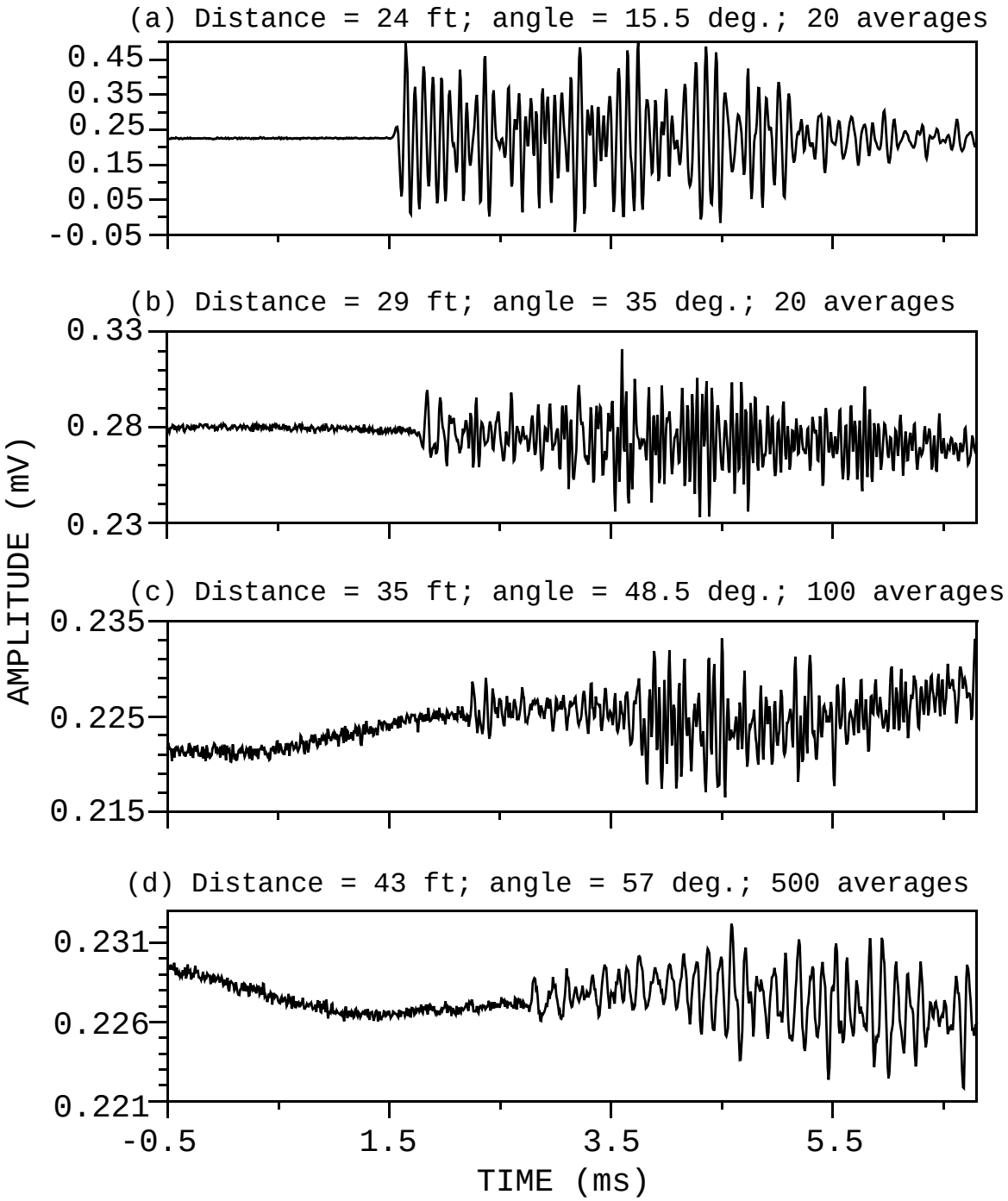


FIGURE 5-11: Data acquired using the sonic logging tool as a source in the reservoir and the unamplified stiffened JODEX sensor (sensor #5) as a receiver on the west gallery wall at Monticello Dam. Each plot contains data recorded with the sonic tool at a different depth in the reservoir. The approximate distance between the source and receiver, ray angle from horizontal, and the number of sonic tool pulses averaged for each response is labeled on each plot.

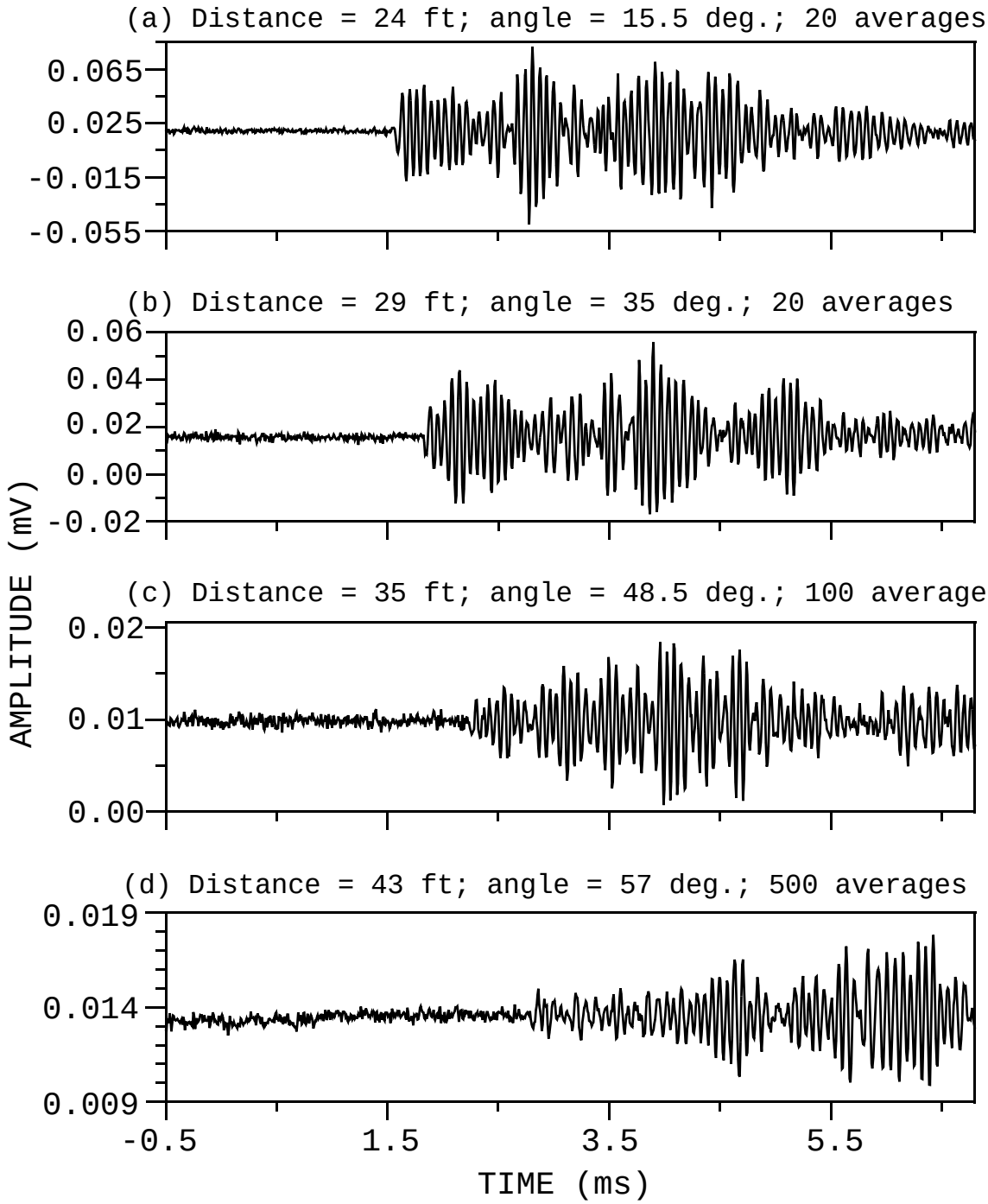


FIGURE 5-12: Data acquired using the sonic logging tool as a source in the reservoir and the PCB accelerometer (sensor #2) as a receiver on the west gallery wall at Monticello Dam. Each plot contains data recorded with the sonic tool at a different depth in the reservoir. The approximate distance between the source and receiver, ray angle from horizontal, and the number of sonic tool pulses averaged for each response is labeled on each plot.

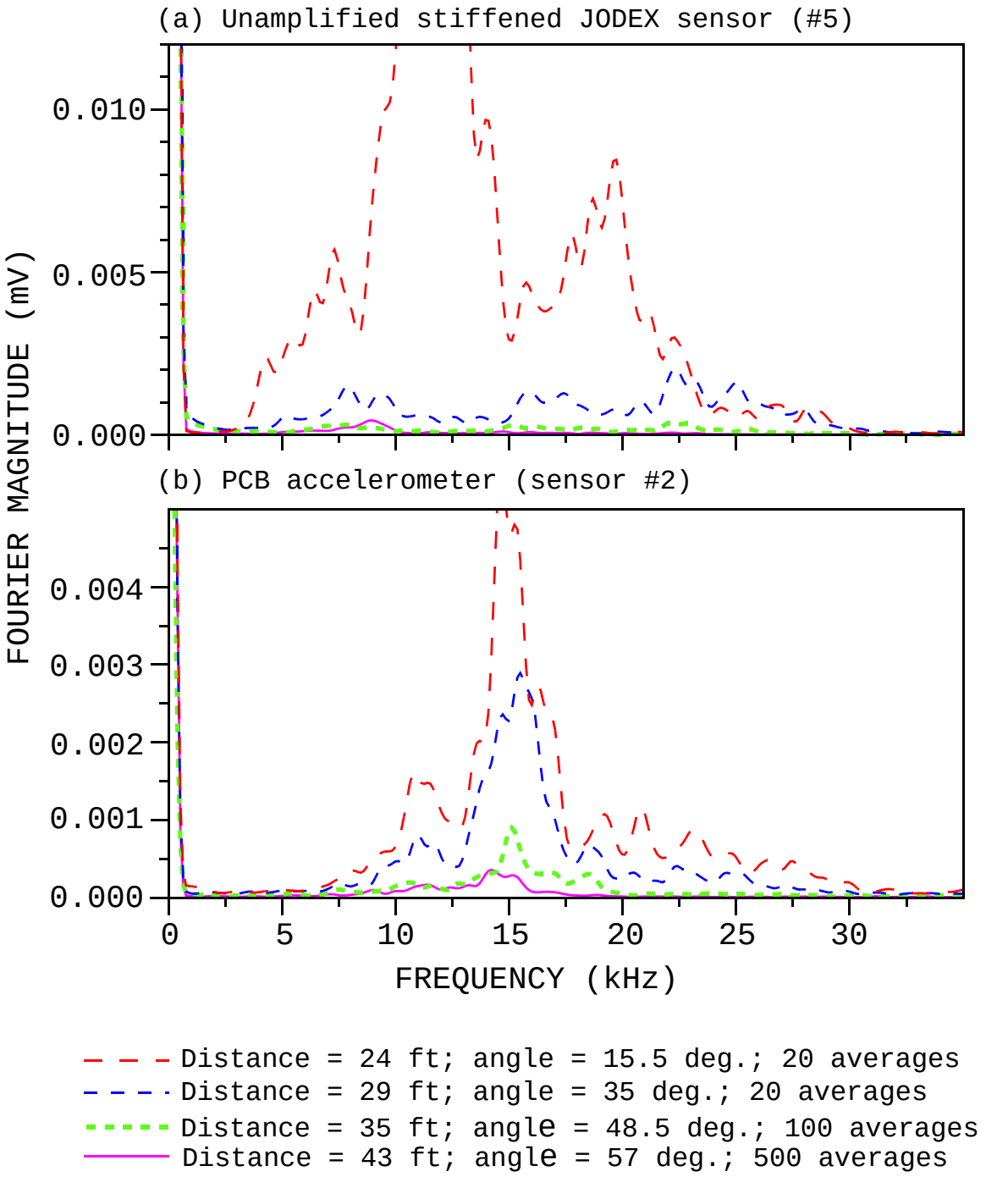


FIGURE 5-13: Frequency spectra of data acquired using the sonic logging tool as a source in the reservoir and two types of receivers on the west gallery wall at Monticello Dam. Each plot contains data recorded with one type of receiver for multiple source depths. The approximate distance between the source and receiver, ray angle from horizontal, and the number of sonic tool pulses averaged for each response is given in the legend.

trigger the frequency analyzer during data acquisition. A recording delay time of -0.5 ms was used, so that some data were acquired before the source was activated (at time 0 ms). The time sampling interval is 15.3 us. Each recorded trace represents a single source activation (i.e, the data were not stacked or averaged). Each receiver response was recorded separately, using a different source activation.

During these tests, responses from the three accelerometers were measured. Measurements were not completed with the piezoelectric transducers because of 60-Hz electromagnetic crossfeed problems (from the nearby power plant) and lack of time. The PCB and Wilcoxon accelerometers were stud-mounted using a 1/4-inch masonry anchor bolt. The Oceana accelerometer was removed from its alluminum mounting block used during the laboratory tests. A 1/4-inch nut was glued to the bottom of the accelerometer housing 6 days before these tests were performed. The accelerometer was directly threaded onto the anchor bolt placed in the downstream face of the dam. The same masonry anchor was used repeatedly for all three accelerometer mountings.

Time and frequency responses recorded by the three accelerometers using the small Schmidt ("N") hammer as a source are presented in Figures 5-14 and 5-15, respectively. (The seismic energy at the beginning of the waveform from the Wilcoxon accelerometer is from another source activation immediately before the trigger. It should be ignored.) The variation in frequency content between the three responses is striking. The PCB accelerometer shows the highest frequency response, with a peak frequency at 11.5 kHz. The Wilcoxon accelerometer shows an intermediate response, with a peak frequency at about 7.1 kHz. The accelerometer from Oceana shows the lowest frequency response, with a peak frequency response at only 2.2 kHz.

Similar trends are seen in data acquired with these three accelerometers using the large Schmidt ("M") hammer and nail gun sources, as well as data acquired between the reservoir and west gallery wall with the sonic logging tool source. The frequency responses from all of these data sets are compared in Figure 5-16. (The response spectra from the laboratory tests are included on these plots for later discussion.) Because of different source strengths and propagation distances, the responses for different data sets have significantly different magnitudes, even when recorded by the same receiver. In Figure 5-16, each frequency spectrum was individually scaled by simply multiplying the spectrum values by a constant scaling factor. This scaling allows the shapes of the frequency spectra to be easily compared on the same plot.

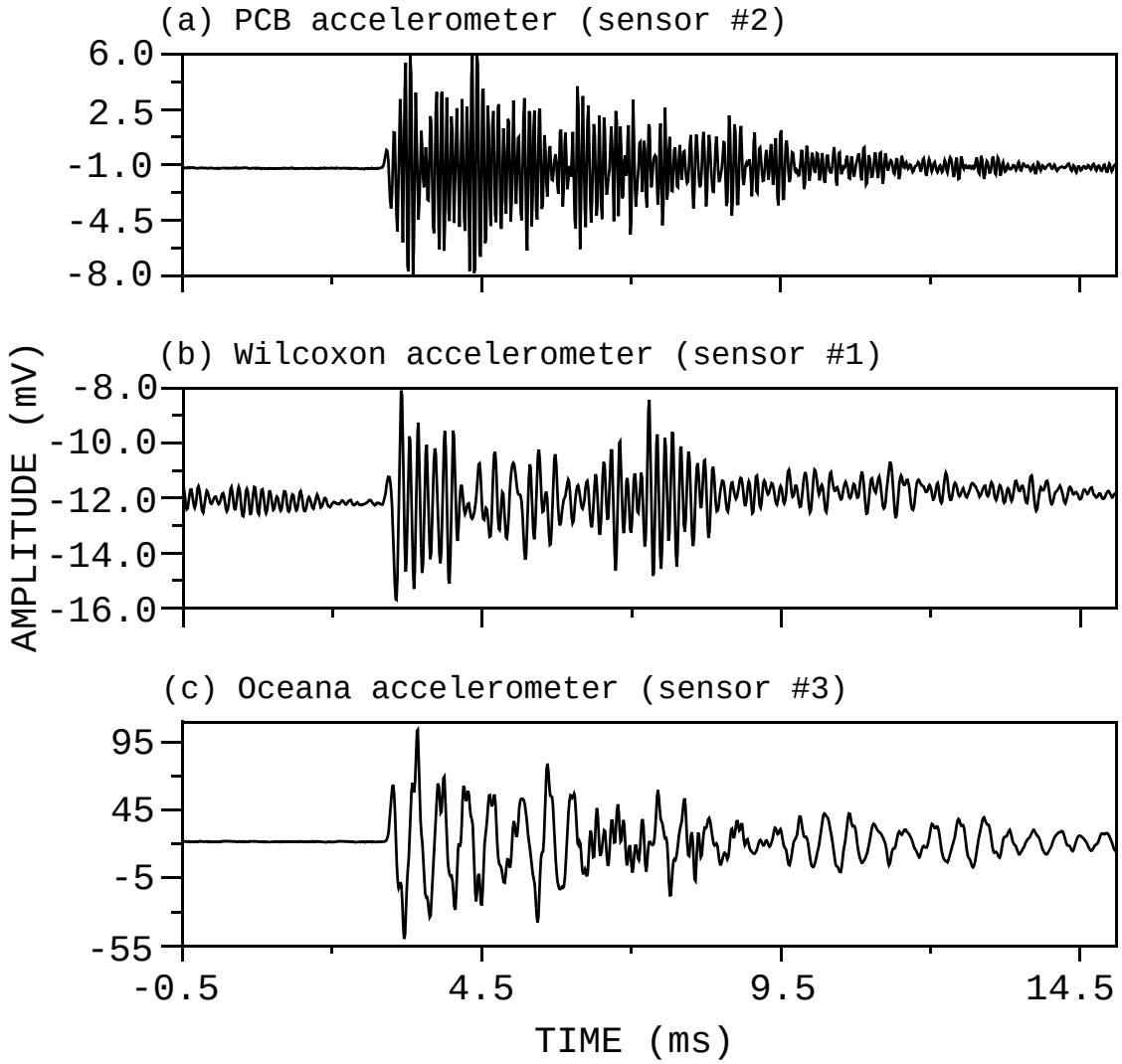


FIGURE 5-14: Time responses recorded with three accelerometers mounted on the downstream face of Monticello Dam. The small Schmidt ("N") hammer was used as the seismic source, on the east gallery wall. The ray path length was 45 feet, and the ray angle was about 5.5 degrees from horizontal. Each waveform represents a single source activation.

The scaling factor used for each data set is given in the legend of Figure 5-16. As can be seen from the figure, data acquired with the accelerometer from PCB consistently contain the highest frequencies, while the data acquired with the Wilcoxon and Oceana accelerometers are dominated by lower frequencies.

Two of the data sets recorded with the Wilcoxon accelerometer have some significant deficiencies. The wire connections were loose during the acquisition of the sonic tool data, resulting in extremely low signal-to-noise ratio of the acquired data. The input range

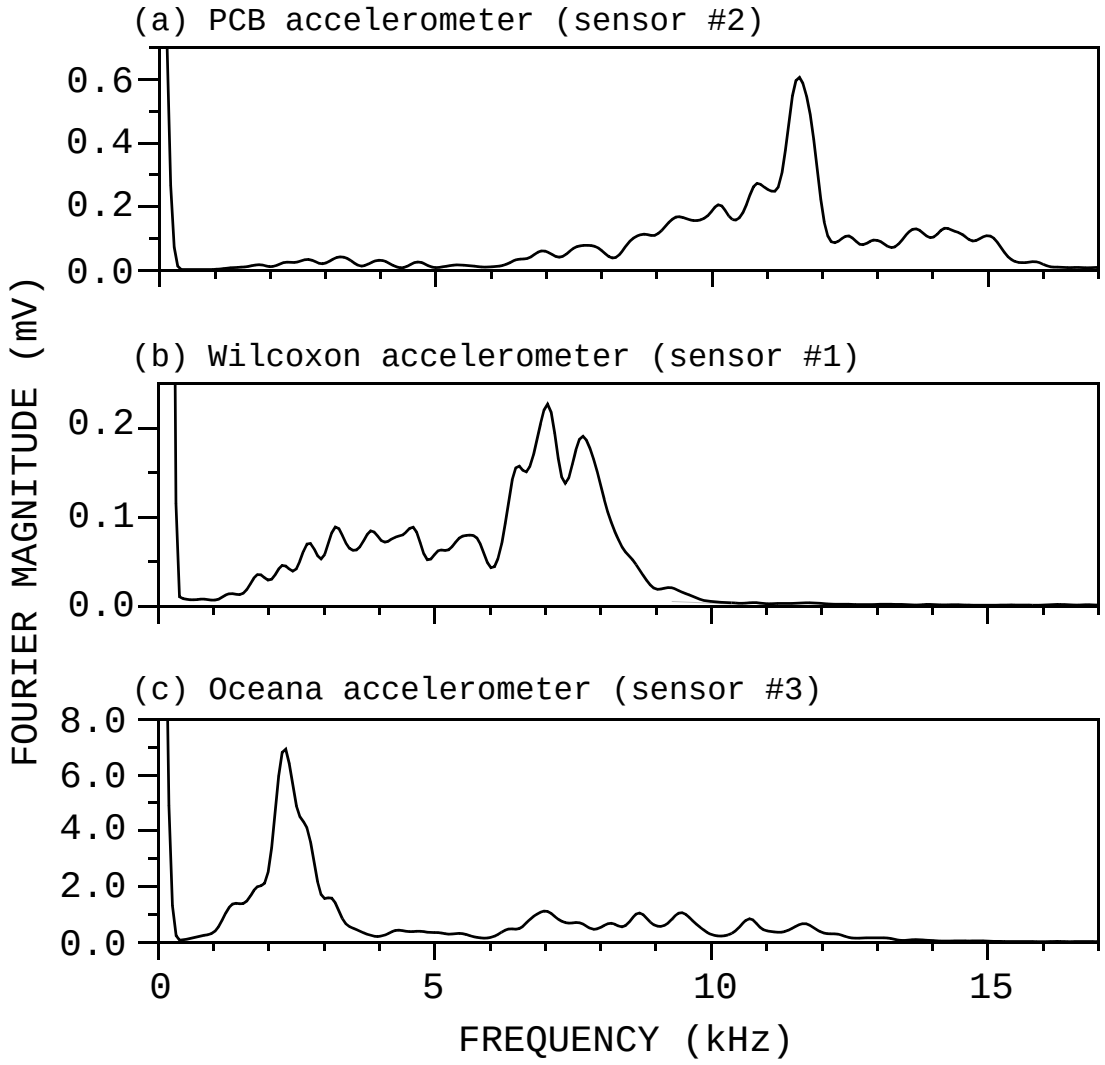


FIGURE 5-15: Frequency responses recorded with three accelerometers mounted on the downstream face of Monticello Dam. The small Schmidt ("N") hammer was used as the seismic source, on the east gallery wall. The ray path length was 45 feet, and the ray angle was about 5 degrees from horizontal. Each waveform represents a single source activation.

on the frequency analyzer was set too low during acquisition of the nail gun data, resulting in significant clipping of the data. This clipping may be causing the harmonic seen at 15 kHz.

Despite these deficiencies, the data recorded with the Wilcoxon accelerometer clearly show a consistent trend. At least below 30 kHz, the data are consistently dominated by frequencies between 7 and 10 kHz, regardless of the source used or the distance the energy traveled (Figure 5-16b). This is true even of the data acquired in the laboratory on the concrete block using the piezoelectric

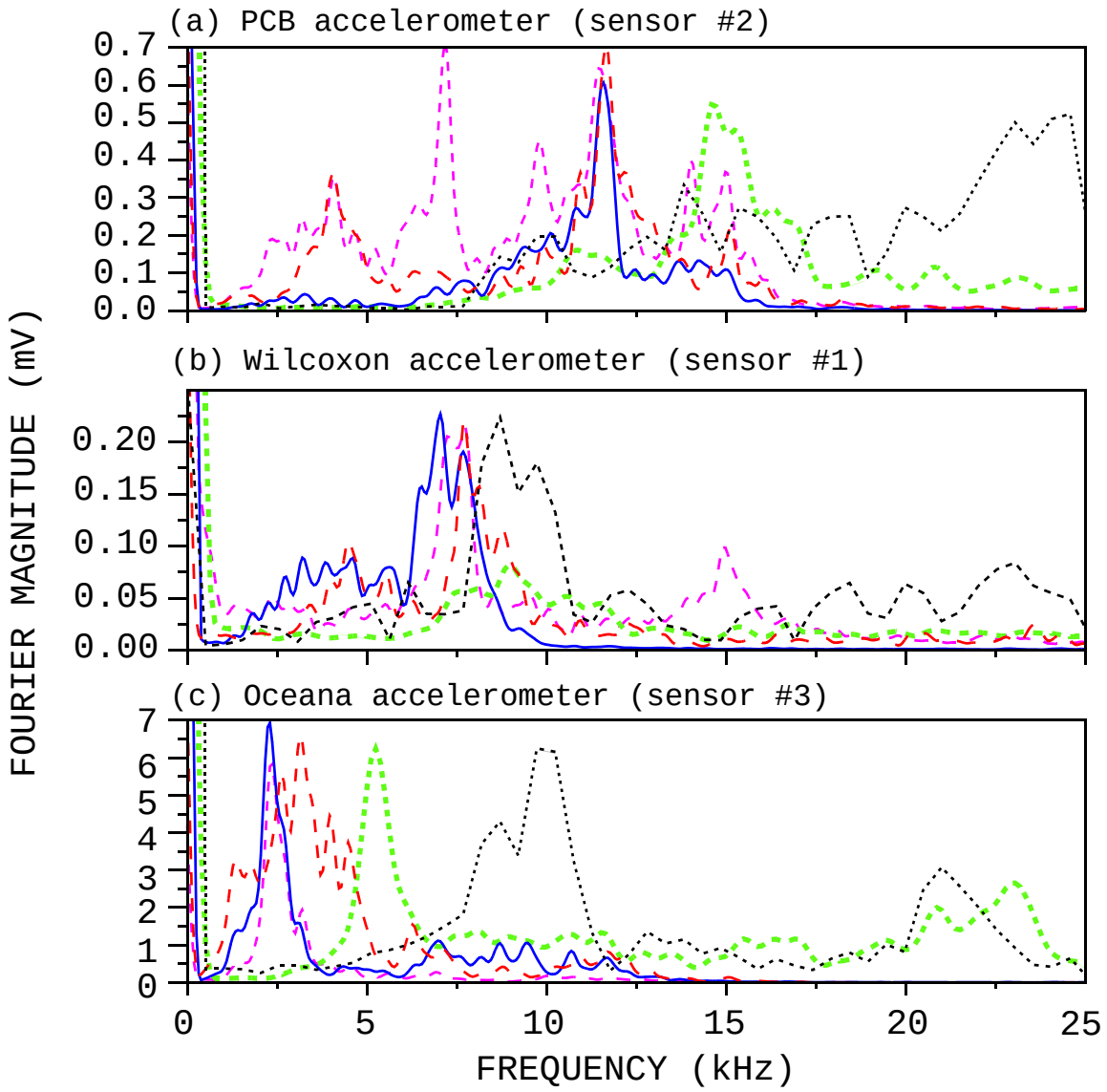


FIGURE 5-16: Frequency response spectra of field and laboratory data recorded by three accelerometers. The field seismic data were acquired between the gallery and downstream face of Monticello Dam using two sizes of Schmidt hammers and a nail gun as sources, and between the reservoir and gallery using a sonic logging tool source. The laboratory data were acquired across a 5-ft concrete block using a piezoelectric transmitter source. The numbers given in the legend are scaling factors applied to each magnitude spectrum (See text for explanation).

transducer source. It is highly unlikely that the 5 different sources and 3 different acquisition geometries represented in Figure 5-16 produced seismic energy at the receiver location having such similar frequency content. Rather, the consistent, large frequency response at 7 to 10 kHz is probably due to either a resonance of the accelerometer itself or the mounting apparatus.

Data acquired with the Oceana accelerometer also show somewhat consistent low-frequency resonances. The data acquired using the three impact surface sources (Schmidt hammers and nail gun) consistently show frequency peaks at 2 to 3 kHz (Figure 5-16c). The response recorded from the sonic logging tool source shows a strong peak at 5 kHz. The frequency spectrum from the laboratory test shows a dominant peak at about 10 kHz. The smaller peaks at about 21 to 23 kHz on the responses from the laboratory and sonic logging tool sources may represent the resonance frequency of the accelerometer itself, which is stated to be >20 kHz.

The large, low-frequency peaks ranging from 2 to 10 kHz recorded with the Oceana accelerometer are interpreted to be due to mounting resonances, with differences between them explained by variations in each individual mounting. The three data sets from the surface impact sources were acquired sequentially with the accelerometer mounted on the same anchor. The accelerometer was not removed until all three data sets were acquired, and the mounting was not adjusted in any way between acquisition of the different data sets. These data sets consistently show the lowest-frequency resonances in Figure 5-16c (2-3 kHz). The data set from the sonic logging tool source was acquired on a different anchor than the anchor used for the surface source testing, but used the same type of mechanism (a nut glued to the bottom of the accelerometer housing, threaded onto a 1/4-inch masonry anchor bolt). These data show a higher resonance (5 kHz) than the data from the impact surface sources. (The sonic logging tool data were acquired 4 days prior to the surface source data. The nut on the bottom of the accelerometer may have loosened between the 2 tests, because shortly after the conclusion of the surface source tests the nut came off the accelerometer housing.) The lab data were acquired with a different accelerometer mounting than that used during the field tests. The accelerometer was glued onto an alluminum block, which was bolted onto the concrete. These data show the highest-frequency resonance (10 kHz).

The frequency spectra of data acquired with the PCB accelerometer show much greater variability than the spectra of data recorded with either of the other two accelerometers (Figure 5-16a). Although the spectra from the three impact surface sources all have a peak

at 11.5 kHz, it is not always the dominant peak. The spectrum of the sonic logging tool data shows only a minor peak at 11.5 kHz, and the spectrum of the laboratory data does not contain any peak at this frequency. While there may be some effect of mounting resonance with this accelerometer, it does not appear to dominate the data as is the case for the other two accelerometers.

## 5.3 Conclusions

Laboratory and field tests demonstrated two important differences between the responses of the receivers investigated. First, the piezoelectric transducers tested in this study are extremely susceptible to electromagnetic crossfeed, whereas the accelerometers show no crossfeed problems. Electromagnetic crossfeed with a frequency of 60 Hz was recorded by the piezoelectric receivers at Monticello Dam. Crossfeed from the piezoelectric source used during the laboratory tests, containing frequencies up to at least 30 kHz, was also picked up by these receivers. The difference in susceptibility to electromagnetic crossfeed between these accelerometers and piezoelectric transducers could be important in electrically noisy environments, such as near power plants.

The second important difference amoung the receivers tested is that the frequency response from the PCB accelerometer (sensor #2) appears to be flatter than that from the piezoelectric transducers. For example, data from the PCB accelerometer acquired from the sonic logging tool source show a frequency response centered at 15 kHz, the center frequency of the tool. The other receivers tested with this source don’t show a single dominant response at this frequency. In addition, the frequency content of sonic tool data acquired with the PCB accelerometer varies systematically with increasing source-receiver separation in a manner consistent with the effects of intrinsic attenuation. Data acquired with one of the piezoelectric transducers (sensor #5) for a variety of source-receiver separations show strong variations in frequency content that are inconsistent with the effects of attenuation.

The deficiencies of the piezoelectric transducers tested during these studies may be overcome if more time is invested in their development. Higher-quality, more expensive piezoelectric crystals might solve the problems with the variable frequency response. Careful shielding and grounding of the receivers may alleviate the electrical crossfeed problem. In addition, tests would have to be performed to determine the variation in receiver response

(amplitude) with angle of incidence, unless this information is available elsewhere. This variation must be expressed in terms of a mathematical formula that can be used in a tomography computer algorithm. (The variation in response as a function of angle of incidence is already known for accelerometers.) Also, piezoelectric crystals are open circuits that can easily short circuit with a slight amount of moisture. They would need to be encased in a water-resistant coating or housing for use on potentially damp surfaces. The only advantage of these types of sensors over accelerometers is their potentially lower cost (excluding development costs), which may be an important factor if disposable receivers are desired. At this time, disposable receivers are not needed, and accelerometers should be used to achieve the best data quality.

Of the three accelerometers tested, the one from PCB Piezotronics showed the broadest frequency response during these laboratory and field tests. The other two accelerometers tested consistently show low-frequency resonances for laboratory and field data acquired using a variety of sources and source-receiver separations. In contrast, data recorded with the PCB accelerometer for the same set of sources and acquisition geometries exhibit a much greater variety of frequency response. As discussed in Section 5.2, the differences in frequency response during these tests may be at least partially due to mounting effects. Effects of various mounting techniques are discussed in the following section.

# 6.0 MOUNTING METHODS FOR SURFACE RECEIVERS

## 6.1 Piezoelectric Transducer Mountings

Two adhesive mountings were compared using one of the piezoelectric transducers. The receiver used was sensor #5, the stiffened but unamplified transducer from JODEX. (The side of the transducer with the quarter was coupled to the concrete surface.) This comparison was performed in the laboratory on the concrete block. The two adhesives tested were silicon grease and epoxy. Glass powder was mixed with the epoxy to make a stiffer bond. The epoxy was allowed to set for 15 and 1/2 hours before data were recorded. For the grease mount, silicon grease was spread on the sensor, and then the sensor was pressed against the concrete surface. Tape was used to support the cables so that their weight wouldn’t pull on the receiver. Data were acquired immediately after mounting the receiver. The laboratory set-up was the same as that described at

the beginning of Section 5.1. (In fact, the data from the silicon grease mounting have already been shown in Figures 5-1b and 5-2b.)

The waveforms acquired using the two mountings are compared in Figure 6-1 . Figure 6-1a shows the entire recorded waveforms (overlaid). The solid curves are from the silicon grease mounting, and the dashed curves are from the epoxy mounting. Figure 6-1b shows the beginning of each trace plotted at an expanded scale so that the P wave can be better seen. The signal strength increases when the receiver is mounted with epoxy rather than silicon grease. The amplitude of the direct P wave (arriving at about 0.38 ms) almost doubles. Later arrivals increase in amplitude by as much as a factor of 4. These arrivals are interpreted to be the direct S wave and reflected arrivals, possibly including P-to-S converted phases. The solid epoxy mounting allows for better coupling of shear wave energy than the silicon grease mounting.

The frequency spectra are compared in Figure 6-2. The magnitude spectrum from the epoxy mounting was scaled by a factor of 0.2 so that its shape could be more easily compared to that of the silicon grease mounting spectrum. Although there are differences between these two spectra, the general frequency content is similar. Both responses contain frequencies between 13 and 43 kHz. In both cases the dominant frequency band is centered about 33 kHz. A smaller frequency peak is seen at 20 or 21 kHz.

## 6.2 Accelerometer Mountings

A few types of receiver mountings for the Wilcoxon and PCB accelerometers were investigated in the laboratory on the concrete block. Because of the difficulty in mounting the Oceana accelerometer (it has no bolt or threaded hole in its housing), its poor performance in earlier tests, and its relatively low resonant frequency (about 20 kHz), it was not included in these experiments. The main purpose of the following tests was to investigate the relative effects of different types of receiver mountings on the frequency response of the Wilcoxon and PCB accelerometers.

The data presented here were acquired on the concrete block using the "burst chirp" source from the piezoelectric transmitter described in Section 3-1 (Figure 3-1). Each data trace presented below represents the averaged response from 200 transmitter firings. All frequency spectra presented below represent the magnitude of the Fourier transform of the entire recorded waveform.

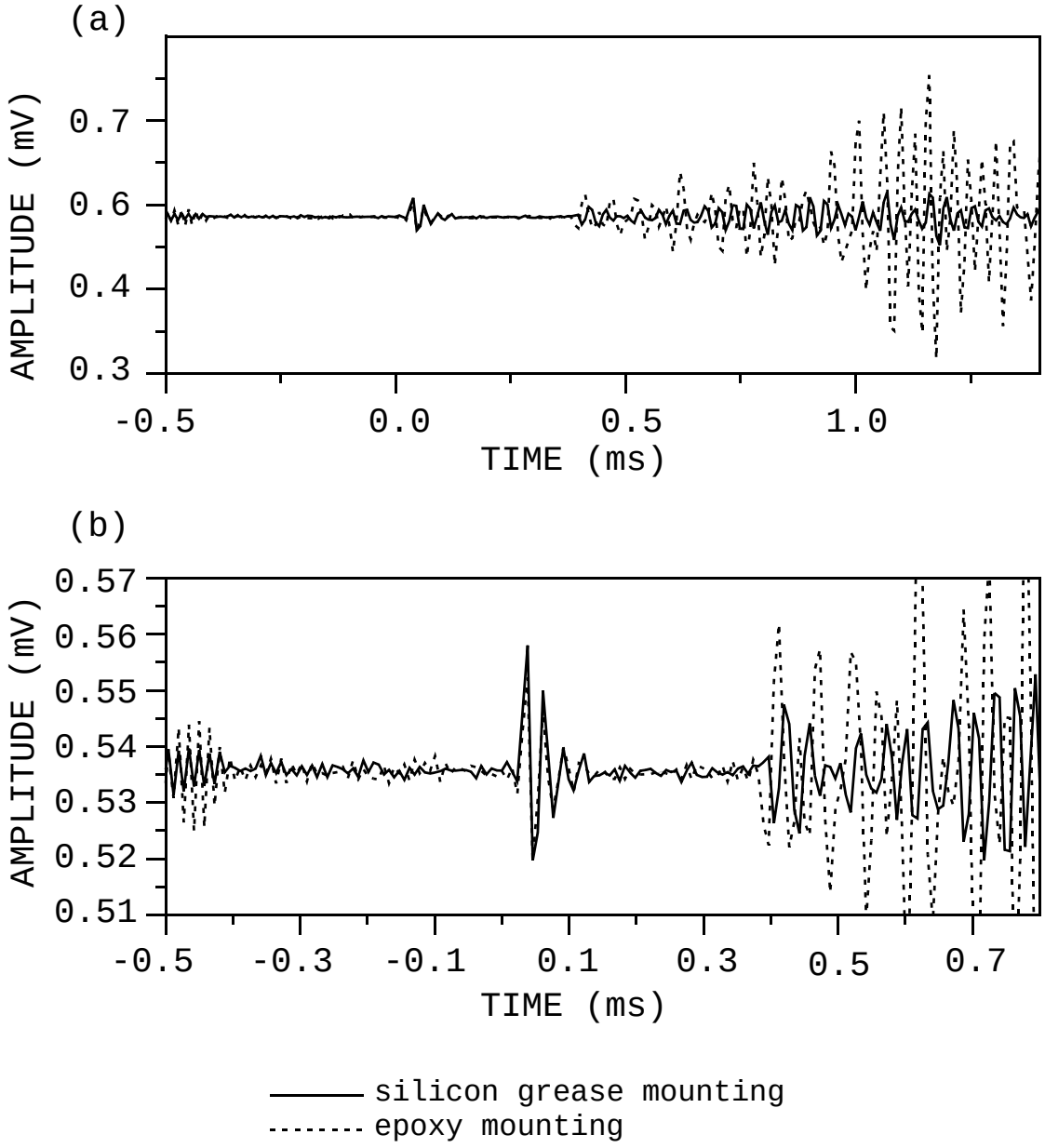


FIGURE 6-1: Time responses from the stiffened JODEX piezoelectric transducer (sensor #5), mounted with silicon grease and epoxy. These data were acquired in the laboratory on the concrete block. (a) Entire recorded trace (b) beginning of trace, plotted with expanded scale to show the P wave (at about 0.38 ms)

Prior to the tests described here, the transmitter amplifier overheated and became inoperable. The output from the HP frequency analyzer was still boosted by the transformer, but not by the

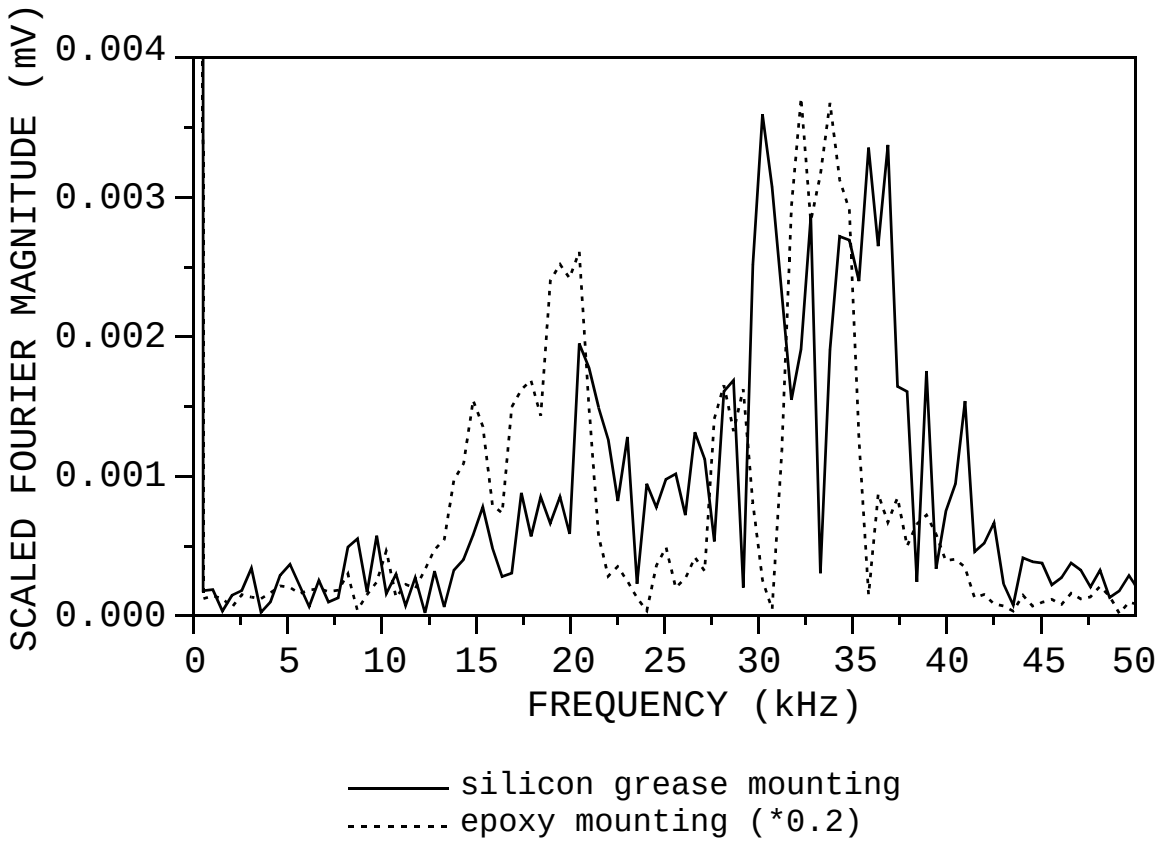


FIGURE 6-2: Frequency responses from the stiffened JODEX piezoelectric transducer (sensor #5), mounted with silicon grease and epoxy. These data were acquired in the laboratory on the concrete block. The number given in the legend for the epoxy mounting is a multiplier used to scale the epoxy mounting magnitude spectrum.

amplifier. For this reason, the signal was not strong enough to be transmitted through the block, and the following tests were performed with the transmitter and receivers on the same side of the block. (Results from limited tests of receiver mountings performed from one block face to the opposite face before the amplifier broke are consistent with the test results presented below.)

The receiver mountings tested were: a stud-mount using a 1-inch steel expansion masonry anchor; two 1-inch square steel plates, 1/4-inch thick, with bolts of different lengths through their centers; a 1/2-inch steel cube; and nuts made of zinc, alluminum, and nylon. Two groups of nuts were glued onto the concrete to help

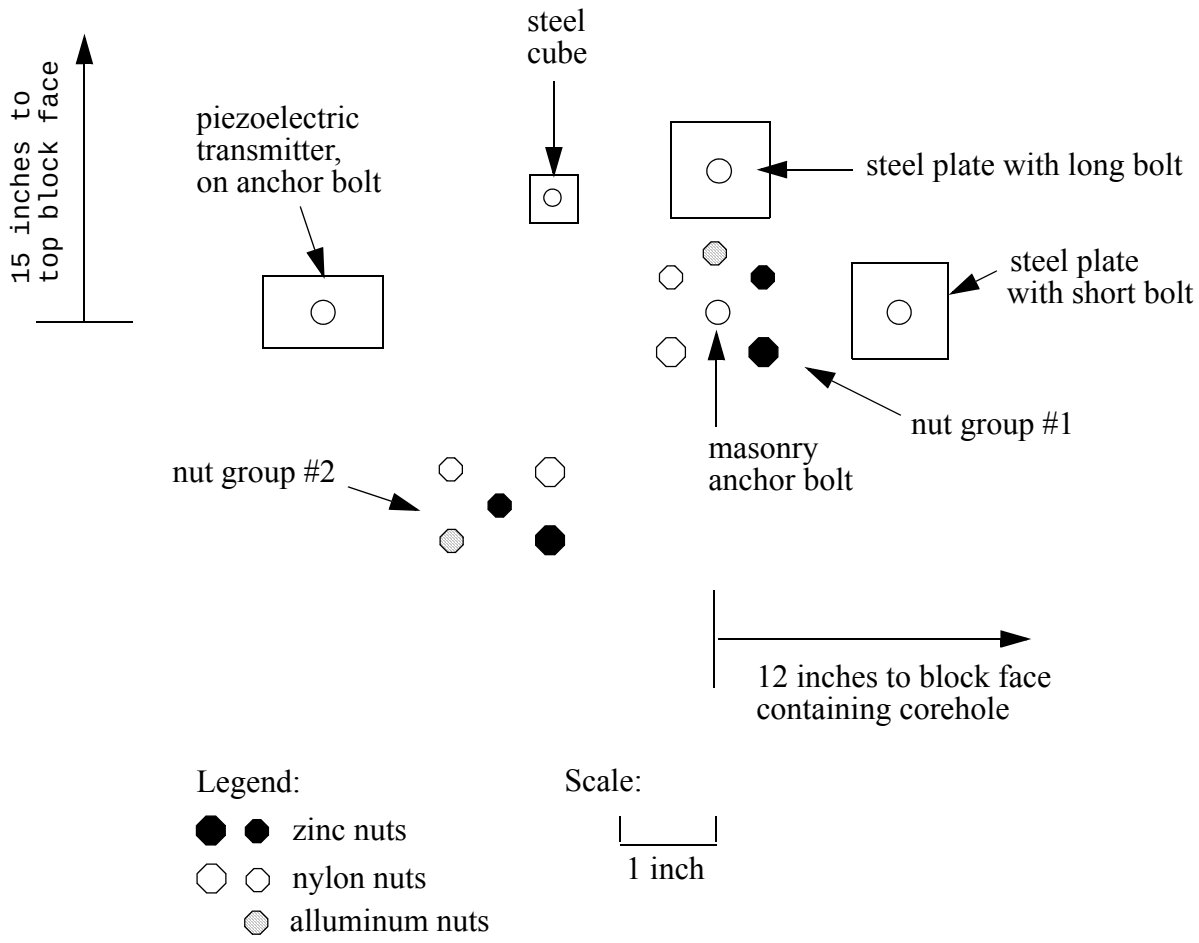


FIGURE 6-3: View of piezoelectric transmitter (source) and receiver mountings on face of concrete laboratory block. Scales are approximate. The smaller nuts were used to mount the PCB accelerometer, and the larger ones were used to mount the accelerometer from Wilcoxon.

evaluate the variability in response due to exact receiver location and coupling characteristics. Alluminum nuts were only available in the size that fits the PCB accelerometer, and therefore no data were acquired on alluminum nuts with the Wilcoxon accelerometer.

Figure 6-3 shows the approximate relative locations of the piezoelectric transmitter (source) and receiver mountings on the side of the concrete block. Due to the scale of the drawing, the edges of the concrete block are not shown. For reference, the masonry anchor bolt shown in Figure 6-3 is located 15 inches from the top face of the block and 12 inches left of one of the block

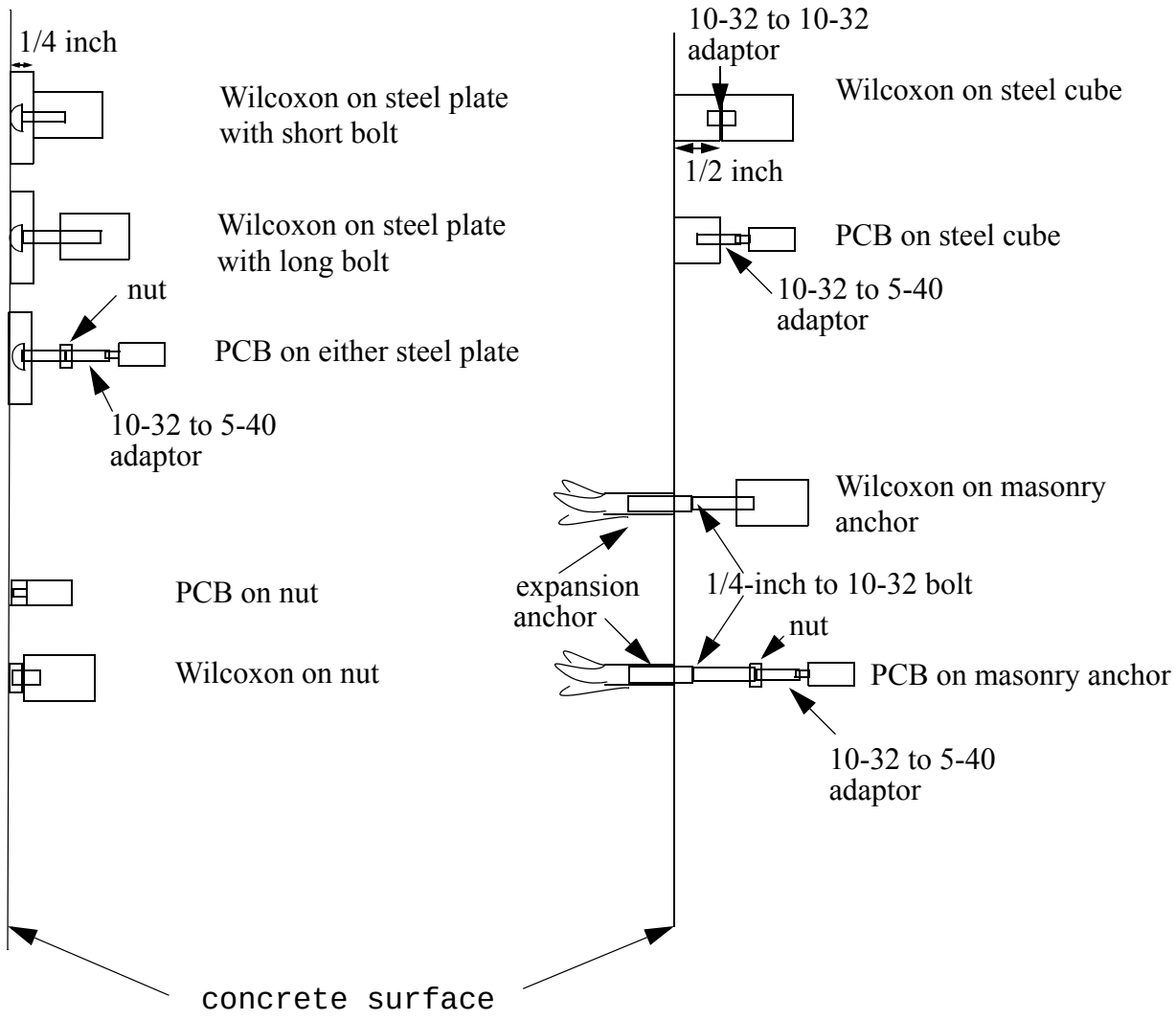


FIGURE 6-4: Profiles of the receiver mounting mechanisms tested with the PCB and Wilcoxon accelerometers. The numbers 10-32 and 5-40 refer to bolt thread sizes.

faces containing the corehole. (See Section 3.1 for an explanation of the corehole.)

Figure 6-4 shows profiles of the receiver mounting mechanisms tested. All of the receiver mountings, other than the masonry anchor, were epoxyed onto the concrete surface at least 45 hours prior to testing. No other type of adhesive (such as silicon grease or wax) was tested because epoxy is believed to produce the strongest bond and the receivers must remain securely in place in the field for at least several hours at a time.

The two steel plates with bolts of different lengths were both used when testing the Wilcoxon accelerometer. For the plate with the long bolt, the accelerometer does not touch the plate, whereas for the plate with the short bolt, the accelerometer is in firm contact with the steel plate (Figure 6-4). The PCB accelerometer does not contact the steel plate in either case. Hence, for this receiver the mounting is nearly identical for the two plates and data from only one plate mounting are presented.

Time responses acquired with the Wilcoxon accelerometer using 6 types of receiver mountings are presented in Figure 6-5. The corresponding frequency responses are shown in Figure 6-6. Some of the fourier magnitude spectra were multiplied by scaling constants. (See the legend in Figure 6-6.) These spectra were scaled so that their shapes could be more easily compared.

All of the receiver responses, except that for the steel cube mounting, show a strong low-frequency resonance of about 8 to 10 kHz. As discussed in Section 5.2, a similar resonance was also seen for this accelerometer when other sources were used in the field (Figure 5-16b). Therefore, the resonance is believed to be unrelated to the seismic energy produced by the transmitter used for these tests. It is not known why this resonance is not present on the response from the steel cube mounting, which clearly shows the highest frequency response (Figures 6-5d and 6-6).

The exceptionally good signal-to-noise ratio seen in the response for the cube mounting for this test (Figure 6-5d) is likely due to the fact that it is the closest mounting to the source. Other tests performed with comparable source-receiver distances (from one block face to the opposite face) indicate that the signal-to-noise ratio of data recorded on the cube mounting is similar to that of data recorded with the stud mounting.

The responses recorded on the nylon and zinc nuts are very poor (Figures 6-5e and f), especially for the nylon nut. They show poorer signal-to-noise than the data recorded on the square steel plate with the short bolt (Figure 6-5c), even though they are much closer to the source.

Time responses acquired with the PCB accelerometer using 6 types of receiver mountings are presented in Figure 6-7. The corresponding frequency spectra are shown in Figure 6-8. The responses obtained on the steel cube, alluminum nut, and nylon nut mountings (Figures 6-7c, d, and e) are clearly dominated by a

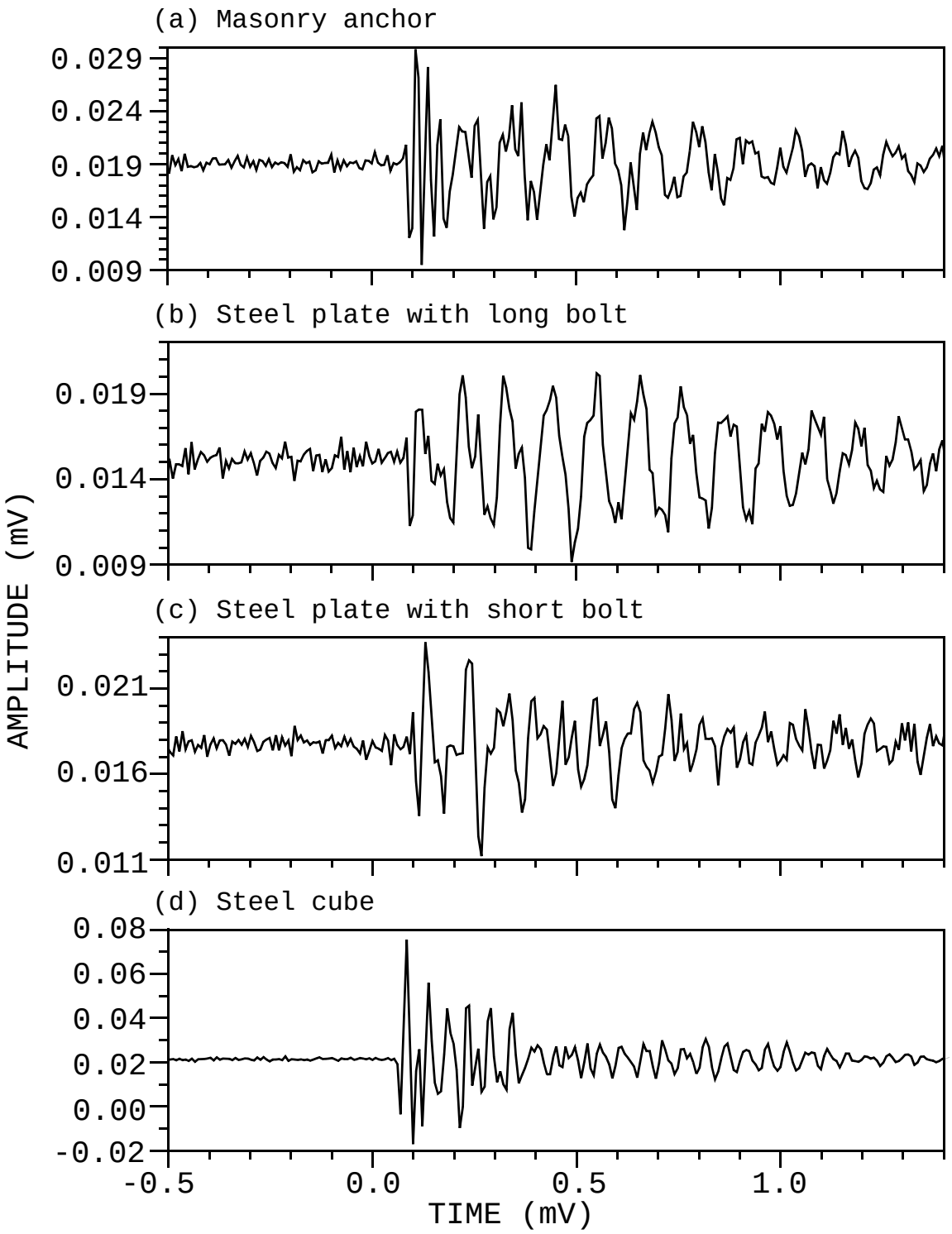


FIGURE 6-5: Time responses recorded with the accelerometer from Wilcoxon using different types of mounting methods. The data were acquired on the concrete laboratory block, using burst chirps from a piezoelectric source.

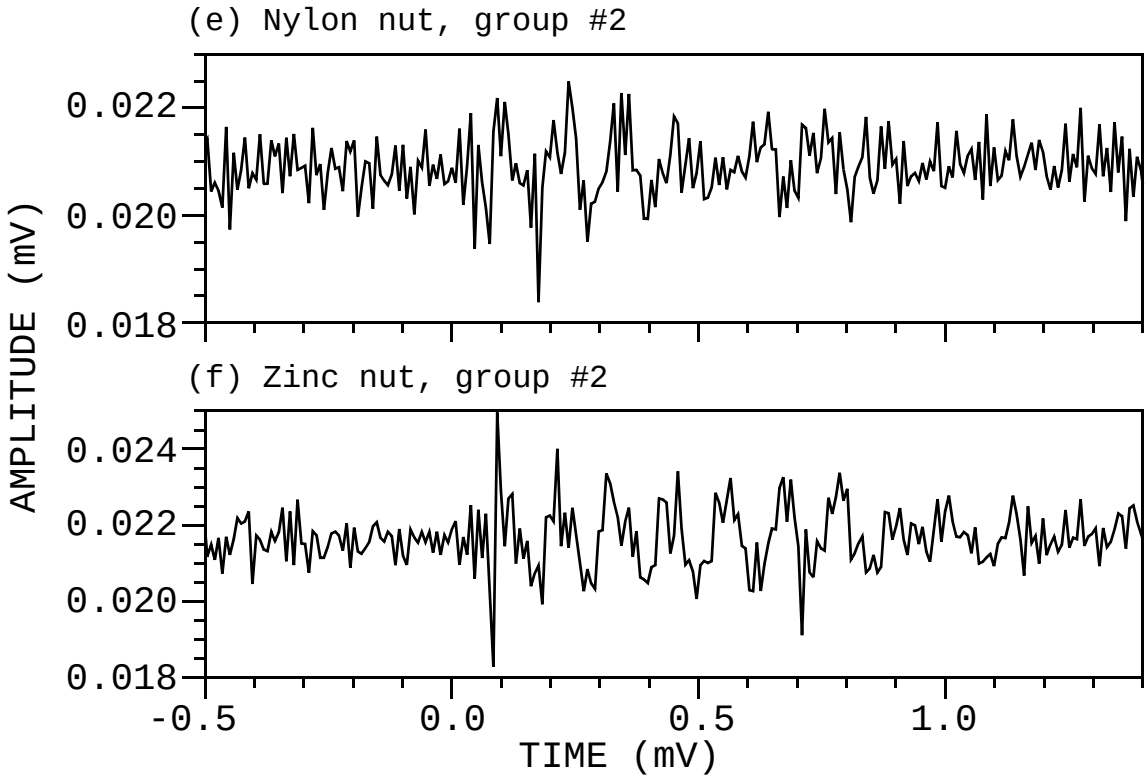


FIGURE 6-5, continued.

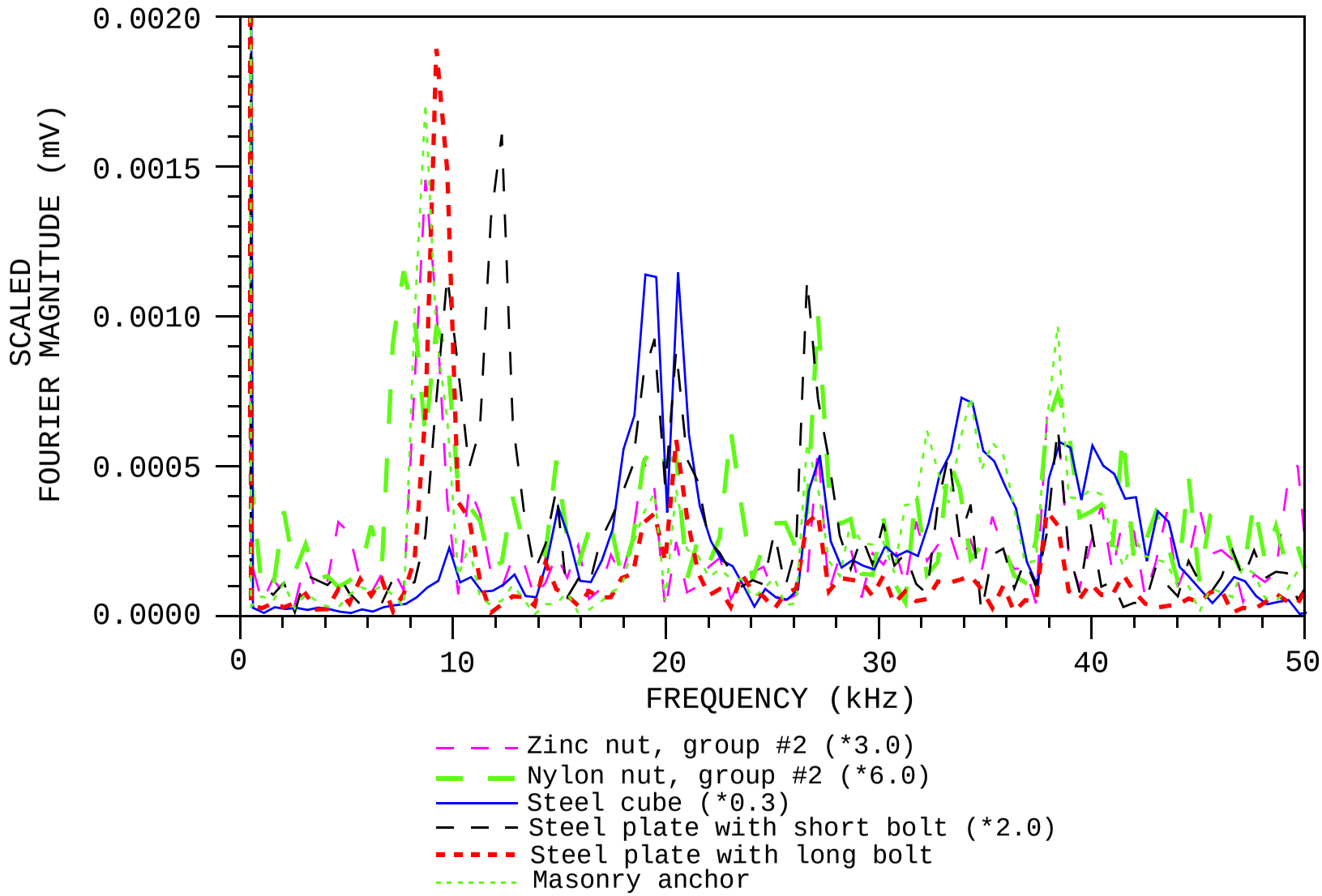


FIGURE 6-6: Frequency spectra of the data in Figure 6-5. The numbers given in the legend are multipliers used to scale each magnitude spectrum.

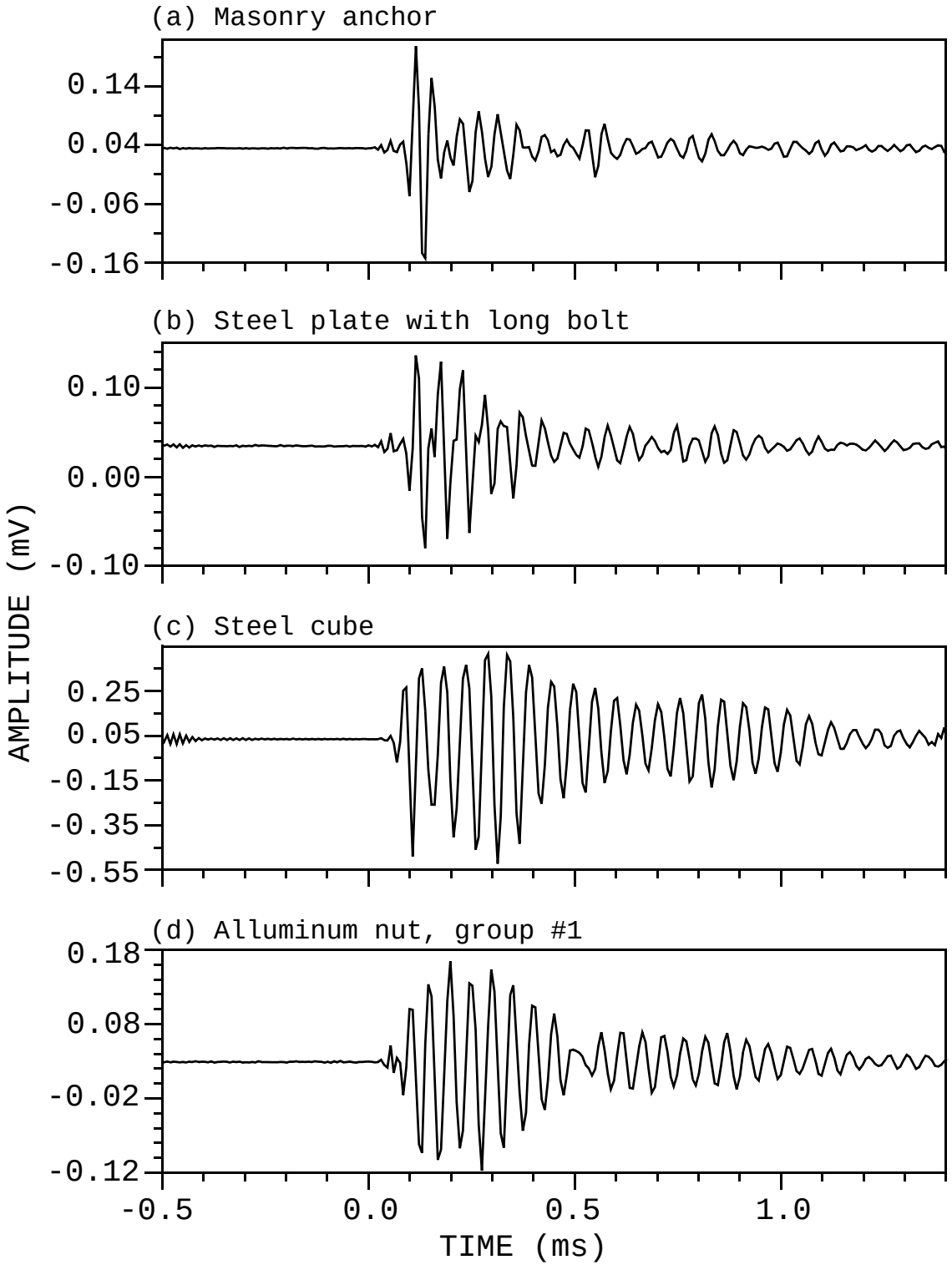


FIGURE 6-7: Time responses recorded with the accelerometer from PCB using different types of mounting methods. The data were acquired on the concrete laboratory block, using burst chirps from a piezoelectric source.

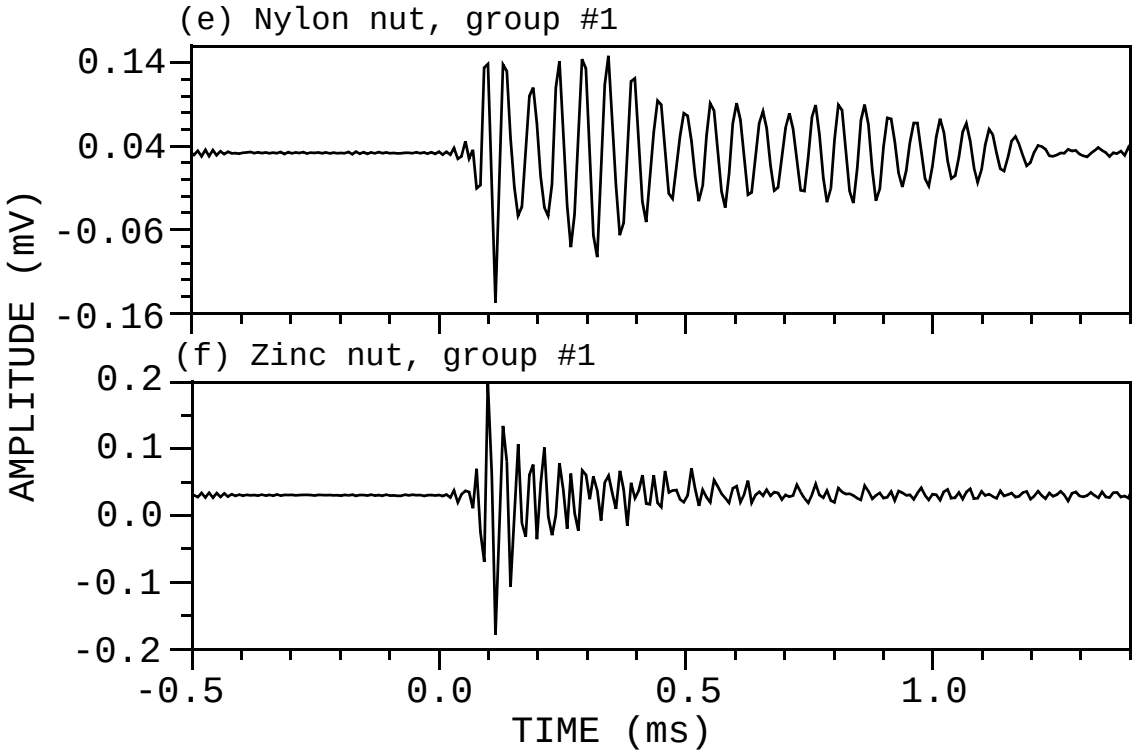


FIGURE 6-7, continued.

resonance at approximately 19.5 kHz. The waveforms ring after the first arrival, obscuring later arrivals. The response from the steel plate mounting displays some ringing for a relatively short amount of time after the first arrival (Figure 6-7b). The responses obtained on the masonry anchor and zinc nut mountings clearly show the most impulsive waveforms (Figure 6-7a and f). Of these two, the data trace from the zinc nut mounting shows the higher frequency response (Figure 6-8).

Time series recorded with the PCB accelerometer on mountings in nut group #2 (refer to Figure 6-3 for nut group locations) are presented in Figure 6-9. Comparison of these waveforms to those from nut group #1 (Figure 6-7d, e, and f) show significant differences for the alluminum and zinc nut mountings. The differences are most dramatic for the alluminum nut mountings. The response recorded on the alluminum nut in group #2 (Figure 6-9a) is much higher in frequency and shorter in duration than the corresponding response from group #1 (Figure 6-7d).

Frequency spectra of the data acquired on the two sets of nut mountings are compared in Figure 6-10. The solid curves represent the spectra from nut mounting group #2, while the dotted curves are the spectra for nut group #1. The dramatic difference in frequency

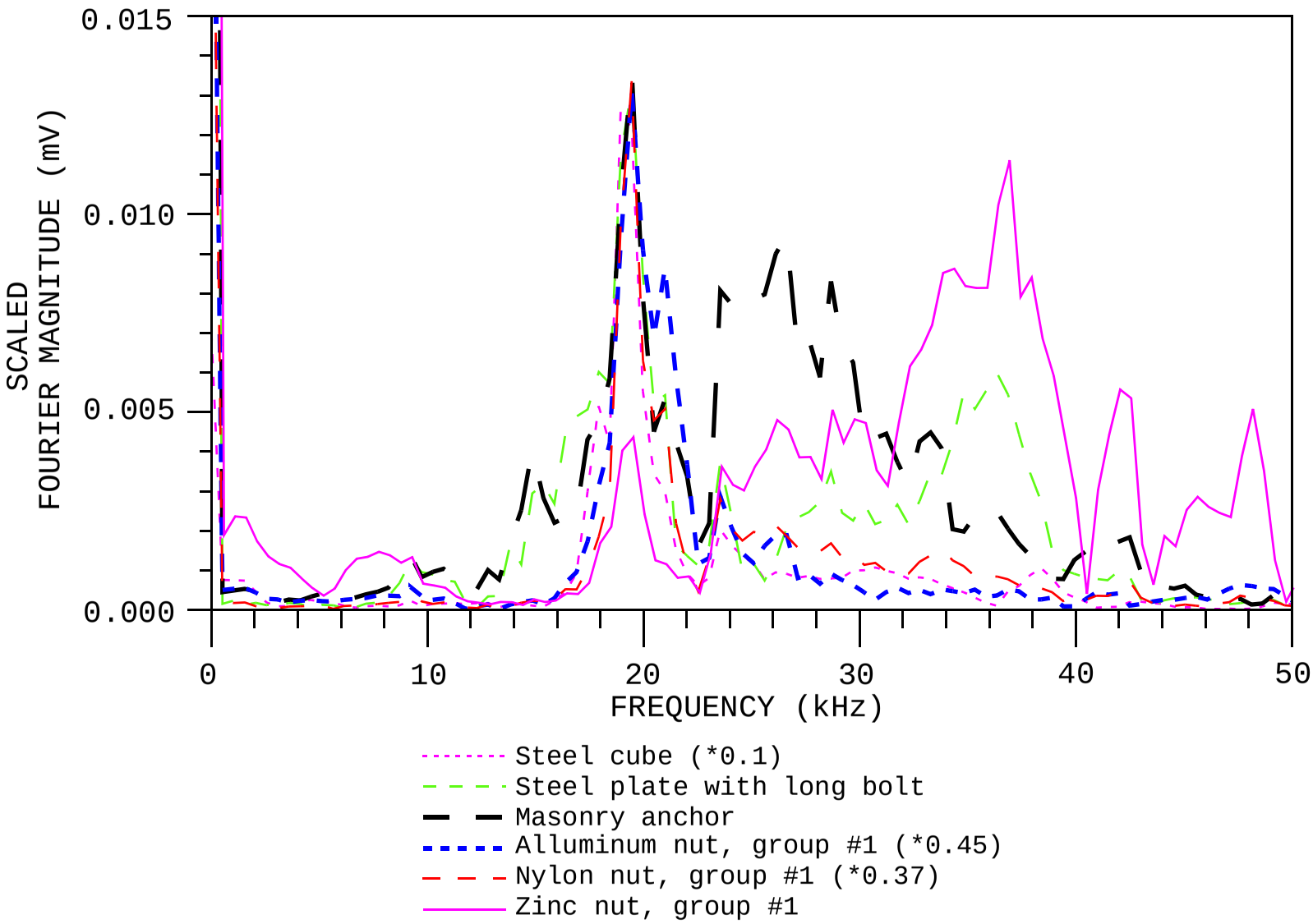


FIGURE 6-8: Frequency spectra of the data in Figure 6-7. The numbers given in the legend are multipliers used to scale each magnitude spectrum.

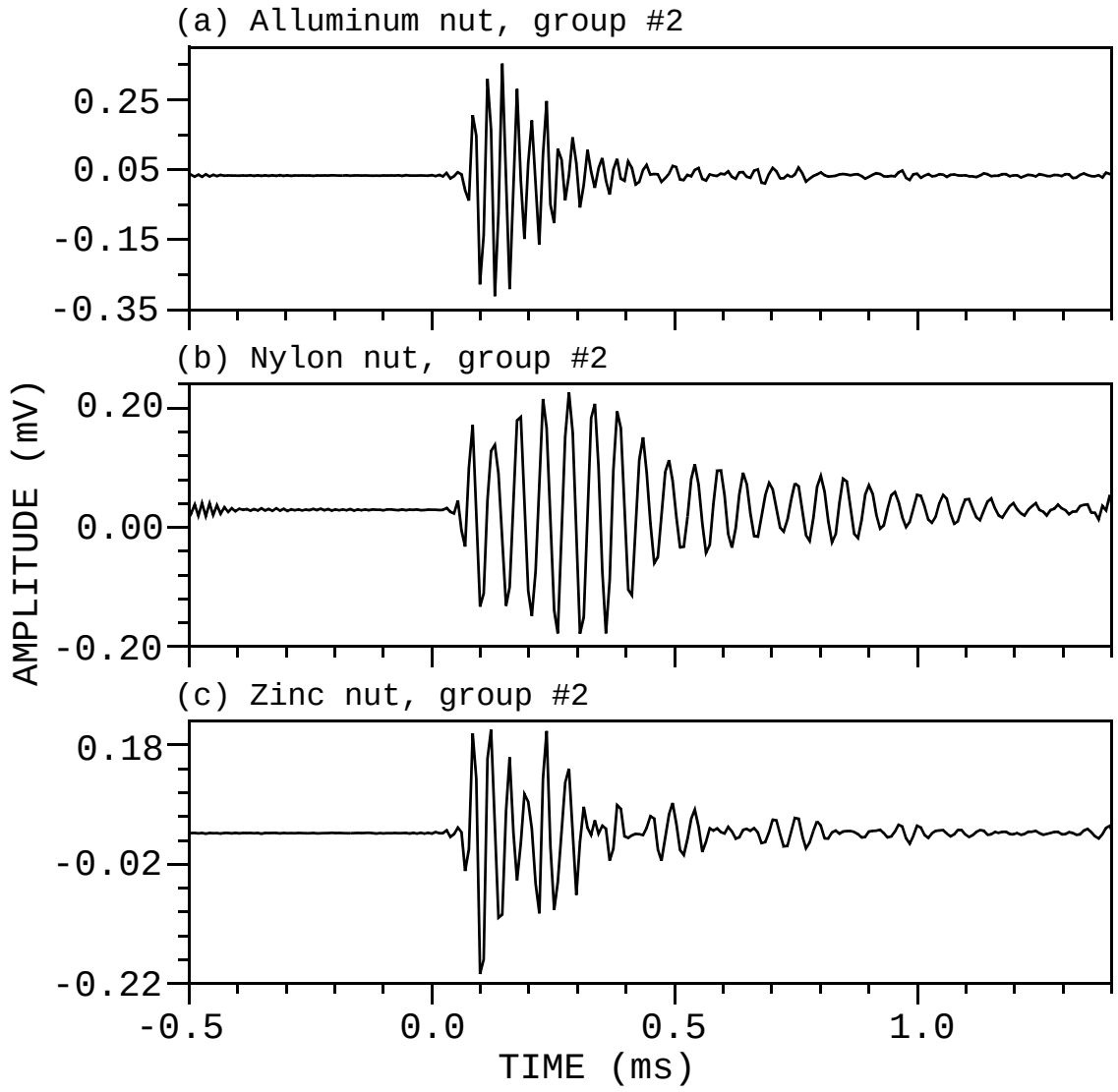


FIGURE 6-9: Time responses recorded with the accelerometer from PCB using the three nut mountings in group #2.

content for the two alluminum nut mountings is clear (Figure 6-10a). The spectra from the two zinc nut mountings also show some substantial differences (Figure 6-10c), whereas the results for the two nylon nuts are nearly identical (Figure 6-10b).

The low-frequency response of the alluminum nut mounting in group #1 compared to that of group #2 is not likely due to actual differences in the seismic energy reaching the two receiver locations. The differences are too dramatic to be due to wave propagation phenomenon, and other receivers very near the alluminum nut in group #1 recorded data with substantially higher frequencies (masonry anchor and zinc nut mountings, Figure 6-8). The differences are more likely due to differences in the coupling of the nuts to

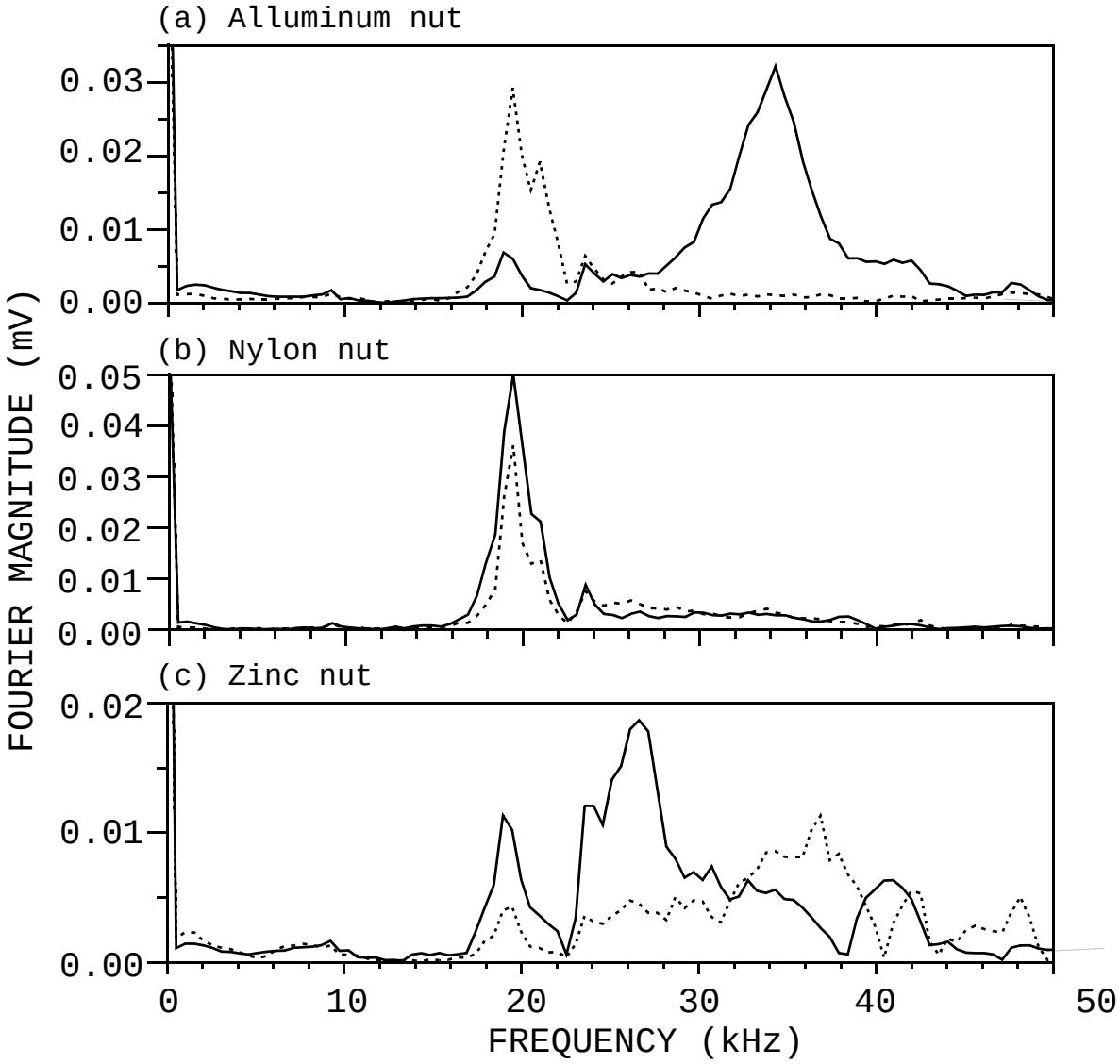


FIGURE 6-10: Comparison of response spectra of data obtained on the nut mountings in group #1 (dotted curves) and group #2 (solid curves).

the concrete surface. The alluminum nuts were epoxyed to the concrete surface after all of the other receiver mountings were in place. Because the alluminum nut in group #1 was surrounded by other nearby receiver mountings, it was difficult to spread out the epoxy thinly on the concrete surface. The epoxy was easier to spread out for the alluminum nut in group #2, since it was not completely surrounded by other mountings. A thicker layer of epoxy could potentially explain the lower-frequency response of the data acquired on the alluminum nut mounting in group #1 compared to the data from the mounting in group #2. Some differences in coupling could also be caused by differences in the roughness and porosity

of the concrete surface in different locations (although the concrete was sanded before the nuts were glued). Such differences in coupling may also account for the differences in the frequency content of the data acquired on the two zinc nut mountings.

## 6.3 Conclusions

Epoxy provided better coupling than silicon grease for one of the piezoelectric transducers (sensor #5). The P-wave amplitude almost doubled when epoxy was used rather than silicon grease. The shear-wave energy was up to 4 times stronger with the epoxy mounting than with the silicon grease mounting. The frequency content of the recorded data was similar for the two types of adhesive mountings.

Data acquired with the Wilcoxon accelerometer on all but one type of receiver mounting are dominated by resonances at about 8 to 10 kHz. The persistence of this resonance for many types of mountings makes the Wilcoxon accelerometer an undesirable choice for seismic tomography data acquisition.

Data acquired with the PCB accelerometer on the masonry anchor and zinc nut mountings show the most impulsive character and highest frequency responses. Some of the data obtained with the alluminum nut mounting also display similar qualities. Two of the four data traces acquired with the alluminum and zinc nut mountings (Figures 6-7f and 6-9a) clearly contain higher frequencies than the data acquired with the masonry anchor mounting (Figure 6-7a). These two nut mountings yield data with dominant frequencies of about 34 to 36 kHz (Figure 6-10a, solid curve, and 6-10c, dotted curve), compared to a dominant frequency of about 26 kHz for the masonry anchor mount (Figure 6-8)

The type of mounting method that produces data with the most consistent character cannot be determined from the limited data that was acquired in the laboratory. These test results indicate that significant changes in the character of the data can potentially be caused by variations in the coupling charactistics of epoxyed receiver mountings. The variability of data obtained on masonry anchor mountings was not investigated. Data should be acquired in the field on several masonry anchors and epoxyed mountings in order to look for trends in the character of the data and determine which type of mounting produces data with the best overall qualities and consistency.

# 7.0 EVALUATION OF SOURCES

## 7.1 Field Tests

### 7.1.1 Sonic Logging Tool Source

Data acquired at Monticello Dam with the sonic logging tool source in the reservoir immediately upstream of the dam (probably within inches of the dam face) and receivers mounted on the west gallery wall have already been presented (See Section 5.2, Figures 5-9 to 5-13). Data were acquired for source-receiver separations up to 43 feet and ray angles up to 57 degrees from horizontal. However, despite averaging as many as 500 pulses of the sonic tool at the higher angles, the signal-to-noise ratio is only fair (Figures 5-11 and 5-12).

Attempts were made to record the sonic tool signal from the reservoir to the downstream face. The PCB accelerometer, which is the least sensitive of the three accelerometers tested, did not detect any obvious signal. No attempts were made to enhance the data with processing or amplifiers. (The other two accelerometers had problems with mounting and wiring at the time of these tests.) The three piezoelectric transducers from JODEX and the tweeter from Radio Shack recorded a weak signal at an angle of 8 degrees from horizontal and a source-receiver separation of about 68 feet. However, these sensors detected nothing at an angle of 51 degrees and a separation of 106 feet.

Base on these tests, we conclude that this sonic logging tool may be used as a seismic source over relatively short distances (up to 30 or 40 feet through concrete). However, it is not strong enough to transmit energy through the thicker sections of a dam.

Another potential disadvantage of this tool as a seismic tomography source is its relatively narrow-band frequency excitation. Assuming that data acquired with the PCB accelerometer yield fairly accurate indications of the seismic frequencies generated, most of the seismic energy lies between 13 and 17 kHz (Figure 5-13b). However, a broader frequency band is desirable for two reasons. The higher the frequency of the recorded data, the better the spatial resolution of the computed tomograms. However, higher frequencies attenuate more severely than lower frequencies. Since it is not known in advance precisely what frequencies will propagate through the dam

for all source-receiver separations needed, it is probably best to input a wide range of frequencies so that good quality data will be obtained for all source-receiver combinations.

Another reason that a wide frequency band may be better than a narrow one is that a narrow frequency band may cause the results of amplitude tomography to be "biased" toward imaging objects that are about the same size as the seismic wavelength corresponding to the dominant frequency. The reason for this is that anomalies of acoustic impedence (density and/or velocity variations) most strongly scatter seismic energy having wavelengths that are about the same size as the anomaly. Our current amplitude tomography processing algorithm does not account for scattering. Areas that produce a large amount of scattering will be imaged as areas having high intrinsic attenuation. For these reasons, a broad-band source is likely to allow the amplitude tomography to image anomalies of varying sizes more uniformly than a narrow-band source.

### 7.1.2 Surface Sources

Surface seismic sources were tested between the east gallery wall and downstream face at Monticello Dam (Figure 3-3a). The sources were used inside the gallery, and a receiver was mounted on the downstream face. The distance between source and receiver was about 45 feet. The angle of the direct raypath was about 5.5 degrees above horizontal from source to receiver. (Some of the data acquired during these tests were presented previously in Section 5.2.)

Although various receivers were used during these tests, only the results from the PCB accelerometer are included in this section. The responses from this receiver were chosen because in other tests it showed the broadest frequency response and least sensitivity to receiver mounting effects (See Sections 5 and 6). This accelerometer was stud-mounted on the downstream face of the dam using a 1/4-inch steel masonry amchor bolt.

The piezoelectric transmitter built and used for the laboratory tests (See Section 3.1) was only partially tested at Monticello Dam. Initial tests indicated that the signal was too weak for the short burst chirp used for the laboratory tests to be transmitted through the 45 feet of concrete between the gallery and downstream face. Very weak responses were obtained of continuous sine waves at some frequencies. Problems with the amplifier and time constraints prevented further field testing of this source. The testing did demonstrate that a stronger piezoelectric source would be required for field work and that it would most likely need to

be driven by some type of long sequence rather than a short impulsive signal.

Three impact surface sources were tested: the small Schmidt hammer (size "N"), the large Schmidt hammer (size "M"), and the nail gun. Section 4 contains a description of these sources. The nail gun piston was driven against a steel plate (approximately 3/8-inch thick) that was bolted to the gallery wall. The Schmidt hammers were used directly on the concrete. All sources were used such that their pistons hit the concrete wall or steel plate at approximately a 90-degree angle. Each recorded trace represents a single source activation (i.e, the data were not stacked or averaged). The time sampling interval was originally set to 7.63 us. After a few test shots, the sampling interval was changed to 15.3 us so that longer records could be recorded.

Recording was triggered using the response of an accelerometer stud-mounted on the gallery wall within two feet of each source. Variations in the precise triggering time are caused by variations in the distance from each source to the accelerometer and variations in the amplitude of each source relative to the specified trigger level. Furthermore, during acquisition of the nail gun data, recording was sometimes triggered by the manual hammer hit to the back of the nail gun. This manual hammer hit fires the 22 mm shot which in turn drives the piston. Because of time constraints, no effort was made to optimize the triggering for these tests.

Figures 7-1 and 7-2 show the time and frequency responses, respectively, recorded by the PCB accelerometer for the two Schmidt hammers and the nail gun with two different shot sizes. (No quantitative measure of shot strength is available.) The relatively weak energy on the traces from the 2 nail gun shots before the arrival of the main energy burst is believed to be caused by the manual hammer hit to the back of the nail gun. When the waveform from the light duty shot shown in Figure 7-1c was acquired, recording was triggered by the energy from the manual hammer hit. When the waveform from the heavy duty shot in Figure 7-1d was acquired, recording was triggered by the energy from the piston hitting the steel plate. The trigger levels were set differently during acquisition of the two tests, because of the different source strengths.

The peak amplitude of the seismic waveform from the large Schmidt hammer source (Figure 7-1b) is slightly more than twice that of the waveform from the small Schmidt hammer (Figure 7-1a). The signal strength from the nail gun using the light duty shot (Figure 7-1c)

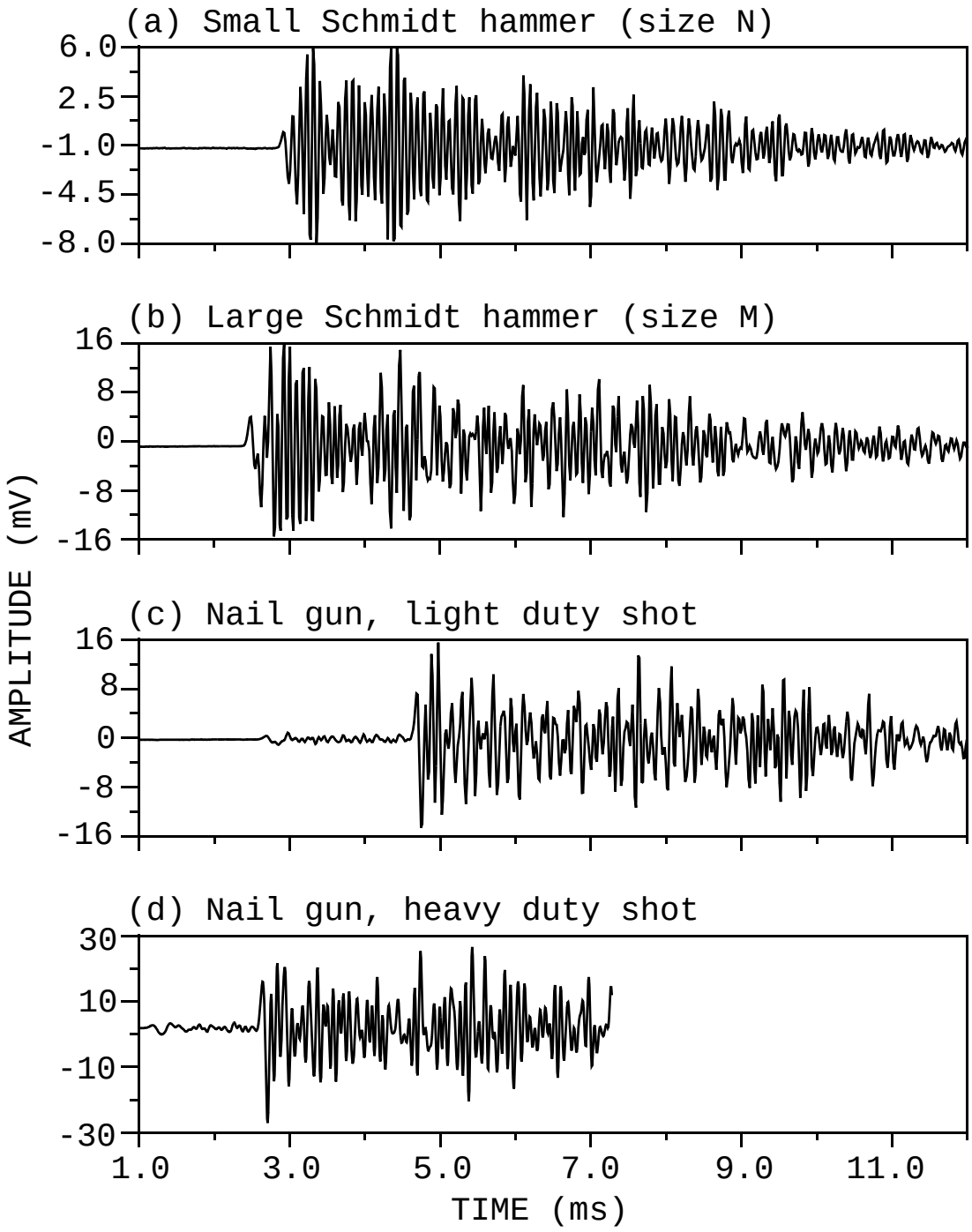


FIGURE 7-1: Time responses recorded with the PCB accelerometer from four different impact surface sources. The sources were activated on the east gallery wall at Monticello Dam, and the accelerometer was mounted on the downstream face. The source - receiver separation was 45 feet, at an angle of about 5.5 degrees from horizontal.

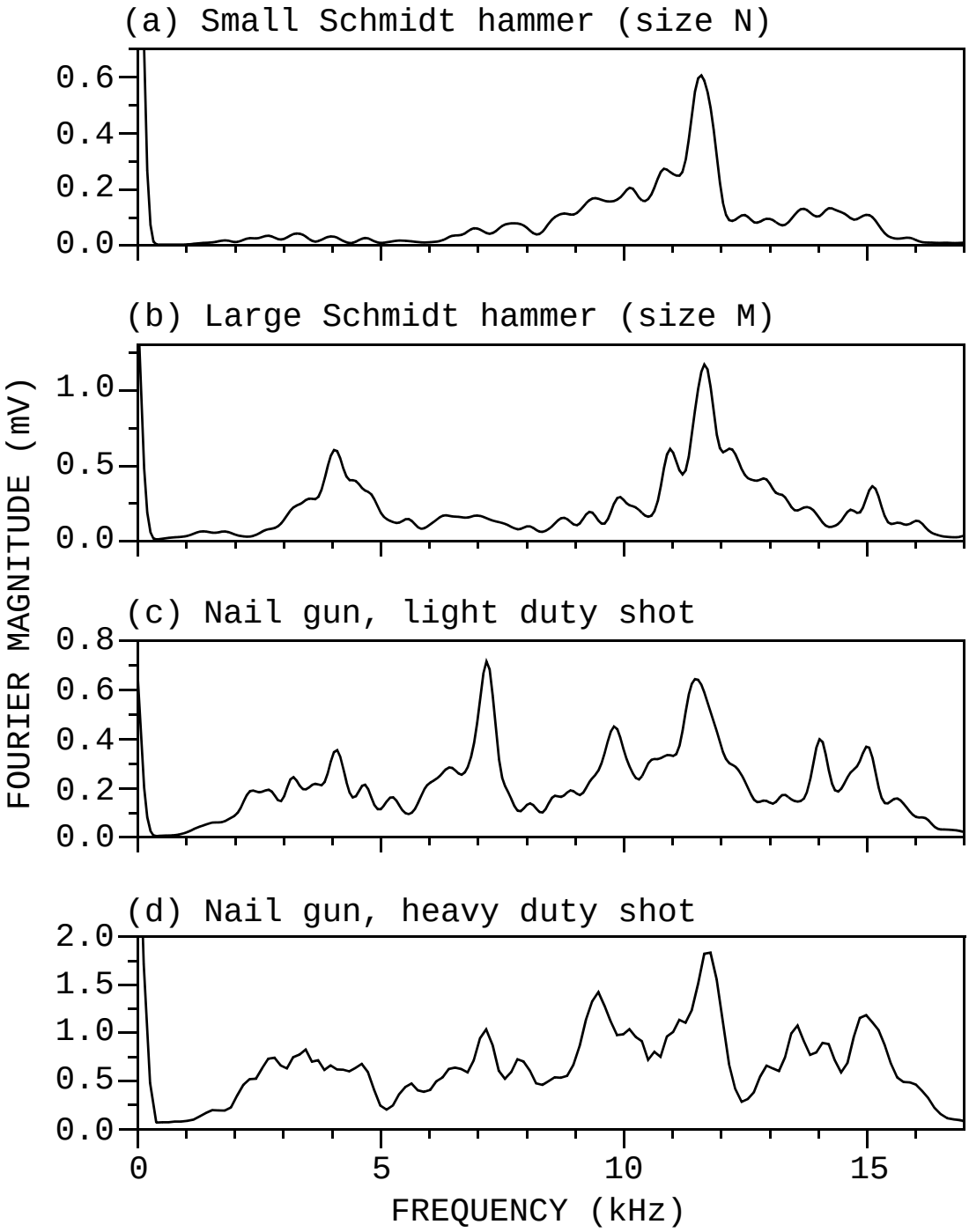


FIGURE 7-2: Frequency responses recorded with the PCB accelerometer from four different impact surface sources. The sources were activated on the east gallery wall at Monticello Dam, and the accelerometer was mounted on the downstream face. The source -receiver separation was 45 feet, at an angle of about 5.5 degrees from horizontal.

is comparable to that from the large Schmidt hammer. The nail gun with the heavy duty shot generates the largest signal (Figure 7-1d), which has a peak amplitude on the order of 50% to 60% larger than the amplitudes of the signals generated with the large Schmidt hammer or the nail gun with the light duty shot.

The frequency spectra from all four sources show a peak at about 11.5 kHz (Figure 7-2). The persistence of this frequency peak for all four sources suggests that there may be some resonance caused by the receiver mounting mechanism. Disregarding the narrow peak at 11.5 kHz, the general frequency trends of the seismic energy generated by the different sources can be discerned. The energy from the small Schmidt hammer is concentrated in the frequency band between about 7 and 15.5 kHz (Figure 7-2a). The spectrum from the data acquired using the large Schmidt hammer source is bi-modal, showing the strongest response between 3 and 5 kHz and between 10.5 and 13.5 kHz (Figure 7-2b). The data from the nail gun shots show the widest range of frequencies. Except for an overall magnitude difference and minor variations in small-scale details, the spectra of the seismic energy recorded from the light duty and heavy duty nail gun shots are very similar (Figures 7-2c and d). These spectra contain strong responses at most frequencies between 2 and 16 kHz.

The nail gun was tested further as a potential seismic source by activating the nail gun on the downstream face of Monticello Dam and recording data with a hydrophone lowered into the reservoir immediately upstream of the dam face. Data were acquired with the nail gun at a fixed position on the downstream face and the hydrophone at various depths in the reservoir (Figure 3-3c). These tests were conducted in order to evaluate the strength of the nail gun source and obtain estimates of the maximum distances and angles over which it can be successfully used.

Heavy duty shots were used for these tests, and the nail gun piston was driven against a steel plate (approximately 3/8-inch thick) bolted onto the downstream face. The nail gun was held approximately perpendicular to the dam face, so that the piston was striking the steel plate at a 90-degree angle. For most of the data acquired, a single source activation was used. For the data acquired with the two largest source-receiver separations, up to 6 nail gun shots were averaged. The time sampling interval is 15.3 us. Recording was triggered using the response of an accelerometer stud-mounted on the downstream face within two feet of the source.

Figure 7-3 shows time responses recorded at source-receiver separations ranging from 67 to 148 feet and ray angles ranging from

19 to 80 degrees above the nail gun axis. (When computing the ray angles, the downstream face was assumed to dip downstream at an angle of 17 degrees from vertical. This value was measured from Reclamation construction drawing no. 413-D-103, cantilever F.) Disregarding the early, low-amplitude signal on some traces believed to be generated by the manual hammer hit to the back of the nail gun and some 60-Hz electromagnetic crossfeed, the responses show good signal-to-noise to a distance of 94 feet and ray angle of 61 degrees from the nail gun axis (Figure 7-3a to e). The last two data traces, at distances of 113 and 148 feet and angles of 71 and 80 degrees, show data with unacceptably low signal strength.

Frequency spectra of the data acquired with the nail gun source between the downstream face and reservoir at Monticello Dam are presented in Figure 7-4. In general, the frequency spectra fall off abruptly between 7.5 and 9 kHz. Recall that data with frequencies up to 16 kHz were acquired with the nail gun source over a distance of 45 feet between the east gallery wall and downstream face (Figure 7-2c and d). The loss of frequencies above 9 kHz in the data acquired in the reservoir is probably not due to the increased source-receiver distances, since the frequency ranges shown in Figure 7-4 for distances varying from 67 to 93 feet are similar. A more likely cause of the lack of higher frequencies in these data is the limited frequency response of the hydrophone used to record the data. This hydrophone was designed for relatively low-frequency applications and was tested by the manufacturer (Geo Space) to only 1 kHz.

## 7.2 Numerical Modeling of the Nail Gun Source

When seismic energy from the nail gun source was recorded by a hydrophone located in the reservoir at Monticello dam, the signal strength decreased as the hydrophone was raised in the reservoir (Figures 7-3 and 7-4). This decrease in signal strength is caused by both increasing source-receiver separation and increasing ray angle from the nail gun axis. In order to determine a mathematical expression for the effects of source-receiver separation and ray angle on the P-wave amplitude, a numerical model was developed that best fits (in a least squares sense) the P-wave amplitudes observed at Monticello Dam. The results from this modeling were then used to predict the P-wave amplitudes that would be observed for a wide range of ray angles and distances. From these results, a general guide about the combinations of ray angles and source-receiver separations for which the nail gun source can be successfully used

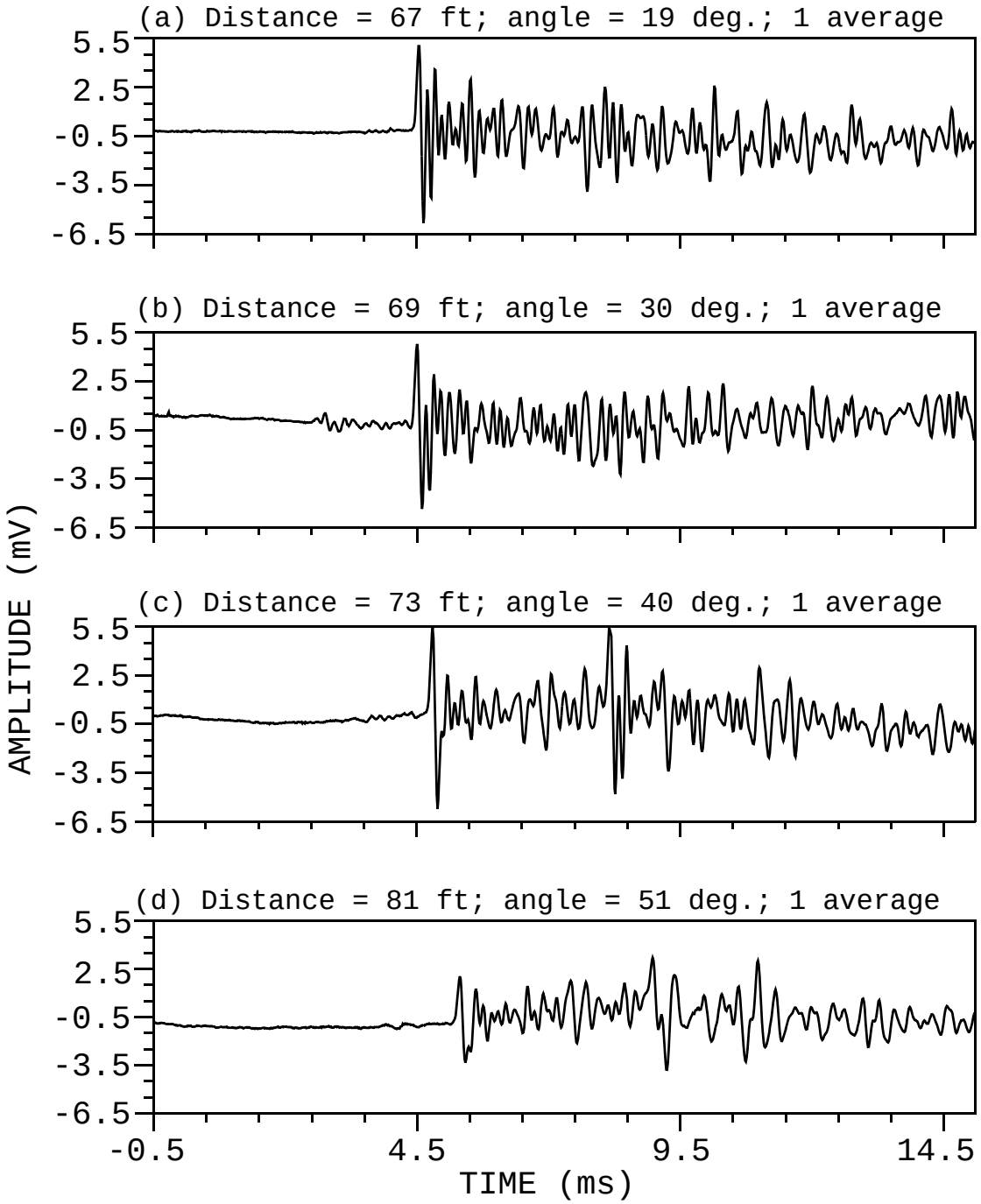


FIGURE 7-3: Time responses of data acquired at Monticello Dam using the nail gun source on the downstream face and a hydrophone receiver located in the reservoir. The distance from the source to receiver, the ray angle from the nail gun axis, and the number of averages for each trace are labeled on the individual plots.

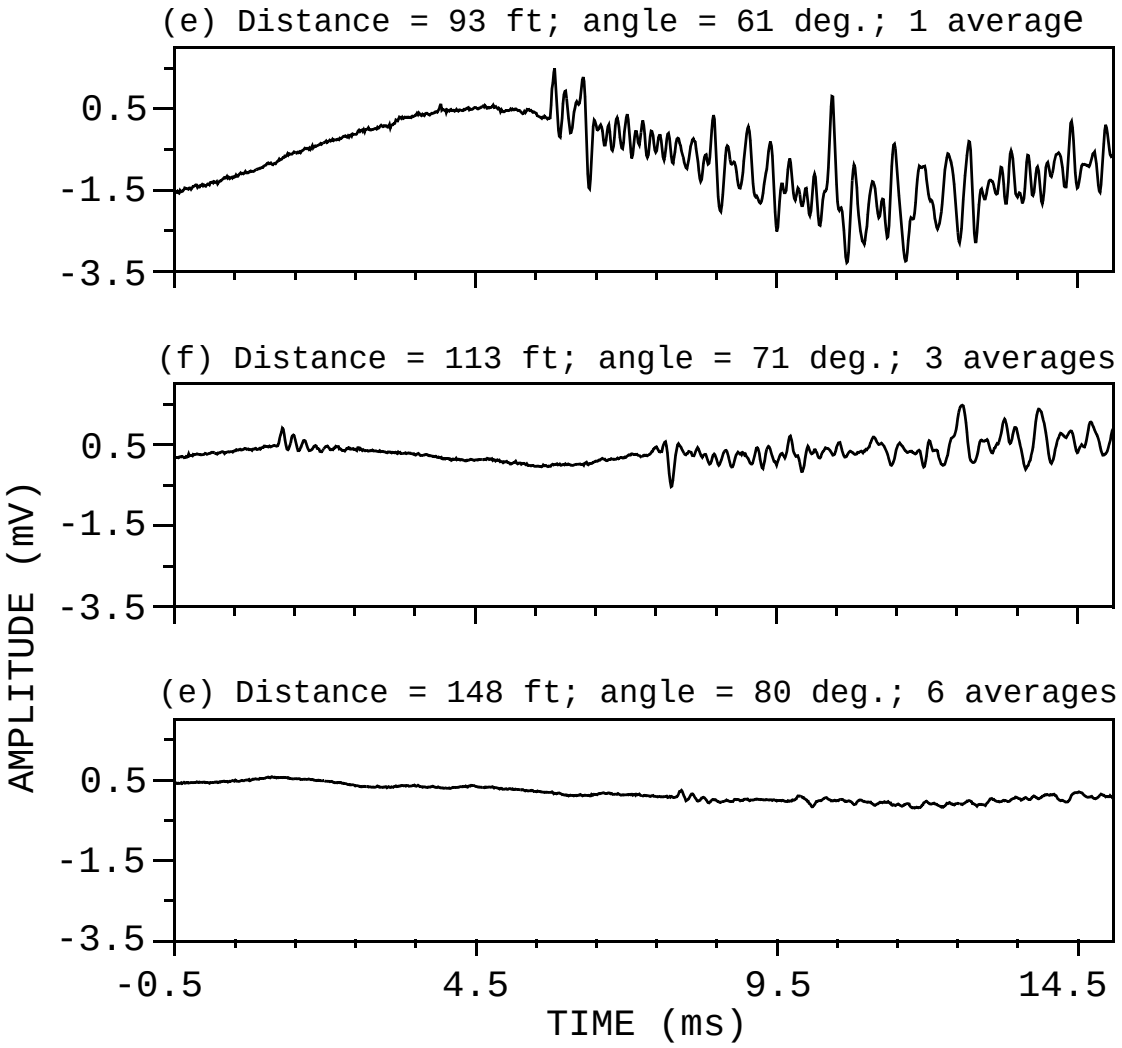


FIGURE 7-3, continued.

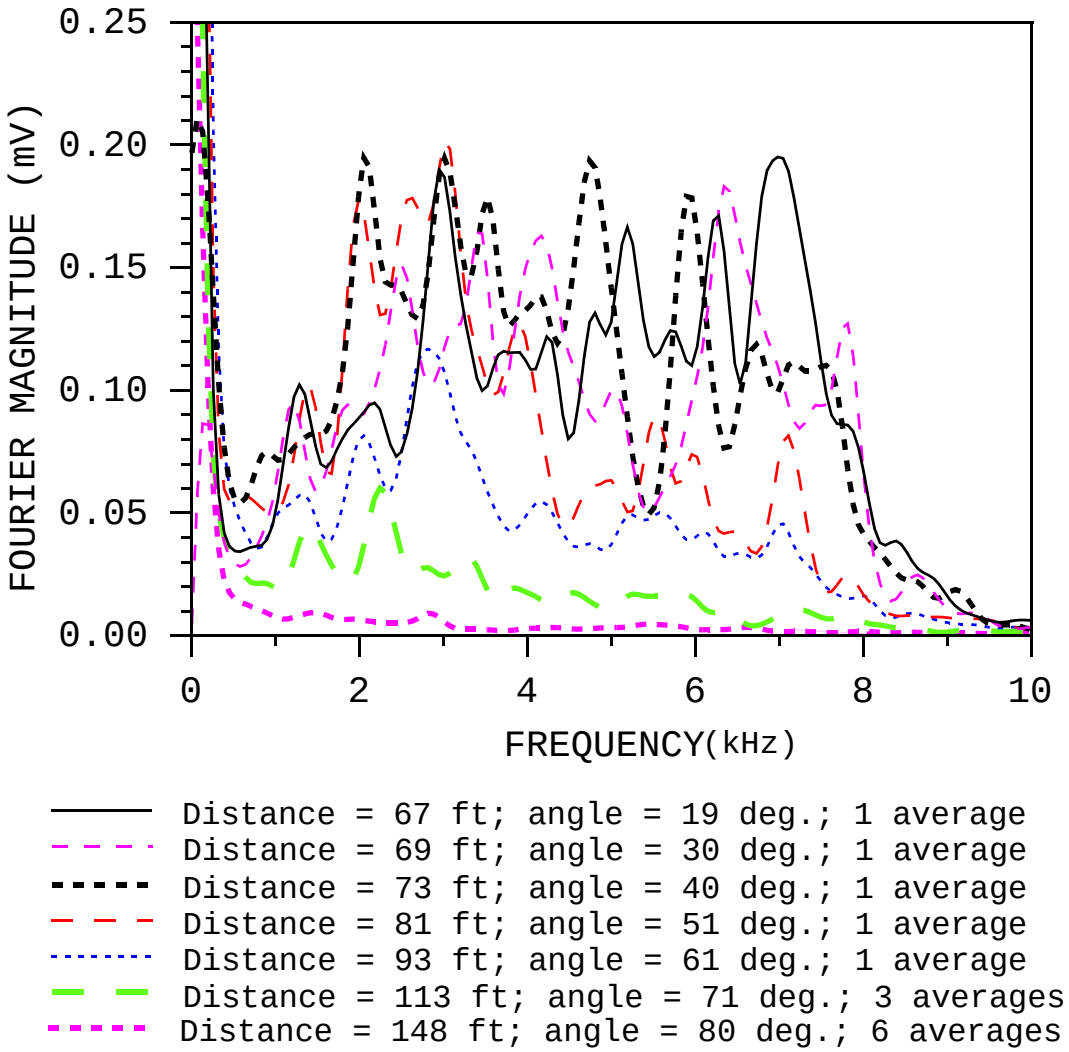


FIGURE 7-4: Frequency responses of data acquired at Monticello Dam using the nail gun source on the downstream face and a hydrophone receiver located in the reservoir. The distance from the source to receiver, the ray angle from the nail gun axis, and the number of averages for each data set are listed above.

on a concrete dam was developed.

As the first step in the modeling procedure, P-wave amplitudes were measured from the data recorded in the reservoir at Monticello Dam (Figure 7-3) using three methods. Peak amplitude values of the first cycle of each P wave were measured. Average absolute amplitude values within a 0.46 ms window immediately following the first break

were also calculated. This window length represents 2 1/2 cycles of the P-wave at its dominant frequency (about 5.4 kHz). Average absolute amplitude values were also computed using a 1.0 ms window length (arbitrarily chosen). The mathematical equations used for measurement of the amplitude values are given in Appendix B.

Amplitudes were measured by more than one method so that we could evaluate how much the model results depend on the particular method used to determine the P-wave amplitudes. The entire modeling procedure discussed below was performed independently for the three sets of amplitude values. If the model results were to vary greatly for the three different sets of amplitudes, then the model would be judged to be unstable and not very useful.

A numerical model was fit (independently) to the three sets of observed amplitude values. This model accounts for the source radiation pattern, geometrical spreading, attenuation, and the loss of energy as the seismic waves cross the concrete/water interface. Details of the modeling procedure are given in Appendix B. Measured amplitude values, plotted as a function of ray angle, and curves generated by the numerical model are presented in Figure 7-5. The measured amplitude values and model curves are also presented in Figure 7-6, plotted as a function of source-receiver distance rather than ray angle. The model curves do not fit the measured amplitude values from the hydrophone traces recorded at the two deepest locations in the reservoir (the 2 data points at the smallest ray angles in Figure 7-5 and shortest distances in Figure 7-6) because these values were not included in the modeling procedure. These amplitude values were omitted because initial model results indicated that they may be strongly affected by scattering from the top of the gallery.

Fitting the numerical model to the observed amplitude values yields estimates of the "effective source amplitude" and attenuation coefficient (See Appendix B). The effective source amplitudes and attenuation coefficients for the three models shown in Figures 7-5 and 7-6 are listed in Table 7-1. In addition, an approximate value of Q for each model is listed in the table. The Q values were computed from the attenuation coefficients using the following formula:

$$Q = \frac{\pi f}{V_p \alpha},$$

where $f$ is the frequency, $V_p$ is the P-wave velocity, and $\alpha$ is the attenuation coefficient. The dominant P-wave frequency of 5.4 kHz and the average P-wave velocity computed from the first breaks of

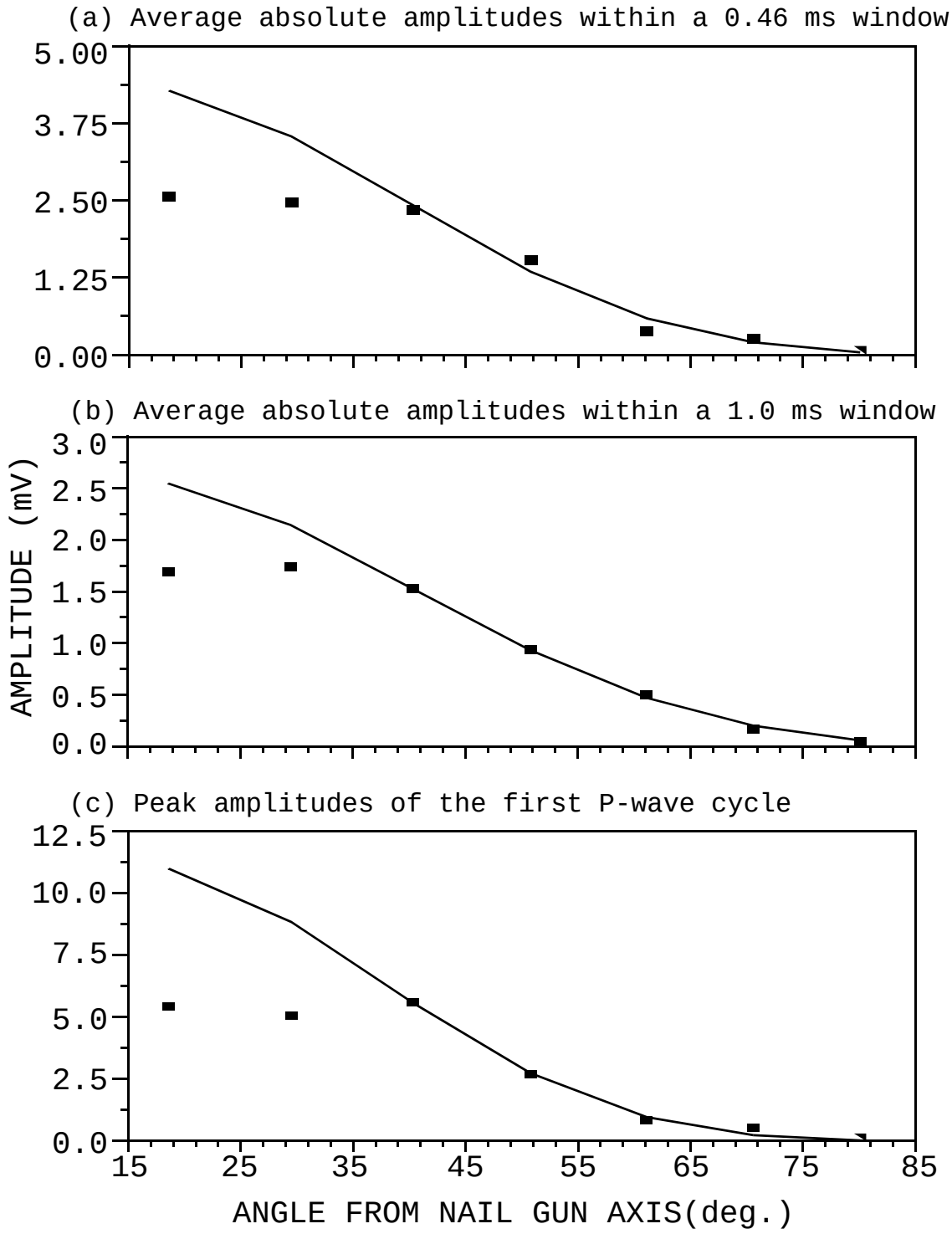


FIGURE 7-5: Measured P-wave amplitude values (points) from the data shown in Figure 7-3, plotted as a function of ray angle, and computed model curves. The first two data points were not included in the modeling procedure (see text for discussion). The model parameters determined by the fit to each data set are given in Table 7-1.

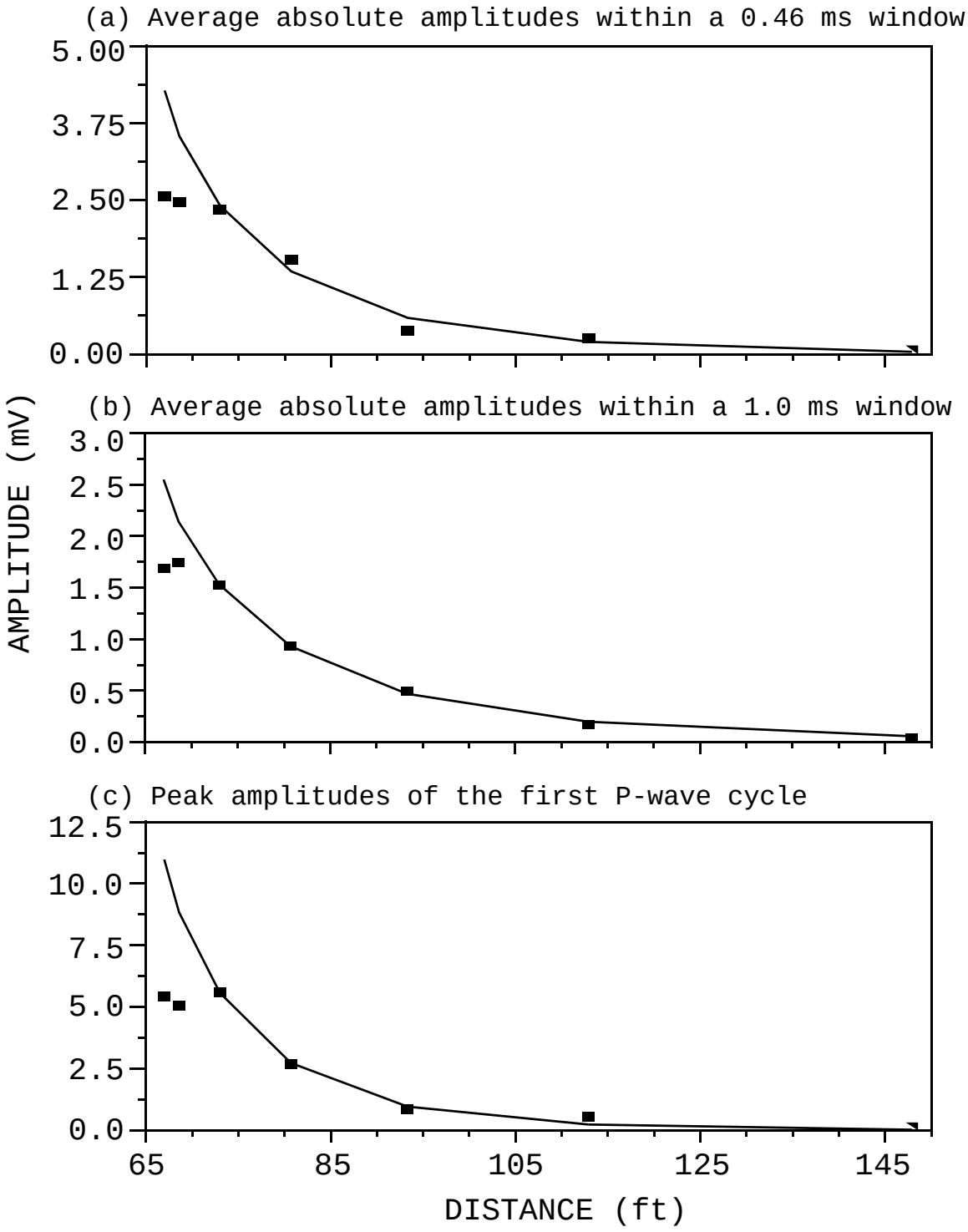


FIGURE 7-6: Measured P-wave amplitude values (points) from the data shown in Figure 7-3, plotted as a function of source-receiver distance, and computed model curves. The first two data points were not included in the modeling procedure (see text for discussion). The model parameters determined by the fit to each data set are given in Table 7-1.

| MODEL NO. | TYPE OF AMPLITUDE MEASUREMENT | EFFECTIVE SOURCE AMPLITUDE (mV ft) | ATTENUATION COEFFICIENT ($ft^{-1}$) | Q | RMS ERROR (mV) |
|---|---|---|---|---|---|
| 1 | average absolute value within 0.46 ms window | 2475 | 0.0228 | 48.3 | 0.118 |
| 2 | average absolute value within 1.0 ms window | 703 | 0.0118 | 93.3 | 0.016 |
| 3 | peak amplitude of first cycle | 19880 | 0.0399 | 27.6 | 0.135 |

TABLE 7-1: Parameters computed by least squares fits to amplitudes measured from seismic data acquired at Monticello Dam using the nail gun source on the downstream face and a hydrophone receiver in the reservoir. The amplitude values used and least squares fits are shown in Figures 7-5 and 7-6.

the 7 traces shown in Figure 7-3, 15414 ft/s, were used in the formula. Values of Q estimated by these models range from 27.6 to 93.3. Published Q values for concrete were not found in the literature searched. However, values of sandstone, limestone, and shale published by Knopoff (1964), measured at frequencies between 1 and 13 kHz, range from 52 to 73. Hence, although the uncertainty in the attenuation coefficients estimated by the amplitude modeling is large, the models yield Q values that are the same order of magnitude as values determined for competent rocks.

The effective source amplitudes and attenuation coefficients given by the three models were used to estimate P-wave amplitudes for a range of ray angles and source-receiver distances. Amplitudes were computed for two types of receivers: an omnidirectional hydrophone located in the reservoir near the upstream dam face, and a unidirectional receiver, such as an accelerometer, mounted on a concrete surface. For the latter case, the receiver axis is assumed to be perpendicular to the surface on which it is mounted. For each type of receiver, two different geometries were considered: measurements between the upstream and downstream faces of a dam, and measurements between the crest and face of a dam. For simplicity, the two dam faces were assumed to be parallel to each other and perpendicular to the crest.

The results for these four situations are presented in Figure 7-7a

to d. The three curves in each plot represent the results obtained using the parameter values from the three models. Each curve in Figure 7-7 indicates the combinations of distances and ray angles that produce P-wave amplitude estimates equal to the measured amplitude of the P wave in Figure 7-3e. During the field tests, the seismogram in Figure 7-3e was acquired with the hydrophone located at the largest distance and ray angle from the nail gun source that produced data of acceptable quality. Therefore, the amplitude of this trace was chosen as the minimum acceptable signal level. Ray angles and distances represented by points below each curve in Figure 7-7 are predicted to yield data of acceptable quality (having a higher signal level than that in Figure 7-3e), while points above each curve are predicted to yield data of unacceptably low signal-to-noise.

When data are acquired between the upstream and downstream faces of a dam for the purpose of tomographic imaging, ray angles of at least 45 degrees are desireable. Figure 7-7a indicates that data may be acquired using the nail gun source with a heavy duty shot at a ray angle of 45 degrees up to estimated source-receiver distances of about 102 to 118 feet (depending on the model used), when an omnidirectional hydrophone is used to record the data. Data of acceptable quality are predicted to be obtained at a ray angle of 60 degrees to distances of 78 to 97 feet. The estimated maximum distances are increased if a surface-mounted unidirectional receiver is used, such as a vertical accelerometer (Figure 7-7b). In this case, the maximum distance for a ray angle of 45 degrees is estimated to be 130 to 177 feet, while the estimated maximum distance for a ray angle of 60 degrees is 118 to 140 feet. The estimated distances for the surface-mounted receiver are larger than those for the hydrophone for two reasons. First, no energy is lost across the concrete-water interface when a surface-mounted receiver is used. Second, the amplitude of a waveform recorded on the concrete surface is increased due to reflection of the seismic energy at the free surface (see Appendix B).

Data acquisition at very large angles to both the source and receiver is required if data are to be obtained between the crest and a face of a dam. This type of geometry is necessary for obtaining high-resolution tomographic images of the upper section of a dam. Figure 7-7d shows the results that are predicted for this situation when a unidirectional surface-mounted receiver is used. This plot indicates that good quality data can be obtained at a ray angle of 80 degrees from the nail gun axis to distances of 115 to 139 feet, Note that the plot in Figure 7-7d is not symmetric. According to these models, acceptable quality data can be acquired at greater

(a) Omnidirectional hydrophone in reservoir and nail gun on opposite dam face

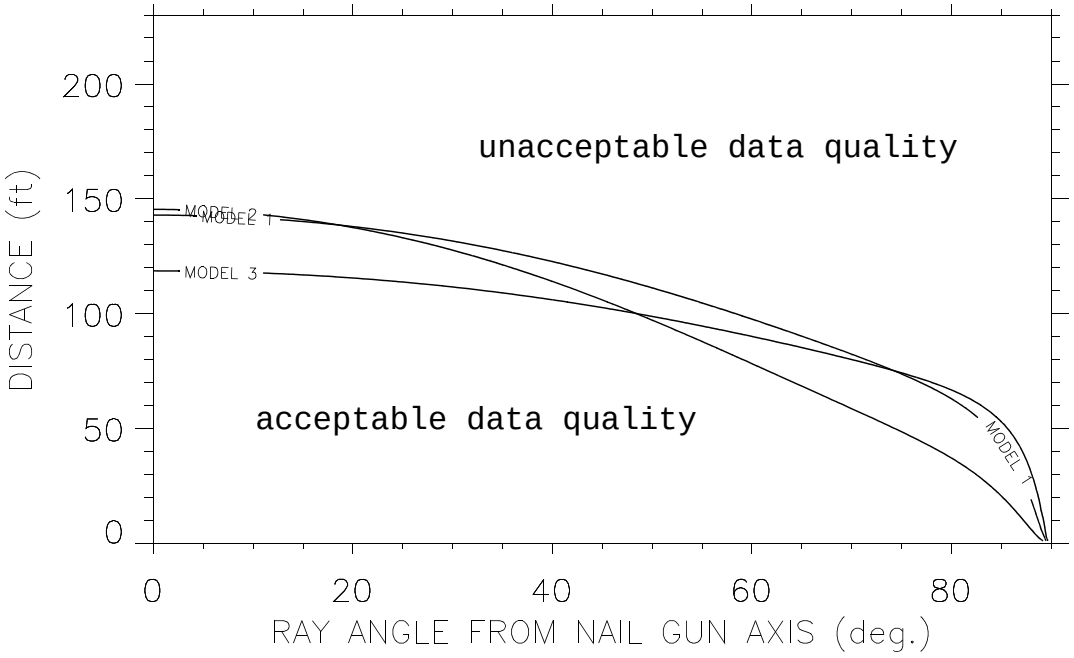


(b) Nail gun source and unidirectional receiver mounted on parallel surfaces.

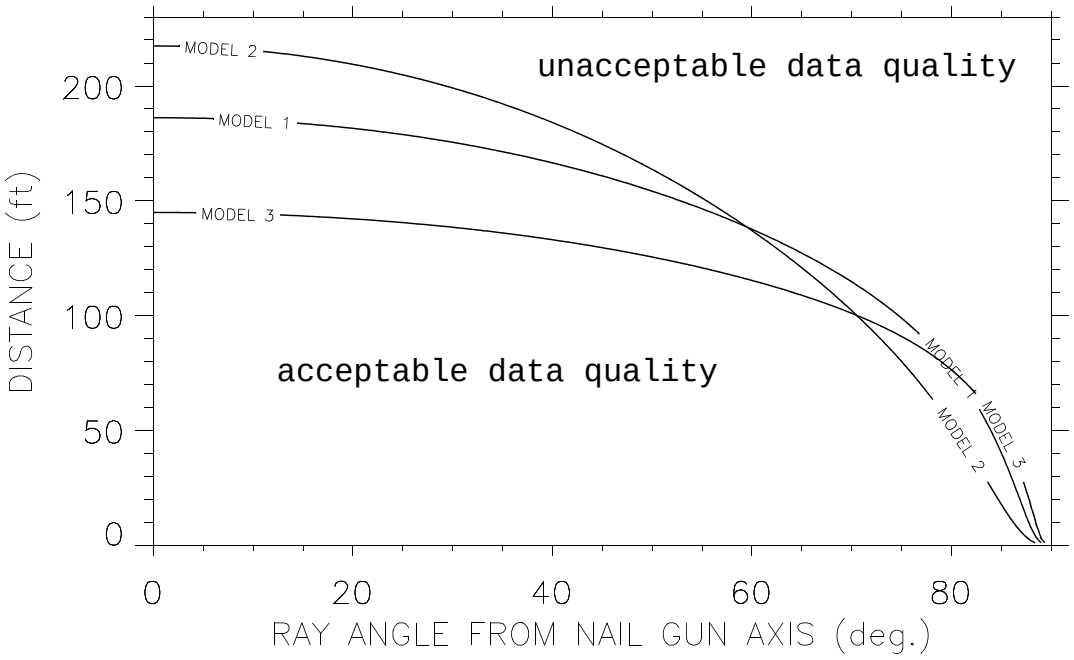


FIGURE 7-7: Combinations of source-receiver distances and ray angles that are predicted to yield acceptable data quality using the nail gun source with a heavy duty shot on a concrete structure. Each plot represents the estimates for a different type of receiver or acquisition geometry, computed using three different sets of parameters (Models 1, 2, and 3, Table 7-1).

(c) Omnidirectional hydrophone in reservoir and nail gun on dam crest

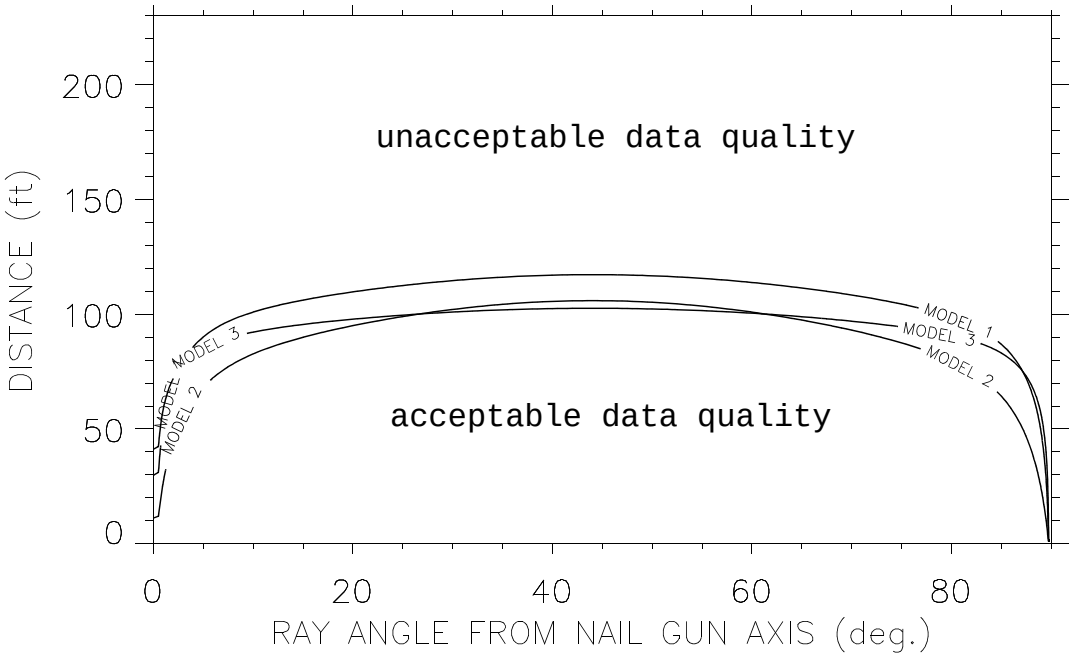


(d) Nail gun source and unidirectional receiver mounted on perpendicular surfaces.

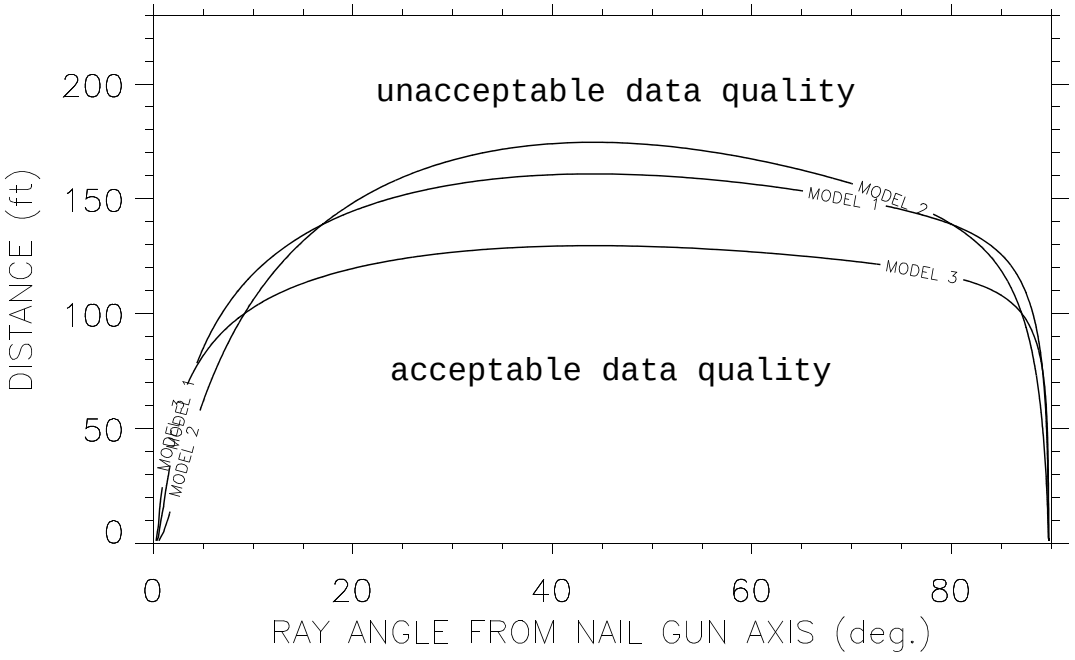


FIGURE 7-7, continued.

distances for very large angles to the nail gun axis than for very large angles to the receiver axis (small angles to the nail gun axis). This result is due to that fact that the response of the unidirectional receiver decreases more quickly with increasing ray angle than does the radiation pattern of the nail gun source. These models indicate that good quality data can be obtained at an angle of 10 degrees from the receiver axis to distances of 101 to 117 feet.

The results obtained for data acquisition using the nail gun source on the dam crest and an omnidirectional hydrophone in the water are shown in Figure 7-7c. Since there is normally at least 15 or 20 feet of freeboard, this geometry does not require data acquisition at very large angles from the nail gun axis (probably not more than 45 degrees for most concrete dams). However, it may require data acquisition at very small angles from the nail gun axis (very steep raypaths). These models indicate that acceptable quality data can be obtained at an angle of 10 degrees from the nail gun axis to distances of 82 to 102 feet.

The plots in Figure 7-7 may be used as general indicators of the results anticipated when a nail gun source is used as a seismic source on a concrete dam. They are especially useful for evaluating the relative effects of ray angle and distance on data quality (i.e., the shapes of the curves are more useful than the absolute distances and ray angles they represent). Several factors may increase or decrease the distances and ray angles for which acceptable quality data is obtained when using the nail gun source for a specific project. The sensitivity and noise characteristics of the particular receiver being used will greatly affect the results, as will the quality of the concrete through which the seismic energy is propagated. The level of background seismic noise will also affect the results, since it will affect the absolute amplitude levels required to obtain good signal-to-noise. Even the type of metal plate that the nail gun is used with (material type and thickness) will affect the results somewhat, since it affects the strength and frequency of the seismic energy that is radiated from the source into the concrete. Finally, the models that these plots are based on were computed from data having frequencies up to about 7.5 to 9 kHz. This frequency cut-off is most likely due to the limited frequency response of the hydrophone used to record the data. Seismic energy may be generated at frequencies up to 16 kHz with the nail gun source (Figure 7-2c and d). However, because of increased attenuation of higher frequencies, the frequencies above 9 kHz are not anticipated to travel to the distances predicted by the models presented here for the lower frequencies.

## 7.3 Conclusions

Of the seismic sources tested, the nail gun powered by a 22 mm shot was found to be the strongest source. Data of acceptable quality were acquired at Monticello Dam with this source from the downstrean face to a hydrophone in the reservoir to a distance of 93 feet and ray angle of 61 degrees from the nail gun axis. Numerical modeling of the amplitudes of seismic data acquired from this source indicate that useable data may potentially be acquired at a ray angle of 45 degrees to distances of about 102 to 118 feet to hydrophones in the reservoir. The nail gun source generates seismic energy having a fairly flat frequency spectrum from 2 to 16 kHz.

The Schmidt hammers produced sufficient energy to yield good quality data through 45 feet of concrete between the gallery and downstream face at Monticello Dam. They are less powerful and have a narrower frequency band than the nail gun source. The large Schmidt hammer (size M) would be too heavy to be used by climbers on the face of a dam and is in general more difficult to use than either the small Schmidt hammer or the nail gun. The small hammer (size N) may be a good seismic source for acquiring data on small concrete structures (over distances of at least 45 feet and possibly farther).

The sonic logging tool source that was tested may be used to transmit seismic energy through concrete to distances of 30 or 40 feet, but is too weak to be used for face-to-face measurements through the thicker sections of a dam. It also has a narrow frequency band (13 to 17 kHz), which is less desireable for seismic tomography than a broad-band source.

The piezoelectric transmitter developed for the laboratory tests can generate frequencies up to at least 50 kHz. However, it is much too weak for field applications.

# 8.0 CONCLUSIONS AND RECOMMENDATIONS

Several types of surface receivers were tested during Phase I of this research program, both in the laboratory and in the field. An accelerometer from PCB Piezotronics (model no. 353B17, cost $275) was found to yield data having the broadest frequency range. The other two accelerometers tested show strong, relatively low-frequency resonances (2 to 10 kHz). We believe these resonances

are related to mounting. (However, they persisted for nearly all of the mounting methods tested.) The piezoelectric transducers tested showed strong susceptibility to electromagnetic crossfeed and poor frequency response. The frequency responses from some of these receivers tested with the sonic tool source were not consistent with the source frequency spectrum. Also, data acquired at various distances and angles with the same source and receiver showed erratic frequency variations.

During laboratory tests epoxy provided better coupling than silicon grease for one of the piezoelectric transducers (sensor #5). The P-wave amplitude almost doubled when epoxy was used rather than silicon grease. The shear-wave energy was up to 4 times stronger with the epoxy mounting than with the silicon grease mounting. The frequency content of the recorded data was similar for the two types of adhesive mountings.

Laboratory tests indicate that the best type of mounting for the PCB accelerometer is either a stud mount using a masonry anchor, or a simple metal nut (zinc and alluminum nuts were tested) epoxyed to the concrete surface. Higher frequencies were obtained in the laboratory for two of the four metal nut mountings tested compared to the single stud mount tested. These two nut mountings yield data with dominant frequencies of about 34 to 36 kHz, compared to a dominant frequency of about 26 kHz for the masonry anchor mount. However, there were also indications that coupling variability for the epoxyed mountings may produce signiciant variations in data quality (frequency content and resonances). Since the consistency of data quality from one location to another is important in seismic tomography work and this issue could not be resolved in the laboratory, it is recommended that both masonry anchor mountings and epoxyed nut mountings be used during the initial tomography data acquisition in order to determine the preferred mounting method.

Of the seismic sources tested, the nail gun powered by a 22 mm shot was found to be the strongest source. It also displays a fairly broad frequency spectrum (2 to 16 kHz), which is preferred to a narrow-band source for seismic tomography measurements. For these reasons, and because it is inexpensive and easy to use, it is recommended as the seismic source to be used during the tomography data acquisition for this research program. A robust triggering mechanism and a method for mounting or temporarily holding metal plates against the concrete surface need to be developed prior to the field program.

Frequencies ranging from 2 to 16 kHz were generated with the nail gun source at Monticello Dam. No other mechanical impact source tested yielded data with higher frequencies. However, frequencies up to 50 kHz were obtained in the laboratory with a piezoelectric transmitter, and frequencies in this range have been obtained in the field by other investigators (Section 2.0). Development of a piezoelectric transmitter that is powerful enough to be used over large distances could potentially increase the frequency content of seismic data obtained in the field significantly, thereby improving the resolution of the tomographic images. The acquisition or development of such a source may be recommended in the future.

The field tests at Monticello Dam demonstrated the feasibility of lowering hydrophones into the reservoir immediately upstream of a concrete dam for recording seismic data below the water level (without the use of divers). Reclamation does not currently have hydrophones capable of recording the full frequency range generated by the nail gun source (up to 16 kHz). A high-frequency hydrophone string is needed to acquire this data. The accuracy to which these hydrophones can be located beneath the water without the use of divers also needs to be investigated.

# 9.0 REFERENCES


Angeloni, P., Bettolo, G., Superbo, S., and Zaninetti, A., 1995, On site sonic tomography data processing and analysis for dam investigations, Proceedings of the 1st meeting of the European Section of the EEGS, Torino, Italy.

Bertacchi, P, Zaninetti, A., Carabelli, E., and Superbo, S., 1991, Geophysical methods for the detection of ageing and effectiveness of repairs in dams: Proceedings of the XVII ICOLD Congress, Vienna, Austria.

Knopoff, L., 1964, Q, Reviews of Geophysics, Vol. 2, No. 4,625-660.

Thomas, M.D.A., Wiese, D., Caratin, H., and Stroczkowski, J., 1995, Ultrasound tomography applied to AAR-affected concrete structures, Proceedings of the Second International Conference on Alkali-Aggregate Reactions in Hydroelectric Plants and Dams, U.S. Committee on Large Dams, October, 1995.

# APPENDIX A

# ACCELEROMETER SPECIFICATION SHEETS

WILCOXON RESEARCH

# SPECIFICATION SHEET

INDUSTRIAL MILITARY RESEARCH

# Model 736/736T

## Small Size, High Sensitivity, High Frequency Accelerometer

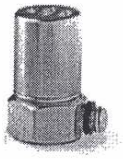

### FEATURES:

- Wide dynamic range
- High sensitivity
- Compact construction to fit in tight spaces
- Wide frequency range
- Standardized sensitivity
- Hermetically sealed

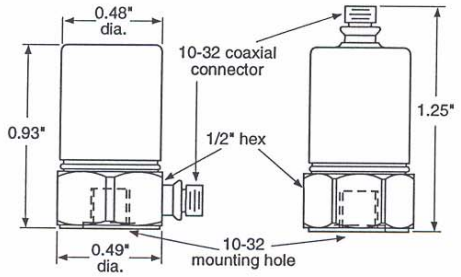


Model 736 Model 736T

### SPECIFICATIONS

| | | |
|---|---|---|
| **DYNAMIC** | | |
| Sensitivity, ±5%, 25°C | | 100 mV/g |
| Acceleration Range [1] | | 50 g peak |
| Amplitude Nonlinearity | | 1% |
| Frequency Response: | | |
| ±5% | | 5.0 - 15,000 Hz |
| ±3 dB | | 2.0 - 25,000 Hz |
| Resonance Frequency, mounted, nominal | | 60 kHz |
| Transverse Sensitivity, max. | | 5% of axial |
| Temperature Response | | see graph |
| **ELECTRICAL** | | |
| Power requirement: | | |
| voltage source | | 18 - 30 VDC |
| current regulating diode[1, 2] | | 2 - 10 mA |
| Electrical Noise, equiv. g, nominal: | | |
| Broadband | 2.5 Hz to 25 kHz | 150 µg |
| Spectral | 10 Hz | 10 µg/√Hz |
| | 100 Hz | 2 µg/√Hz |
| | 1,000 Hz | 1 µg/√Hz |
| | 10,000 Hz | 0.8 µg/√Hz |
| Output Impedance, max. | | 150 Ω |
| Bias Output Voltage, nominal | | 10 VDC |
| Grounding | | case grounded |
| **ENVIRONMENTAL** | | |
| Temperature Range | | –50 to 120°C |
| Vibration Limit | | 500 g peak |
| Shock Limit | | 5000 g peak |
| Electromagnetic Sensitivity, equiv. g | | 100 µg/gauss |
| Base Strain Sensitivity | | 0.005 g/µstrain |
| **PHYSICAL** | | |
| Weight | | 13 grams |
| Material | | 316L stainless steel |
| Mounting | | 10-32 tapped hole |
| Output Connector | | 10-32 coaxial |
| Cabling: Mating Connector | | Wilcoxon R1 (10-32 coaxial) |
| Cable | | J93, coaxial, Teflon jacket, 30 pF/ft |

**NOTES:**

[1] To minimize the possibility of signal distortion when driving long cables with high vibration signals, 24 to 30 VDC powering is recommended. The higher level constant current source should be used when driving long cables (please consult Wilcoxon Customer Service).

[2] A maximum current of 6 mA is recommended for operating temperatures in excess of 100 °C.

**ACCESSORIES SUPPLIED:** SF1 mounting stud, calibration data

**ACCESSORIES AVAILABLE:** R1-2-J93-10 cable assembly, power supplies, amplifiers, signal conditioners, SF5 cementing studs, magnetic mounting bases, SF4 isolating studs.

### TYPICAL TEMPERATURE RESPONSE

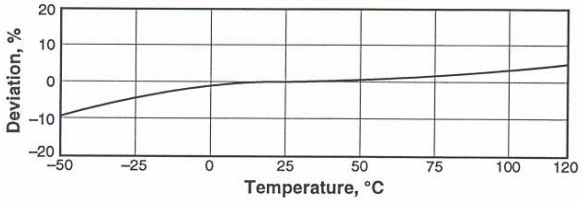


### TYPICAL FREQUENCY RESPONSE

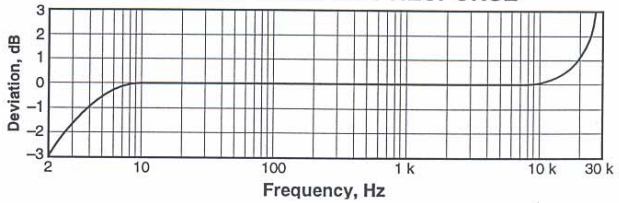


Due to continued research and development, Wilcoxon Research reserves the right to amend this specification without notice.

98093 Rev. B.1 3/96

WILCOXON RESEARCH, Inc. 21 Firstfield Road, Gaithersburg, Maryland 20878 • 1-800-WILCOXON • 301-330-8811 • FAX 301-330-8873

WR

# WILCOXON RESEARCH

(301) 330-8811 • 1-800-WILCOXON • Fax: (301) 330-8873

21 Firstfield Road • Gaithersburg, Maryland 20878

PIEZOELECTRIC VIBRATION INSTRUMENTATION

## High Sensitivity, High Frequency Accelerometer
## CALIBRATION DATA

| | | | |
|---|---|---|---|
| | Accelerometer Model... | 736 | |
| | Serial Number..... | 2581 | |
| * | Voltage Sensitivity... | 104 | mV/g |
| | Mounted Resonance..... | 52 | kHz |
| | Max Amplitude Range... | 50 | g peak |
| | Transverse Sensitivity | 2 | % of axial |
| | Bias Output Voltage... | 10.4 | Vdc |

Frequency Response:

| | | | | |
|---|---|---|---|---|
| ±5% | 5 | Hz to | 23.8 | kHz |
| ±3dB | 2 | Hz to | >25.0 | kHz |

Calibrated By: F. FUNES Date: 03/24/97

Calibration Station Number: 2

* Reference sensitivity at 100 Hz, 1g, 25°C.

*This calibration is traceable to National Institute of Standards and Technology, Gaithersburg, MD 20879. Frequency Response is traceable 10 Hz to 10 kHz.*

| Model Number | QUARTZ SHEAR ICP® ACCELEROMETER SPECIFICATIONS | Revision: H |
|---|---|---|
| 353B17 | | ECN #: 7752 |

| | | | |
|---|---|---|---|
| **DYNAMIC PERFORMANCE** | | | |
| Voltage Sensitivity | mV/g [mV/(m/s²)] | 10 [1,02] | (±10%) |
| Measurement Range | ±g pk [±m/s² pk] | 500 [4 905] | |
| Frequency Range: (±5%) | Hz | 1 to 10,000 | |
| (±10%) | Hz | 0.7 to 20,000 | |
| (±3 dB) | Hz | 0.35 to 30,000 | |
| Mounted Resonant Frequency | kHz | ≥70 | |
| Resolution - Broadband | g pk [m/s² pk] | 0.01 [0,1] | |
| Amplitude Linearity | % | ±1 | [1] |
| Transverse Sensitivity | % | ≤5 | [2] |
| **ENVIRONMENTAL** | | | |
| Shock Limit (Maximum) | ±g pk [±m/s² pk] | 10,000 [98 100] | |
| Operating Temperature Range | °F [°C] | -65 to +250 [-54 to +121] | |
| Temperature Response | | See Graph | [3] |
| Strain Sensitivity | g/με [(m/s²)/με] | ≤0.002 [≤0,02] | |
| **ELECTRICAL** | | | |
| Excitation Voltage/Constant Current | VDC/mA | 18-30/2-20 | |
| Output Impedance | ohms | <100 | |
| Output Bias | VDC | 8 to 12 | |
| Discharge Time Constant | sec | ≥0.5 | |
| Warm Up Time (within 10% of output bias) | sec | <5 | |
| Broadband Electrical Noise: (1-10 kHz) | µV rms | 40 | |
| Spectral Noise: (1 Hz) | µg/√Hz [(µm/s²)/√Hz] | 3,200 [31 392] | [4] |
| (10 Hz) | µg/√Hz [(µm/s²)/√Hz] | 700 [6 867] | |
| (100 Hz) | µg/√Hz [(µm/s²)/√Hz] | 180 [1 766] | |
| (1 kHz) | µg/√Hz [(µm/s²)/√Hz] | 64 [628] | |
| Ground Isolation | ohms | None (Optional) | |
| **MECHANICAL** | | | |
| Sensing Element | material/geometry | Quartz/Shear | |
| Housing | material/sealing | Titanium/Welded | |
| Size (hex x height) | inch [mm] | 0.28 x 0.55 [7,1 x 14,0 ] | |
| Weight | oz [gm] | 0.06 [1,7] | |
| Electrical Connector | type/location | 2-Pin Solder/Top | |
| Cable (standard 10 ft supplied) | type/termination | 031D010W Twisted Pair/10-32 | |
| Mounting Thread | size | 5-40 Male | |
| **Mounting Torque** | **in-lb [N-cm]** | **8-12 [90-135] Must Be Applied** | |

## OPTIONAL VERSIONS

Optional versions have identical specifications and accessories as listed for the standard model except where noted by the letter prefixes below. More than one option may be used.

☐ A - Adhesive Mount
Additional Accessory: (1) Model 080A90 "quick bonding gel"
Note: Adhesive mounting base is not required.

☐ B - Low Output Bias

| | | | |
|---|---|---|---|
| Output Bias | | VDC | 4.5 - 6.5 |
| Excitation Voltage/Constant Current | | VDC/mA | 12 - 30/1 - 20 |
| Measurement Range | | ±g pk [±m/s² pk] | 300 [2 943] |
| Resolution-Broadband | | g pk [m/s² pk] | 0.02 [0,2] |
| Broadband Electrical Noise: (1-10 kHz) | | µV rms | 120 |
| Spectral Noise: | (1 Hz) | µg/√Hz [(µm/s²)/√Hz] | 4,600 [45 126] [4] |
| | (10 Hz) | µg/√Hz [(µm/s²)/√Hz] | 1,120 [10 987] |
| | (100 Hz) | µg/√Hz [(µm/s²)/√Hz] | 460 [4 513] |
| | (1 kHz) | µg/√Hz [(µm/s²)/√Hz] | 130 [1 275] |

☐ J - Ground Isolated

| | | |
|---|---|---|
| High Frequency Range: (+5%)/(+10%) | Hz | 8,000/15,000 |
| Mounted Resonant Frequency | kHz | ≥56 |
| Electrical Base Isolation | ohms | >10⁸ |
| Size (hex x height): | inch [mm] | 0.37 x 0.69 [9,5 x 17,5] |
| Weight | oz [gm] | 0.10 [2,9] |

☐ M - Metric

| | | |
|---|---|---|
| Mounting Thread | size | M3 x 0.5 Male |
| Supplied Accessories: | (1) Model M080A15 base replaces Model 080A15 | |

☐ Q - Extended Time Constant

| | | |
|---|---|---|
| Low Frequency Range: (-5%)/(-10%) | Hz | 0.15/0.1 |
| Discharge Time Constant: | sec | ≥5 |
| Warm Up Time (within 10% of output bias) | sec | 45 |

☐ W - Water Resistant

| | | |
|---|---|---|
| Cable (standard 10 ft supplied) | type/termination | 018D010A/10-32 |

PCB® PIEZOTRONICS

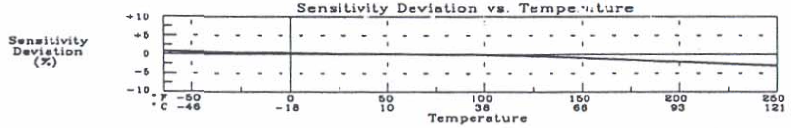


**NOTES:**
[1] Zero based best straight line method.
[2] Transverse sensitivity is typically ≤3%.
[3] Specification within ±2% of typical curve.
[4] Acceleration level equivalent.

**SUPPLIED ACCESSORIES:**
080A15 Adhesive Mounting Base (1)
(except A option)
080A24 Petro Wax Sample (1)
NIST Traceable Calibration Certificate

| Drawn: | Engineer: | Sales: CSA | Approved: | Spec Number: |
|---|---|---|---|---|
| Date: 4/3/97 | Date: 03APR97 | Date: 4/3/97 | Date: 4/3/97 | 353-2170-80 |

*In the interest of constant product improvement, we reserve the right to change specifications without notice.*

CP* is a registered trademark of PCB Piezotronics, Inc.

13,M140

# — Calibration Certificate —

Per ISA-RP37.2

Model No. 353B17

Serial No. 38672

PO No. _____ Customer _____

Calibration traceable to NIST thru Project No. 822/256889

**ICP® ACCELEROMETER**
with built-in electronics

Calibration procedure is in compliance with ISO 10012-1, and former MIL-STD-45662A and traceable to NIST.

## CALIBRATION DATA

| | | |
|---|---|---|
| Voltage Sensitivity | 10.49 | mV/g |
| Transverse Sensitivity | 2.1 | % |
| Resonant Frequency | 81.0 | kHz |
| Output Bias Level | 9.3 | V |
| Time Constant | 1.0 | s |

## KEY SPECIFICATIONS

| | | |
|---|---|---|
| Range | 500 | ±g |
| Resolution | 0.01 | g |
| Temp. Range | -65/+250 | °F |

**METRIC CONVERSIONS:**
$ms^{-2}$ = 0.102 g
°C = 5/9 x (°F - 32)

Reference Freq.

| Frequency Hz | | 10 | 15 | 30 | 50 | 100 | 300 | 500 | 1000 | 3000 | 5000 | 7000 | 10000 | | |
|---|---|---|---|---|---|---|---|---|---|---|---|---|---|---|---|
| Amplitude Deviation % | | -2.0 | -1.8 | -1.4 | -0.5 | 0.0 | 0.3 | 0.5 | 0.4 | 0.5 | 0.1 | 2.8 | 2.7 | | |

FREQUENCY RESPONSE

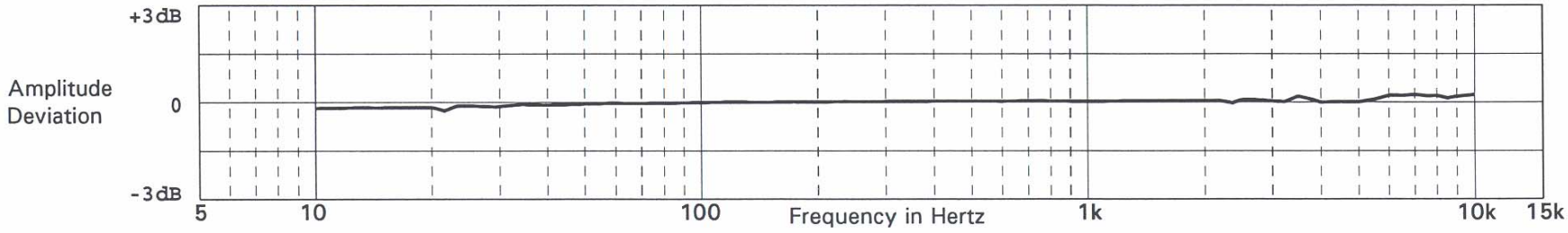


PCB® Piezotronics, Inc. 3425 Walden Avenue Depew, NY 14043-2495 USA
716-684-0001

Calibrated by Jonathan Molnar

Date 03-17-1997

Oceana Accelerometer

## Model A8000

| | | | |
|---|---|---|---|
| Voltage Sensitivity [1] | (± 20%) | mV/g [mV/(ms$^{-2}$)] | 1000 [102] |
| Measurement Range (for ± 5V output) | | ± g pk [± ms$^{-2}$ pk] | 5 [50] ("01" option) |
| Measurement Range (for ± 1V output) | | ± g pk [± ms$^{-2}$ pk] | 1 [10] ("02" option) |
| Frequency Range [2] | (± 5%) | Hz | 0.25 to 4000 |
| | (± 10%) | Hz | 0.17 to 6000 |
| | (± 3dB) | Hz | 0.08 to 10000 |
| Mounted Resonant Frequency | | Khz | >20 |
| Phase Response ± 5° (at 70°F[21°C]) | | Hz | 1 to 4000 |
| Broadband Resolution | | g pk [ms$^{-2}$ pk] | 0.00003 [0.0003] |
| Amplitude Linearity [3] | | % | ≤1 |
| Transverse Sensitivity | | % | ≤5 |
| Shock Limit - All Axes (Maximum) | | ± g pk [± ms$^{-2}$ pk] | 6000 [60000] |
| Operating Temperature Range | | °F [°C] | -65 to +200 [-48 to +93] |
| Storage Temperature Range | | °F [°C] | -65 to +250 [-48 to +121] |
| Temperature Coefficient | | %/°F [%/°C] | 0.10 [0.18] |
| Strain Sensitivity [4] | | g/με [(ms$^{-2}$)/]με] | 0.001 [0.01] |
| | [5] | g/με [(ms$^{-2}$)/]με] | 0.01 [0.1] |
| Excitation Voltage/Constant Current | | VDC/mA | 18 to 28 / 2 to 20 ("01" option) |
| | | VDC/mA | 5 to 28 / 0.3 to 20 ("02" option) |
| Output Impedance | | ohms | <100 |
| Output Bias | | VDC | 8 to 12 ("01" option) |
| | | VDC | 1 to 3 ("02" option) |
| Discharge Time Constant | | seconds | ≥2.0 |
| Warm Up Time (within 10% of output bias) | | seconds | 10 |
| Spectral Noise [6] | (1 Hz) | μg/√Hz [(μms$^{-2}$)/√Hz] | 15 [150] |
| | (10 Hz) | μg/√Hz [(μms$^{-2}$)/√Hz] | 1.0 [10] |
| | (100 Hz) | μg/√Hz [(μms$^{-2}$)/√Hz] | 0.3 [3] |
| | (1 Khz) | μg/√Hz [(μms$^{-2}$)/√Hz] | 0.2 [2] |
| Ground Isolation | | ohms | No |
| Sensing Element | | material/Geometry | PZT/Shear |
| Housing | | material | Stainless Steel |
| | | sealing | Welded Hermetic |
| Size (diameter x height) | | inch (mm) | 0.645 x 0.580 [16.38 x 14.73] |
| Weight | | oz [gm] | 0.88 [25] |
| Electrical Connector | | type/location | TO-8 (three pins) |
| Mounting | | type | Adhesive/Solder |

**NOTES:**

[1] Consult factory for tighter tolerances
[2] Adhesive mounted on cap
[3] Zero based straight line
[4]Socket mounted on pins
[5] Adhesive mounted on cap
[6] Acceleration level equivelant

The use of adhesive is recommended for both cap and pin mounting in order to achieve maximum high frequency response.
All specifications are subject to change. Contact factory for latest information.

Oceana Sensor Technologies, Inc.
1632 Corporate Landing Parkway, Virginia Beach, VA. 23454
PHONE: 804-426-3OST (3678) FAX: 804-426-3633
A Subsidiary of PCB Piezotronics, Inc.

*The Future In Motion*

# CALIBRATION DATA

DATE: 4/15/97

CUSTOMER: Matrix-5 Technologies, Inc.

MODEL: A8000-C01

| | SERIAL NO. | SENSITIVITY | | BIAS VOLTAGE | |
|---|---|---|---|---|---|
| 1 | 252 | 8.58 | mV/g | 9.8 | VDC ← accelerometer tested |
| 2 | 253 | 871 | mV/g | 9.1 | VDC |
| 3 | | | mV/g | | VDC |
| 4 | | | mV/g | | VDC |
| 5 | | | mV/g | | VDC |
| 6 | | | mV/g | | VDC |
| 7 | | | mV/g | | VDC |
| 8 | | | mV/g | | VDC |
| 9 | | | mV/g | | VDC |
| 10 | | | mV/g | | VDC |
| 11 | | | mV/g | | VDC |
| 12 | | | mV/g | | VDC |
| 13 | | | mV/g | | VDC |
| 14 | | | mV/g | | VDC |
| 15 | | | mV/g | | VDC |
| 16 | | | mV/g | | VDC |
| 17 | | | mV/g | | VDC |
| 18 | | | mV/g | | VDC |
| 19 | | | mV/g | | VDC |
| 20 | | | mV/g | | VDC |
| 21 | | | mV/g | | VDC |
| 22 | | | mV/g | | VDC |
| 23 | | | mV/g | | VDC |
| 24 | | | mV/g | | VDC |
| 25 | | | mV/g | | VDC |
| 26 | | | mV/g | | VDC |
| 27 | | | mV/g | | VDC |
| 28 | | | mV/g | | VDC |
| 29 | | | mV/g | | VDC |
| 30 | | | mV/g | | VDC |
| 31 | | | mV/g | | VDC |
| 32 | | | mV/g | | VDC |
| 33 | | | mV/g | | VDC |
| 34 | | | mV/g | | VDC |
| 35 | | | mV/g | | VDC |
| 36 | | | mV/g | | VDC |
| 37 | | | mV/g | | VDC |
| 38 | | | mV/g | | VDC |
| 39 | | | mV/g | | VDC |
| 40 | | | mV/g | | VDC |
| 41 | | | mV/g | | VDC |
| 42 | | | mV/g | | VDC |
| 43 | | | mV/g | | VDC |
| 44 | | | mV/g | | VDC |
| 45 | | | mV/g | | VDC |
| 46 | | | mV/g | | VDC |
| 47 | | | mV/g | | VDC |
| 48 | | | mV/g | | VDC |
| 49 | | | mV/g | | VDC |
| 50 | | | mV/g | | VDC |

# APPENDIX B

## MODELING P-WAVE AMPLITUDES OF SEISMIC DATA RECORDED AT MONTICELLO DAM

Seismic body waves generated by a point source can be approximated by plane waves at distances that are several wavelengths from the source (Aki and Richards, 1980). At Monticello Dam, frequencies of about 1 to 8 kHz were recorded with a hydrophone in the reservoir using the nail gun as the seismic source on the downstream face (Figure B-1). The P-wave velocity in the concrete structure is approximately 15,000 ft/s, and therefore the wavelengths of these data range from about 2 to 15 ft. Since we are interested in modeling data at source-receiver distances of 67 to 148 ft, a plane wave solution is appropriate.

The nail gun creates a unidirectional force acting perpendicular to the surface on which it is used. Since the size of the nail gun piston is small compared to the wavelengths of the seismic energy generated, it may be considered a point source. White (1983, p.209),

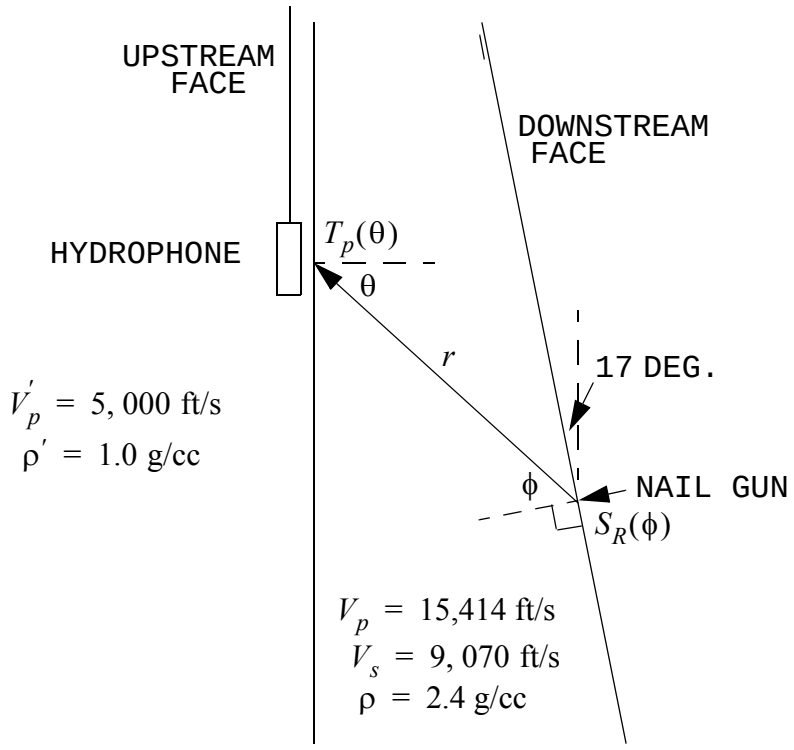


FIGURE B-1: Geometry and parameters used for modeling amplitudes of seismic data acquired at Monticello Dam.

reproducing work by Miller and Pursey (1954), gives a plane wave solution for the radial (compressional) displacement $u_r$ generated by a point force acting perpendicular to the surface of an elastic isotropic solid:

$$u_r(r,t) = \frac{G_o}{2\pi\rho V_p^2 r} S_R(\phi) e^{i\omega(t - r/V_p)} \qquad (1)$$

where:

$G_o$ = force magnitude

$\rho$ = density of solid

$V_p$ = P-wave velocity of solid

$r$ = distance from source

$\omega$ = angular frequency

$t$ = time

$S_R(\phi)$ = source radiation pattern

The term $1/r$ accounts for the decrease in displacement with increasing distance from the source due to geometrical spreading. The source radiation pattern, $S_R(\phi)$, describes how the displacement varies as a function of the angle $\phi$ from the direction of the applied force (Figure B-1):

$$S_R(\phi) = \frac{\cos\phi\left[1 - 2(V_s/V_p)^2 \sin^2\phi\right]}{\left[1 - 2(V_s/V_p)^2 \sin^2\phi\right]^2 + 4(V_s/V_p)^3 \sin^2\phi \cos\phi\left[1 - (V_s/V_p)^2 \sin^2\phi\right]^{1/2}}$$

$V_s$ represents the S-wave velocity of the solid.

For the case of an inelastic solid, intrinsic attenuation can be incorporated into the plane wave solution given by equation 1 by including the term $e^{-\alpha r}$, where $\alpha$ is the attenuation coefficient of the solid. The attenuation coefficient is a function of frequency. When modeling the seismic data recorded at Monticello Dam, P-wave amplitudes were measured in the time domain from unfiltered data recorded at various distances and angles. Since in this case all frequencies are used at one time, the attenuation coefficient computed by fitting the model to the measured amplitudes is an average value for the frequency range of the data analyzed. This type of approach is appropriate if the frequency content of the

data being modeled doesn't vary much, as is the case for the data acquired at Monticello Dam (see Figure 7-4).

When data is recorded in the reservoir upstream of a dam using a source located on the downstream face or crest, the seismic energy crosses the concrete/water boundary before being recorded. Hence, a term representing the transmission coefficient for this boundary is needed. White (1983, p.35) gives the boundary conditions that must be satisfied for the general case of seismic waves impinging upon a solid/liquid boundary. By using only the terms related to a P wave incident upon the boundary from the solid, the following relationships were derived for the P-wave transmission coefficient $T_p(\theta)$ . The primed variables in the equations below represent values for the liquid, whereas the unprimed variables represent the values for the solid.

$$T_p(\theta) = \frac{2a(\theta)f(\theta)}{d(\theta)b(\theta)(f(\theta)+g(\theta))}$$

$$a(\theta) = \sqrt{1/V_p^2 - p^2(\theta)}$$

$$b(\theta) = \sqrt{1/V'^2_p - p^2(\theta)}$$

$$c(\theta) = \sqrt{1/V_s^2 - p^2(\theta)}$$

$$d(\theta) = 1 - 2p^2(\theta)V_s^2$$

$$f(\theta) = c^2(\theta) - p^2(\theta)$$

$$g(\theta) = \frac{4p^2(\theta)c(\theta)a(\theta)}{f(\theta)} + \frac{\rho' a(\theta)}{\rho V_s^2 d(\theta)b(\theta)}$$

$$p(\theta) = \frac{\sin\theta}{V_p}$$

$\theta$ is the angle of the incident P wave, measured from the perpendicular to the solid/liquid boundary (Figure B-1). As a check on the algebra, these equations were also derived using the approach of Aki and Richards (1980, Section 5.2).

The exact distance of the hydrophone from the concrete/water boundary during data acquisition at Monticello Dam is unknown. As the hydrophone was lowered into the reservoir upstream of the dam, it slid along the concrete surface. If the hydrophone did not drift much in the upstream direction as it was lowered beneath the water, then the seismic ray path through the water is a very small fraction

of the total source-receiver distance. For these reasons, the wave propagation in the water is not included in this numerical model.

Incorporating the terms for intrinsic attenuation and transmission across the concrete/water boundary into equation 1, the expression for the particle displacement at the hydrophone becomes:

$$u_{r'}(r,t) = \frac{G_o}{2\pi\rho V_p^2 r} S_R(\phi) T_p(\theta) e^{-\alpha r} e^{i\omega(t - r/V_p)} \qquad (2)$$

The prime on the displacement subscript $r$ indicates that the direction of the compressional displacement in the water is different than that in the concrete due to refraction at the concrete/water boundary. The variable $r$ represents the distance from the nail gun source on the downstream face to the concrete/water boundary near the hydrophone (Figure B-1).

The hydrophone measures pressure rather than displacement. From the equation of motion (Aki and Richards, 1980, p. 17):

$$\rho' \frac{\partial^2 u_{r'}}{\partial^2 t} = \sum_j \frac{\partial \tau_{r'j}}{\partial j},$$

where $\tau_{r'j}$ are components of stress. In a liquid, no shear stresses exist. The only component of stress for this case is $\tau_{r'r'}$, which by definition is equal to the negative of the $r'$ component of pressure, $-P_{r'}$. Hence, the equation of motion for this case becomes:

$$\rho' \frac{\partial^2 u_{r'}}{\partial^2 t} = - \frac{\partial P_{r'}}{\partial r'}$$

Representing pressure by the plane wave solution $P_{r'}(r', t) = P_o e^{i\omega\left(t - r'/V_p'\right)}$, and taking the appropriate partial derivatives, the expression relating displacement and pressure becomes:

$$\rho' \omega u_{r'}(r,t) = - \frac{P_{r'}(r,t)}{V_p'} i$$

$$= \frac{P_{r'}(r,t)}{V_p'} e^{-\frac{\pi}{2} i}$$

Rearranging the terms and substituting the expression in equation 2 for $u_{r'}(r,t)$, the solution for the pressure recorded by the hydrophone becomes:

$$P_{r'}(r,t) = \frac{G_o V_p' \rho' \omega}{2\pi\rho V_p^2 r} S_R(\phi) T_p(\theta) e^{-\alpha r} e^{i\omega\left(\frac{\pi}{2} + t - r/V_p\right)} \qquad (3)$$

Assuming that the frequency content of the P-wave data being modeled doesn't vary drastically, $\omega$ may be considered constant. Then the constant variables may be grouped into one term that is referred to here as the "effective source amplitude", $A_S$. A constant term representing the hydrophone sensitivity that relates the acoustic pressure detected to the electrical voltage generated is also needed, and may be incorporated into $A_S$. Letting $S$ represent the hydrophone sensitivity:

$$A_S = \frac{G_o V_p' \rho' \omega S}{2\pi\rho V_p^2}$$

The peak P-wave amplitude (measured voltage, represented by $A$) is then given by:

$$|A_{r'}(r)| = \frac{A_S}{r} S_R(\phi) T_p(\theta) e^{-\alpha r} \qquad (4)$$

Note that the hydrophone is assumed to be omnidirectional (for the dominant wavelengths recorded), since we have not included a receiver directivity term.

Equation 4 was used to model the measured P-wave amplitudes of the data acquired at Monticello Dam using the nail gun source on the downstream face and a hydrophone receiver in the reservoir. A least squares matrix inversion was performed using QR factorization (Golub and Van Loan, 1983) to solve for values of the effective source amplitude $A_S$ and attenuation coefficient $\alpha$. Angles and distances $(\theta, \phi, r)$ were calculated based on measurements made in the field and assuming a dip of 17 degrees for the downstream face of the dam at the location of the nail gun source (measured from construction drawing 413-D-103, cantilever F). A P-wave velocity of 15,414 ft/s, the average velocity computed from the P-wave arrival times of the recorded seismic data, was used in the equations for $S_R(\phi)$ and $T_p(\theta)$. The values used for the S-wave velocity (9070 ft/s) and density (2.4 g/cc) of the concrete are the average values obtained from sonic and density logs performed previously in two boreholes in block 8 at Monticello Dam. Standard density and velocity values of fresh water were used (1.0 g/cc and 5000 ft/s, respectively). Figure B-1 shows the model geometry and parameters.

P-wave amplitudes were measured in two ways. The peak amplitude value of the first cycle of each P wave was measured using:

$$\frac{\text{amplitude of first peak} - \text{amplitude of first trough}}{2}$$

Average absolute amplitude values within two windows of different lengths were also calculated for each trace:

$$\overline{|A_{r'}(r)|} = \frac{1}{N} \sum_{t = t_n}^{t_p + wlen} |A(r, t) - \text{bias}|$$

where

$$\text{bias} = \frac{1}{N} \sum_{t = t_p}^{t_p + wlen} A(r, t)$$

$A(r, t)$ = amplitude of seismic trace recorded at distance $r$ from the source, at time $t$

$t_p$ = P-wave arrival time

$wlen$ = length of amplitude window

$N$ = number of samples in amplitude window

The two window lengths used during this modeling are 0.46 ms (which represents 2 1/2 cycles of the P wave at its dominant frequency of 5.4 kHz) and 1.0 ms (chosen arbitrarily). If the number of cycles within the amplitude window is fairly consistent for all of the data used (the frequency content doesn't vary much), then the average absolute amplitude values are related to the peak amplitudes by a constant scaling factor. This constant factor can be absorbed into the unknown constant term $A_S$ in equation 4. Least squares fits were performed independently for the three sets of measured P-wave amplitudes.

Initially, the amplitudes measured from all 7 seismic traces recorded in the reservoir at Monticello Dam (Figure 7-3) were used in the inversions. However, satisfactory fits to the data could not be obtained. After considering possible explanations for this problem, the most likely cause was judged to be that scattering from the top of the gallery is affecting the measured P-wave amplitudes of the two data traces recorded nearest the source (and nearest the gallery). After eliminating these two values from the inversion, good fits were obtained to the remaining 5 data points for all three amplitude data sets (Figures 7-5 and 7-6).

The effective source amplitudes and attenuation coefficients computed from the least squares inversions were used to predict

amplitudes for a large range of source-receiver distances and ray angles. This forward modeling was performed for two types of receivers: an omnidirectional hydrophone located in the reservoir, and a uni-directional receiver mounted on either a dam face or crest. For the hydrophone, equation 4 was used for the forward modeling. For the surface-mounted uni-directional receiver, the transmission coefficient for the concrete/water boundary ($T_p(\theta)$) was omitted and a $\cos\theta$ term was included to account for the directivity of the receiver. The free surface correction, which accounts for reflection and phase conversion of seismic energy at the concrete surface, was also included. The equation used to predict P-wave amplitudes recorded by a surface-mounted, uni-driectional receiver is therefore:

$$|A_{r'}(r)| = \frac{A_S}{r} S_R(\phi) FSC(\theta) \cos\theta e^{-\alpha r}, \qquad (5)$$

where $FSC(\theta)$ is the free surface correction. The free surface correction for an incident P wave is given by Aki and Richards (1980, p. 190). In the notation used here, the free surface correction becomes:

$$FSC(\theta) = \frac{\sqrt{(4p(\theta)\cos\theta c(\theta))^2 + (2\cos\theta f(\theta))^2}}{V_S^2\left[f^2(\theta) + \frac{4p^2(\theta)\cos\theta c(\theta)}{V_p}\right]}$$

The definitions of $p(\theta)$, $c(\theta)$, and $f(\theta)$ are given on page B-3.

REFERENCES


Aki, K., and Richards, P.G., 1980, *Quantitative Seismology, Theory and Methods,* Vol. 1, W.H. Freeman and Company, New York.

Golub, G.H., and Van Loan, C.F., 1983, *Matrix Computations*, The John Hopkins University Press, Balitmore, Maryland.

Miller, G.F., and Pursey, H., 1954, The field and radiation impedance of mechanical radiators on the free surface of a semi-infinite isotropic solid, Proc. R. Soc. London, Ser. A., 223: 521-541.

White, J.E., 1983, *Underground Sound, Application of Seismic Waves,* Methods in Geochemistry and Geophysics Series, No. 18, Elsevier Science Publishers B.V., New York.